Cosmological Structure Formation using Wave Mechanics

Aoibhinn Gallagher B.Sc.

Thesis presented for the degree of

Doctor of Philosophy

to the

National University of Ireland Maynooth

Department of Physics

February 2025

Department Head

Dr. Neil Trappe

Research Advisor

Prof. Peter Coles

To my parents, Barry and Pamela.

Declaration

This thesis has not been submitted in whole, or in part, to this or any other university for any other degree and is, except where otherwise stated, the original work of the author.

Aoibhinn Gallagher, August 19, 2025

Acknowledgements

I would like to first thank my supervisor Peter Coles for many years of guidance and mentorship. I would like to thank my friends and family for support. I would like to thank all past and present members of the Departments of Mathematical Physics, Theoretical Physics and Physics. I want to extend my gratitude to the examiners for their efforts in reading and examining this thesis.

The work in this thesis would not be possible without the Astrophysics Data System [1] and the ArXiv [2].

Abstract

This thesis explores cosmological structure formation through the Schrödinger-Poisson (SP) framework, building on the foundational work of Widrow and Kaiser [3]. By treating dark matter as a wave-like field, the SP formalism provides a novel perspective that addresses challenges in traditional approaches, such as the Zel'dovich approximation's (ZA) failure in nonlinear regimes. The main contributions of this work lie in advancing theoretical understanding, developing computational techniques, and applying the SP framework to foundational models of cosmic evolution.

The thesis begins by outlining the limitations of the standard ΛCDM paradigm and establishes the SP system as an alternative framework. A detailed study of cosmic voids demonstrates the SP method's ability to model void expansion beyond shell-crossing, naturally accommodating multistreaming regions using wave interference effects. These features circumvent the unphysical predictions of particle-based and traditional fluid models.

A key innovation introduced in this thesis is the exploration of viscosity within the SP framework, resulting in a novel scaling solution analogous to the Reynolds number in classical fluid dynamics. This insight enriches our understanding of how small-scale quantum effects influence large-scale structure formation. Furthermore, the SP formalism is evaluated as a reconstruction tool for cosmological initial conditions. Preliminary results show its potential to outperform standard methods in certain scenarios, particularly in simplified power-law universes, while

maintaining competitive accuracy in ΛCDM contexts.

The findings underscore the versatility of the SP approach, not only as a theoretical tool for understanding dark matter dynamics but also as a practical method for reconstructing initial conditions and analysing observational data. The thesis concludes by highlighting potential applications, including filament dynamics, redshift-space reconstructions, and the integration of SP into future observational pipelines, particularly in the context of upcoming surveys like Euclid and DESI.

Through its contributions, this thesis advances both theoretical and computational cosmology, demonstrating the promise of the Schrödinger-Poisson framework as a powerful tool for exploring the complex dynamics of the universe.

Published Works

A large proportion of the work presented in this thesis is found in these two papers

(i) Aoibhinn Gallagher and Peter Coles. "Evolution of Cosmic Voids in the Schrödinger-Poisson Formalism". In: *The Open Journal of Astrophysics* (2022). DOI: 10.21105/astro.2208.13851

(ii) Peter Coles and Aoibhinn Gallagher. "Classical Fluid Analogies for Schrödinger-Newton Systems". In: *preprint* (2025). arXiv: 2507.08583 [astro-ph.CO]. URL: https://arxiv.org/abs/2507.08583

Chapters 3 and 4 each contain work presented in (i). Chapter 4 contains the bulk of the work presented in (ii).

Contents

List of Figures

Chapter 1

Introduction

From the ancient world until the 19th century, *natural philosophy* was the term used for what we now call physics. It represented humanity's attempt to make sense of the natural world, blending observation, logic, and speculation. Over time, as our tools and methods evolved, this broad field gave rise to the specialised sciences we recognize today, including physics, chemistry, and biology. Within the realm of modern physics lies the study of one of humanity's most profound questions: the origin, structure, and ultimate fate of the observable universe. This field, now known as *physical cosmology*, continues the ancient pursuit of understanding the cosmos, albeit with the precision of mathematics and the power of advanced technology.

Cosmology sits at the intersection of science and philosophy, where empirical data meets existential wonder. While it is firmly rooted in the scientific method—analysing cosmic microwave background radiation, mapping the distribution of galaxies, and simulating the evolution of structure—it remains deeply tied to humanity's age-old questions about existence. How did the universe begin? Why does it have the structure we observe? What is its ultimate fate? These are not merely scientific inquiries but also reflections of our innate curiosity and search for meaning.

The shared scope of cosmology and philosophy brings the narrative of natural philosophy full circle. In many ways, cosmology continues the work of ancient thinkers like Aristotle, who envisioned the outer realms as part of a grand, interconnected whole, and later philosophers like Kant, who speculated on the vastness and eternity of space. What distinguishes modern cosmology is its empirical foundation: observations from telescopes, satellites, and detectors have turned abstract ideas into testable theories, transforming speculation into knowledge.

Beyond its scientific achievements, cosmology profoundly influences human nature and society. By situating us within a vast, dynamic universe, it reshapes our perspective on existence. The realisation that we inhabit a planet orbiting an average star in a galaxy among billions has a humbling effect, fostering a sense of interconnectedness and shared destiny. At the same time, cosmology inspires a sense of awe. Concepts like the Big Bang, dark matter, and black holes challenge the boundaries of human imagination, compelling us to think beyond the confines of everyday experience.

Moreover, the progress of cosmology reflects the evolution of human ingenuity. From the development of the telescope by Galileo to the launch of the James Webb Space Telescope, our pursuit of the cosmos has driven technological innovation and international collaboration. It is a testament to humanity's resilience and creativity, showing how we can transcend divisions to seek answers to universal questions.

As we delve deeper into the mysteries of the universe, cosmology remains a bridge between what is known and the infinite unknown. It reminds us of our origins while pointing toward our potential. In doing so, it reaffirms the timeless connection between science and philosophy, bringing us back to the very essence of natural philosophy. The search for understanding the cosmos is, at its core, a search for understanding ourselves.

1.1 Cosmological Context

The standard model of modern physical cosmology is known as ΛCDM . Named after the the cosmological constant Λ and cold dark matter (CDM). The cosmological constant, initially known as Einstein's biggest blunder, now dominates modern cosmology. The cosmological constant first appears in Einstein's *General Theory of Relativity* [6]. In general relativity (GR), events in space-time are labelled by coordinates $x^\mu = (ct, x, y, z)$, where c is the speed of light in a vacuum. The invariant infinitesimal space-time interval ds between two events is given by

$$ds^2 = g_{\mu\nu} dx^\mu dx^\nu, \tag{1.1}$$

where repeated indices are summed over (known as Einstein summation convention), and $g_{\mu\nu}$ is the metric tensor that describes the geometry of space-time. GR relates the geometry of space-time to the contents of the universe by the field equations

$$R_{\mu\nu} - \frac{1}{2} g_{\mu\nu} R - \Lambda g_{\mu\nu} = \frac{8\pi G}{c^4} T_{\mu\nu}, \tag{1.2}$$

where G is Newton's graviational constant [7], $R_{\mu\nu}$ is the Ricci tensor, R is the Ricci scalar, $T_{\mu\nu}$ is the total energy-momentum of the universe and Λ is the cosmological constant. The Ricci tensor is constructed from the second derivatives of the metric tensor and encodes how volumes deviate from flat space due to curvature.

The cosmological constant was initially introduced by Einstein on the right-hand side of the field equation to create a static universe, which was believed at the time. An expanding universe was not considered until Hubble [8] showed

that galaxies were receeding from us with a velocity proportional to their distance from us (*Hubble's Law*), causing Einstein to remove Λ from his equations. It was then later discovered by the Supernova Cosmology Project that not only is the universe expanding, but its expansion is accelerated [9, 10]. Thus, the reintroduction of Λ to the famous equations.

To maintain the current level of accelerated expansion, Λ is required to account for approximately 68% of the total energy density of the of the universe. The exact nature of this energy density remains unknown, thus named *dark energy*. The rest of the universe is made up of matter; with ordinary matter (baryons) accounting for $< 5\%$, and *cold dark matter* making up the remaining 26%. Dark, to keep the same naming convention as with dark energy; we don't know what it's made of. Cold generally referes to weakly interacting. Thus, ΛCDM . These percentages are estimated by based on Planck's observations of the Cosmic Microwave Background (CMB) Radiation [11].

ΛCDM relies on the *Cosmological Principle*, which assumes that the universe is homogeneous and isotropic on large scales. We ask that all positions and directions in the universe be equivalent. We are not special. The Cosmological Principle can be reformulated as "the part of the universe we can see is a fair sample" and "the universe is knowable", Keel [12]. This is a strong philosophical assumption. However, this can be tested.

We began by measuring the Cosmic Microwave Background (CMB) Radiation, with COBE [13, 14], establishing that it is blackbody radiation. The CMB is the relic radiation from the early universe, when photons and matter decoupled. Photon decoupling is known as the surface of last scattering. At this epoch the universe had cooled enough for neutral Hydrogen to form, making it transparent to radiation, thus decoupling. The CMB is a nearly perfect blackbody, with only microscopic anisotropies from which the the primordial density fluctuations grew into the vast structure we see today.

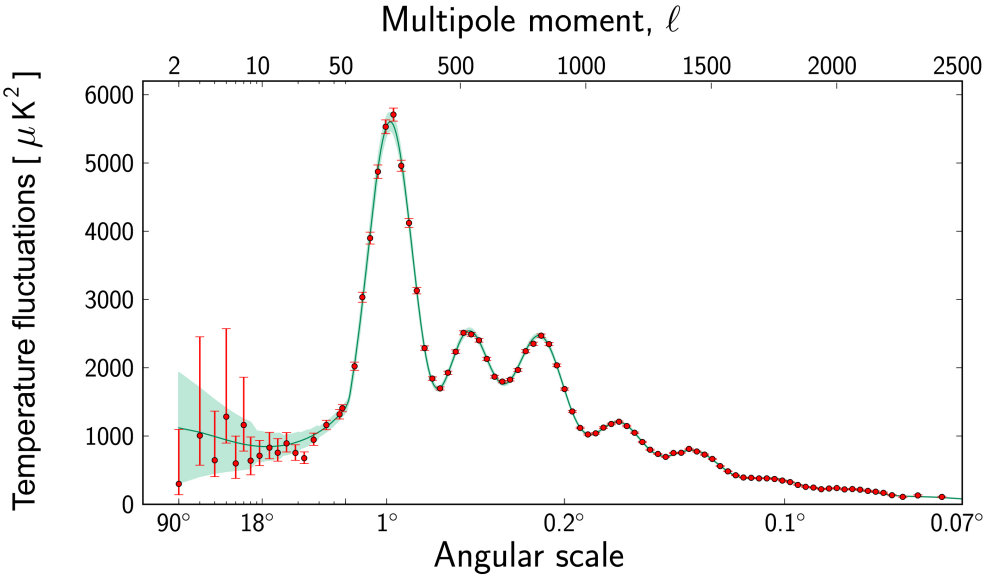

Figure 1.1: Temperature fluctuations of the CMB. The red dots depict the measurements with error bars as taken by Planck. The green curve is the best fit of the standard model of cosmology. Image credit to the Planck Collaboration and ESA [17].

Instrumentation improved with WMAP [15]. And even better with Planck [11, 16]. Figure 1.1 shows the angular power spectrum of these measurements plotted on what a ΛCDM model with the best fit parameters predicts. The temperature power spectrum (Figure 1.1) is a statistical representation of how temperature fluctuations vary across different angular scales on the sky.

Though this is a great success, it had also pointed us toward new challenges. With the measurements of the CMB becoming more precise so are the measurements of the *Hubble Constant*, $H_0 = \dot{a}/a|_{\text{now}}$. Recent measurements from the CMB give $H_0 = 67.66 \pm 0.42$ (km/s)/Mpc [16]. However, if we measure H_0 more directly, with *Cepheids* [18] for example, we get $H_0 = 73.2 \pm 1.3$ (km/s)/Mpc. These measurements disagree at 4.4σ, beyond a plausible level of chance, see Riess [18]. The disagreement of these measurements is known as the *Hubble Tension* and is cause for great concern in the community. This is the largest piece of evidence we have for the failure of ΛCDM. Some propose this can be solved

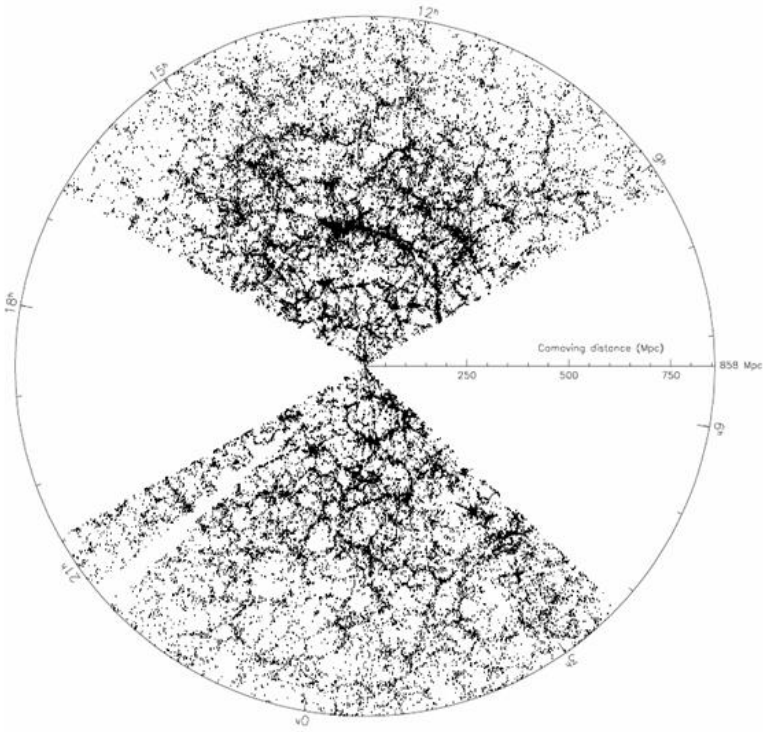

Figure 1.2: Image of the Large-Scale Structure (LSS) of the Universe as taken by the Sloan Digital Sky Survey [22]

with physics beyond ΛCDM , such as Modified Newtonian Dynamics (MOND) [19, 20] or a time-dependent $\Lambda = \Lambda(t)$ [21].

Further evidence challenging the validity of the ΛCDM model is emerging, specifically in large-scale structure. Figure 1.2 is an image from the *Sloan Digital Sky Survey* [22] which shows the rich hierarchical structure of the cosmic web, as theorised by ΛCDM . However, it hides a multitude of unsolved problems beneath the surface.

Issues with Galaxies and Galaxy clustering

The small-scale structure problem refers to the inconsistencies between the predictions of ΛCDM and observations on sub-galactic scales. Key issues include the *missing satellites problem* (the overprediction of small satellite galaxies), the *too big to fail problem* (massive dark matter haloes predicted by simulations failing to host observed galaxies) and the *cusp-core problem* (discrepancy in the density

profiles of dark matter haloes).

CDM predicts a rich heirarchical structure formation, meaning smaller structures form first and merge to create larger ones. This leads to the expectation of hundreds of small satellite galaxies orbiting larger galaxies. Fewer than 50 satellite galaxies have been identified around the Milky Way, far fewer than the hundreds predicted, shown by the Milky Way Census, Drlica-Wagner et al. [23]. This implies either a limitation in the ΛCDM model and gaps in our understanding of galaxy formation, or such satellite galaxies are too faint to be observed, for an undetermined reason. For a more in depth read on missing satellites see; e.g. Mateo et al.[24], Moore [25], Klypin et al. [26].

Included in the rich hierarchical structure expected from ΛCDM, are very massive dark matter sub-haloes. The model predicts the existence of several dark matter sub-haloes that are too massive to avoid forming, yet corresponding luminous galaxies are not observed. Unlike missing satellites, it would be impossible for too-big-to-fail galaxies to be unobservable, see Boylan-Kolchin et al.[27].

There is a discrepancy between the inferred dark matter density profiles of low-mass galaxies from observations and the density profiles predicted by cosmological simulations. With few exceptions, cosmological simulations form dark matter haloes with steeply increasing density at small radii, “cuspy” dark matter distributions. Meanwhile, the rotation curves of most observed dwarf galaxies suggest that they have a flat central dark matter density profile, they have a “core”.

The evidence suggests that the observations are unlikely to become more cuspy as we improve our techniques, equipment and understanding, Moore [28]. Therefore many efforts are being made to adjust cosmological simulations to move towards a theory that forms dark matter haloes with cores; see e.g. Koudmani et. al. [29].

Other issues of the ΛCDM model come from particle physics such as no direct detection or no evidence for super-symmetry.

1.2 Background Cosmology

This thesis has been conducted in a Friedman-Lemaître-Robertson-Walker (FLRW) Universe [30].

This means that the universe is assumed to be spatially homogeneous and isotropic (The Cosmological Principle). This means that we operate under the assumption that the following metric is the metric for our universe

$$\mathrm{d}s^2 = -c^2\,\mathrm{d}t^2 + a(t)^2\left[\frac{\mathrm{d}r^2}{1-\kappa r^2} + r^2\,\mathrm{d}\mathbf{\Omega}^2\right], \tag{1.3}$$

where,

$$\mathrm{d}\mathbf{\Omega}^2 = \mathrm{d}\theta^2 + \sin^2\theta\,\mathrm{d}\phi^2.$$

The parameter κ determines the curvature of the space-time. $\kappa = \{-1, 0, 1\}$ yeilds a $\{$open, flat, closed$\}$ universe. The time coordinate t is *Cosmological Proper Time*, which measures time as if from the perspective of an observer co-moving with the universe from the beginning of time. The expansion of the universe is accounted for by $a(t)$, known as the *Cosmic Scale Factor*. The dynamics of a FLRW universe are determined by the Einstein gravitational field equations,

$$3\left(\frac{\dot{a}}{a}\right)^2 = 8\pi G\rho - \frac{3\kappa c^2}{a^2} + \Lambda c^2, \tag{1.4}$$

$$\frac{\ddot{a}}{a} = -\frac{4\pi G}{3}\left(\rho + 3\frac{p}{c^2}\right) + \frac{\Lambda c^2}{3}, \tag{1.5}$$

$$\dot{\rho} = -3\frac{\dot{a}}{a}\left(\rho + \frac{p}{c^2}\right). \tag{1.6}$$

These equations are known as the Friedman equations [31, 32] (when considered in a FLRW universe) and determine the time evolution of the cosmic scale factor $a(t)$, the dots denote a derivative with respect to proper time t. These equations therefore, describe the global expansion (or contraction) of the universe. It is convenient to define the *Hubble parameter* $H = \dot{a}/a$ and the *density parameter* $\Omega = 8\pi G\rho/3H^2$. A suffix of "0" on any of the defined parameters denote the present epoch $t = t_0$.

1.3 Structure Formation

This section will give the necessary background for structure formation in cosmology to understand the work presented in this thesis. In this thesis we primarily work within the Newtonian approximation for the dynamical equations in either Eulerian or Lagrangian formalisms. Works that proved useful for writing this section are; Peebles [33], Islam [34], Ma and Bertschinger [35], Hawking [36], Kodama and Sasaki[37], Bernardeau [38].

The theory of structure formation is the central theme of this thesis. We wish to understand how the universe evolved from an almost homogeneous state, as evidenced by CMB, to the complex and diverse structure of the cosmic web we see today (Figure 1.2).

In the early universe, slight quantum fluctuations during the inflationary epoch seeded these density perturbations. As the universe expanded and cooled,

these fluctuations grew over time through gravitational instability, a process where overdense regions attract more matter, becoming denser and forming potential wells for galaxies and larger structures. This theory is supported by two major observational pillars, the CMB and large-scale galaxy surveys, and further understood by numerical simulations.

The growth of structure is driven by the competition between gravitational attraction and the expansion of the universe. The nature of both dark matter and dark energy being crucial in understanding what's going on. This thesis does not touch on the nature of dark energy, but has some skin in the game on the nature of dark matter. The current leading theory on the nature of dark matter is the Cold Dark Matter (CDM) model. Its simplicity and success at describing observations has lead to its rise to fame. However, it is not without its issues, as seen in earlier sections.

This Section aims to walk the reader through a brief history and outline of structure formation.

1.3.1 Vlasov Equation

Our story begins with the Vlasov Equation [39], also often referred to as the collisionless Boltzmann eqaution. It is a fundamental equation which describes the evolution of the distribution function of a system of particles under the influence of a collection of forces. Typically, gravitationl and electromagnetic forces are those included in the Vlasov equation. However, for this thesis, we will only consider the graviational forces.

We start by imagining a sea of identical collisionless particles moving under a potential V, that interact only by gravity. The Newtonian equations of motion for such particles with position $\boldsymbol{r} = \boldsymbol{r}(t)$ are

$$\frac{d\boldsymbol{r}}{dt} = \boldsymbol{u}(t), \tag{1.7}$$

$$\frac{d\boldsymbol{u}}{dt} = -\boldsymbol{\nabla} V, \tag{1.8}$$

where $\boldsymbol{u} = \boldsymbol{u}(\boldsymbol{r}, t)$ is the velocity of the a particle and $V = V(\boldsymbol{r}, t)$ is the previously mentioned gravitational potential in which the particles are moving under. The potential is caculated from the density field $\rho = \rho(\boldsymbol{r}, t)$, created by our particles, via the Poisson Equation [6, 7, 40],

$$\nabla^2 V = 4\pi G\rho - \Lambda c^2. \tag{1.9}$$

Here, Λ is the cosmological constant, c is the speed of light, and G is the gravitational constant.

To make our lives easier, we will consider everything in comoving coordinates $\boldsymbol{x} = \boldsymbol{x}(t)$, where $\boldsymbol{r} = a\boldsymbol{x}$, and $a(t)$ is the scale factor of the universe normalised to unity at the present epoch. As well as comoving coordinates, it is very convenient to work in terms of peculiar velocity $\boldsymbol{v} = \boldsymbol{v}(\boldsymbol{x}, t)$, which is the velocity of these particles relative to the expansion of the universe. Using comoving coordinates, we see

$$\boldsymbol{u} = H\boldsymbol{r} + a\dot{\boldsymbol{x}} = \overline{\boldsymbol{u}} + \boldsymbol{v}. \tag{1.10}$$

Here, $H = \dot{a}/a$ is the Hubble parameter and $\overline{\boldsymbol{u}}$ is the expansion velocity of the universe, as described above in Section 1.2.

Similarly, we can describe a peculiar gravitational potential, $V = \overline{V} + V_{\mathrm{p}}$, where $\overline{V}$ is the potential in the background and V_{p} is the peculiar potential.

Using the Friedman eqautions, the comoving equations of motion become

$$\frac{d\boldsymbol{x}}{dt} = \frac{\boldsymbol{p}}{ma^2}, \tag{1.11}$$

$$\frac{d\boldsymbol{p}}{dt} = -m\nabla_x V_p, \tag{1.12}$$

with $\boldsymbol{p} = \boldsymbol{p}(\boldsymbol{x}, t)$ being the momentum (subscript p denoting peculiar), and subscript $\boldsymbol{x}$ denoting the comoving gradient. We can now define a Poisson equation similarly,

$$\nabla^2 V = 4\pi G a^2 \overline{\rho}\delta, \tag{1.13}$$

dropping subscripts and assuming we are comoving from context, among other notational cues. $\overline{\rho}$ is the background density, and δ is the *density contrast*

$$\delta \equiv \frac{\rho - \overline{\rho}}{\overline{\rho}}. \tag{1.14}$$

Now if we expand this into phase-space, with a phase-space distribution function $f = f(\boldsymbol{x}, \boldsymbol{p}, t)$, where all particles are found when f is integrated over $d^3\boldsymbol{x}d^3\boldsymbol{p}$. Invoking Louville's Theorem, vanishing total derivative of f, we find ourselves at the Vlasov Equation:

$$\frac{\partial f}{\partial t} + \frac{\boldsymbol{p}}{ma^2} \cdot \nabla f - m\nabla_{\boldsymbol{x}}\Phi \cdot \nabla_{\boldsymbol{p}} f = 0. \tag{1.15}$$

The Vlasov Equation (1.15), describes the evolution of a phase-space distribution of particles, including Poisson Equation (1.13), under a gravitational field.

The first building block in describing structure formation in cosmology.

1.3.2 Eulerian Formalism

Eulerian Formalism, treats all of the particles we imagined in Section 1.3.1 as a fluid, which makes solving Equation (1.15) much easier. In order to describe such a fluid we need the standard Eulerian fluid equations [41]; *Euler's equation,*

$$\frac{\partial \boldsymbol{v}}{\partial t} + (\boldsymbol{v} \cdot \boldsymbol{\nabla})\boldsymbol{v} + \frac{1}{\rho} p + \boldsymbol{\nabla} V = 0, \tag{1.16}$$

the *continuity equation,*

$$\frac{\partial \rho}{\partial t} + \boldsymbol{\nabla} \cdot (\rho \boldsymbol{v}) = 0, \tag{1.17}$$

which are moments of the Vlasov Equation (1.15), when v is derived from f. We consider these equations with Poisson's Equation (1.9), describing Newtonian gravity. The Newtonian treatment of cosmic structure is still expected to be valid in expanding world models, given the perturbations are sufficiently small; see Buchert [42]. Sufficiently small meaning perturbations are on a length scale much smaller than the Hubble Horizon $d_H = c/H$. This is the distance at which the recessional velocity of an object due to the expansion of the universe equals to the speed of light. Objects within the Hubble Horizon have recessional velocities less than c. Beyond this radius, objects recede faster than c, as allowed by general relativity.

Linear Perturbation Theory - Euler

The process for handling perturbations is to linearise the Euler, continuity and poisson equations by perturbing physical quantities defined as functions of Eulerian coordinates. The near-isotropy of the CMB radiation signifies that CDM density perturbations must have been of small amplitude $|\delta| \ll 1$ at the time of last scattering. At the present epoch, the Cosmological Principle implies that density fluctuations must be much smaller than the mean density on suitably large scales, therefore, it is a good approximation to only consider first-order (linear) terms in the perturbative expansions. Expanding ρ, $\boldsymbol{v}$ and ϕ linearly yeilds the following equation,

$$\frac{\partial \delta}{\partial t} = -\frac{1}{a}\nabla_x \cdot \boldsymbol{v}, \tag{1.18}$$

which can be solved, with a suitable choice of boundary conditions, yielding,

$$\delta = -\frac{1}{aHf}\nabla_x \cdot \boldsymbol{v}. \tag{1.19}$$

The function $f \simeq \Omega_0^{0.55}$ is a fitting formula to the full solution in [33]. The linearized Euler and Poisson equations are

$$\frac{\partial \boldsymbol{v}}{\partial t} + \frac{\dot{a}}{a}\boldsymbol{v} = -\frac{1}{\rho a}\nabla_x p - \frac{1}{a}\nabla_x V, \tag{1.20}$$

$$\nabla_x^2 V = 4\pi G a^2 \rho_0 \delta. \tag{1.21}$$

In Equations (1.19-1.21), $|\boldsymbol{v}|$, $|V|$, $|\delta| << 1$. Ignoring pressure forces we can use these equations to obtain an evolution equation for δ,

$$\ddot{\delta} + 2H\dot{\delta} - \frac{3}{2}\Omega H^2 \delta = 0. \tag{1.22}$$

The general solution to Equation (1.22) is

$$\delta = D_+(t)A(\boldsymbol{x}) + D_-(t)B(\boldsymbol{x}), \tag{1.23}$$

where $A(\boldsymbol{x})$ and $B(\boldsymbol{x})$ are determined from the initial conditions, and $D_\pm(t)$ satisfy

$$\ddot{D}_\pm + 2H\dot{D}_\pm - 4\pi G\overline{\rho} D_\pm = 0. \tag{1.24}$$

Heath [43] showed that the solutions to the growing mode D_+ and decaying mode D_- are

$$D_+ \propto H \int \frac{da}{(aH)^3}, \tag{1.25}$$

$$D_- \propto H. \tag{1.26}$$

It is conventional to neglect the decaying mode D_- since only the growing mode is responsible for the formation of cosmic structure via gravitational instability. Therefore, we will just write $D_+ = D$ for convenience.

The integral in Equation (1.25) can be directly evaluated in the cosmologically relevant case of a spatially flat universe with $\Omega_m + \Omega_\Lambda = 1$:

$$D \propto \frac{5}{6}\mathcal{B}_\alpha(5/6, 2/3)\Big(\frac{\Omega_{m,0}}{\Omega_{\Lambda,0}}\Big)^{1/3}\Big(1+\frac{\Omega_{m,0}}{\Omega_{\Lambda,0}a^3}\Big)^{1/2}, \tag{1.27}$$

where $\mathcal{B}_\alpha$ is the incomplete beta function (Paris [44]). In mathematics, the Euler integral is a special function closely related to the gamma function and the binomial coefficients. The incomplete beta function,

$$\mathcal{B}_\alpha(a,b) = \int_0^\alpha t^{a-1}(1-t)^{b-1}dt, \tag{1.28}$$

is a generalisation of the solution to the Euler integral (also known as the beta function). The term $\alpha = \alpha(a)$, in our case, is defined by

$$\alpha = \frac{\Omega_{\Lambda,0}a^3}{\Omega_{m,0}+\Omega_{\Lambda,0}a^3}. \tag{1.29}$$

The solution to Equation (1.22) then becomes

$$\delta = D\delta_i, \tag{1.30}$$

which is known as the *Linear Growth Law*. Here $\delta_i = \delta(\boldsymbol{x}, t_i)$ is some initial CDM density perturbation and the constant of proportionality is chosen so that $D_i = D(t_i) = 1$. The linear growth factor D approaches a constant at late times and thus it follows from the linear growth law that the growth of CDM density perturbations slows to a halt. This is because the dominant cosmological constant drives the expansion of the universe too rapidly for matter to respond.

The linearised fluid approach provides and excellent description of gravita-

tional instability while the amplitude of the fluctuations remain small $|\delta| \ll 1$. This condition will eventually be violated as density perturbations grow. In hierarchical clustering scenarios, such as CDM, where a significant amount of small-scale power survives the radiation era, fluctuations first become non-linear ($|\delta| \sim 1$) on small scales, with progressively larger scales entering the non-linear regime as the Universe evolves. However, on sufficiently large scales, the amplitude of density perturbations remains small and linear perturbation theory still applies.

The above can only be used for a single Fourier mode of the density field δ. This is not realistic. The more realistic scenario is that we would have a superposition of waves, resulting from some kind of stochastic process in which the density field would be a superposition of multiple Fourier modes with different amplitudes, see Soda and Suto [45]. A statistical description of the initial perturbations is therefore required, and any comparison with observations will also need to be statistical. It is predicted by versions of the inflationary scenario for the very early universe that the initial density fluctuations are Gaussian in nature, with perturbations of the Fourier modes having random phases.

In the linear regime, each Fourier mode evolves independently, but in reality, Fourier modes couple to each other, leading to shifts in the phases of the Fourier components (Scherrer et al. [46]). As a result of the mode-coupling, the distribution loses its Gaussian nature. In order to describe the non-Gaussian properties it is necessary to go into the non-linear regime.

1.3.3 Lagrangian Formalism

The Eulerian formalism deals with the dynamics on a macroscopic scale, dealing with holistic features of the fluid, e.g. density and velocity fields. Alternatively, one can follow the trajectories of individual fluid elements, this is the Lagrangian approach. In this regime, the trajectory of a singular fluid element is $\boldsymbol{x} = \boldsymbol{x}(\boldsymbol{q}, t)$

where the Lagrangian coordinate $\boldsymbol{q}$ is the initial comoving position of the fluid element.

The Zel'dovich Approximation

The Zel'dovich Approximation (ZA) is the widely used analytical approximation in cosmology. Proposed by Zel'dovich [47], it provides an intuitive and mathematically straightforward way to understand how intial density fluctuations in the early universe evolve. The ZA models matter as a collection of particles that move along trajectories determined by the intial gravitational potential, making it particular useful to describe the formation of filaments and sheets in the cosmic web. White [48] shows that the ZA can be used to calculate the two-point correlation function and provides a good fit to N-body simulations. Grinstein and Wise [49] provide an interesting discussion on when ZA is an appropriate regime.

The Eulerian coordinates at time t are given in terms of the Lagrangian coordinates,

$$\boldsymbol{r}(\boldsymbol{q}, t) = a(t)[\boldsymbol{q} + b(t)\boldsymbol{s}(\boldsymbol{q})], \tag{1.31}$$

where $a(t)$ is the cosmic scale factor, $b(t)$ describes the evolution of a perturbation in the linear regime, and is defined by

$$\ddot{b} + 2\left(\frac{\dot{a}}{a}\right)\dot{b} - 4\pi G\rho b = 0. \tag{1.32}$$

It is clear to see that this is very similar to the linear growth equation (1.24) above. Equation (1.24) is defined in terms of the density contrast, whereas, here we define b for a density field. In a flat matter-dominated universe $b \propto t^{2/3}$. Where $\boldsymbol{s}(\boldsymbol{q})$ in Equation (1.31) is the displacement, described by the initial velocity potential ϕ_0,

$$\nabla\phi_0(\boldsymbol{q}) = \boldsymbol{s}(\boldsymbol{q}). \tag{1.33}$$

Mass conservation requires $\rho(\boldsymbol{r}, t)d\boldsymbol{r} = \rho_0 d\boldsymbol{q}$, so the Eulerian density field as a function of Lagrangian coordinates is

$$\rho(\boldsymbol{q}, t) = \rho_0 \left|\frac{\partial \boldsymbol{q}}{\partial \boldsymbol{r}}\right| = \overline{\rho} \left|\delta_{ij} - b(t)\frac{\partial s_i}{\partial q_j}\right|^{-1} \tag{1.34}$$

where $\overline{\rho} = (a_0/a)^3\rho_0$. Here $\frac{\partial \boldsymbol{r}}{\partial \boldsymbol{q}}$ is the deformation tensor, which accounts for the gravitational evolution of the density field. Due to the nature of $\boldsymbol{s}(\boldsymbol{q})$, the deformation tensor is a real symmetric matrix with eigenvectors that define a set of three principal (orthogonal) axes. Rewriting Equation (1.34) in terms of the eigenvalues $-\alpha(\boldsymbol{q})$, $-\beta(\boldsymbol{q})$ and $-\gamma(\boldsymbol{q})$, we get

$$\rho(\boldsymbol{q}, t) = \frac{\overline{\rho}}{[1 - b(t)\alpha(\boldsymbol{q})][1 - b(t)\beta(\boldsymbol{q})][1 - b(t)\gamma(\boldsymbol{q})]}. \tag{1.35}$$

While this approximation is very accurate in the linear regime, it breaks down in the non-linear. Shell-crossing is the moment different particle trajectories intersect. If we look only in one dimension, the Zel'dovich approximation is exact up until shell-crossing. Figure 1.3 shows how this can happen. At shell-crossing, multiple streams of matter begin to occupy the same spatial location, resulting in a multivalued velocity field, this is known as multistreaming. Figure 1.3 depicts the multi-streaming region. This marks the onset of highly nonlinear evolution, where the approximation's linear assumptions about particle motion fail. The difficulty in predicting the displacement beyond the linear regime undermines the approximation's validity and can no longer predict the growth of structures such as haloes or filaments accurately.

In this regime, gravitational dynamics dominate, and the simple assumptions of the ZA no longer suffice. Accurately modeling the evolution of structures requires more sophisticated approaches, often relying on N-body simulations, which

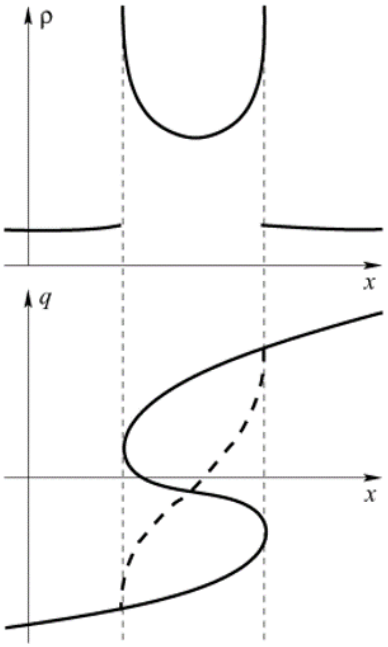

Figure 1.3: Illustration of the Zel'dovich approximation after shell-crossing. The top panel shows the density field, see the undefined nature of the density field at the boundary of the multistreaming region. The bottom panel shows how the initial coordinate maps to the later coordinate. The dashed line and solid line show two different possibilities for that trajectory.

numerically solve for the gravitational interactions between millions of particles to capture the complex, nonlinear behavior of matter after shell-crossing. However, N-body simulations can be computationally expensive and may obscure some of the underlying physical insights.

This limitation opens the door for alternative frameworks, such as the wave-mechanical approach, which we introduce as a complementary perspective to the ZA. By treating dark matter as a classical wave function, this method incorporates interference patterns and quantum pressure effects, offering new insights into structure formation, particularly on small scales. In the rest of this section and subsequent chapters, we will use the ZA as a baseline, contrasting it with our proposed wave-mechanical approach. This comparison will help highlight the strengths and weaknesses of each method and underscore the potential advantages of adopting a quantum-inspired framework for understanding cosmic evolution.

1.4 Thesis Motivation and Outline

The title of this thesis suggests the main topic of this thesis is the theory of large-scale structure (Figure 1.2) formation, from a wave-mechanical perspective. In particular, we are interested in how this wave mechanical approach can be used to explain key features of structure formation, and provide a new perspective from which to frame our understanding of phenomena observed.

The formation of structure via gravitational instability is well understood in the linear regime, when density fluctuations are much smaller than the mean density. However, galaxies and galaxy clusters are fluctuations far beyond the mean. We need to go beyond linear theory to understand the formation of such objects.

In an era dominated by large-scale simulations and extensive galaxy surveys, it's crucial to remember the value of toy models. These models distill complex behaviour into essential insights, offering a deeper understanding of key phenomena. Consider, for example, the significance of this Doroshkevich study [50] on galaxy clustering by focussing solely on the simplicity and power of the spherical collapse model.

Having established the fundamental results of cosmological structure formation to date, this thesis wishes to acomplish the following:

- To provide the necessary background and context to understand the wave-mechanical approach for structure formation as it is used in this thesis and in the literature. We wish to provide the reader with the tools to compare and contrast this method to our industry gold standard *Lagrangian Perturbation Theory* (LPT); see Buchert [51].

- To use the wave-mechanical approach to formulate a new approximation scheme that is capable of evolving cosmic voids beyond shell-crossing and into the non-linear regime.

- To carry out a detailed investigation of the role of the "viscosity" parameter ν, including a scaling solution of the system. The viscosity parameter is an integral part of the wave-mechanical framework, whether it be as a coarse grain or as a function of $\hbar$ and mass, therefore it is very useful to investigate.

- To determine if the wave-mechanical model would be a viable candidate to replace the current method of initial condition reconstruction (Zel'dovich-Bernoulli).

- To identify other structure formation problems this method could potentially tackle, along with provide a path for which to extend the work in this thesis to implement these methods into a simulation or observation pipeline.

The outline of the thesis is as follows:

Chapter 2 introduces the Schrödinger-Poisson (SP) framework for treating cosmological structure formation. We re-establish previously studied results such as *free-particle* collapse and spherical collapse. Comapring these to the ZA and discussing the implications of these results.

In Chapter 3 we investigate the implications of modelling an isolated void in this regime. Highlighting the benefits this regime has for void analysis, and discussing further implications of this model.

Chapter 4 extends the fluid mechanical analogies and introduces a scaling solution analogous to the Reynolds number.

In Chapter 5 we use the SP model to reconstruct initial conditions from which cosmological structure has formed. We also compare this method to previously and currently used methods.

Chapter 6 concludes the findings of this thesis, analyses the implications of the work presented and discusses some areas to continue and extend this work.

Chapter 2

A Wave Mechanical Perspective

This approach was first proposed in the cosmological context by Widrow and Kaiser [3] and has subsequently generated a great deal of interest, see e.g. Uhlemann et al. [52], Gosença et al. [53], Gough et al. [54, 55] and for a relativistic extension see Widrow [56]. This approach treats dark matter as a massive scalar field, described by a wave function evolving according to a modified Schrödinger equation, while the grvaitational potential is determined by the Poisson equation 1.9. This regime describes a dark matter with a wave-like nature, key features of this being interference effects, solitonic cores and suppression of small scale structure. It serves as a natural extension to classical fluid theory, while allowing for a description beyond the linear, making it an interesting contrast to particle based theory. This approach not only serves as a theoretical tool to circumvent issues with small scale structure and non-linear discriptions, it is also a promising canditate for the nature of dark matter itself.

2.1 The Schrödinger - Poisson System

Coles shows in [57, 58] that the wave mechanical approach introduced by Widrow and Kaiser can be linked to the Eulerian Fluid approach described in Section 1.3.2. To see this we need to first assume an irrotational comoving velocity field,

$$\boldsymbol{v} = \nabla_x \phi, \tag{2.1}$$

which is gauranteed by Kelvin's circulation thoerem if the primordial vorticity vanishes and there is no shell-crossing. We note that, as mentioned by [55, 59], that a posteriori the purely wave-mechanical system can actually generate localised and quantised vorticity Inserting Equation (2.1) into the Euler Equation (1.16) and integrating we get the *Bernoulli Equation* (also derived by Euler in [41])

$$\frac{\partial \phi}{\partial t} + \frac{1}{2}(\boldsymbol{\nabla}\phi)^2 = -V. \tag{2.2}$$

Applying the *Madelung Transformation* [60] takes us from the classical fluid approach into the realm of wave mechanics. Letting $\psi = \alpha e^{i\phi/\nu}$, where $\rho = \psi\psi^* = \alpha^2$. This gives

$$i\nu \frac{\partial \psi}{\partial t} = -\frac{\nu^2}{2}\nabla^2\psi + V\psi + P\psi, \tag{2.3}$$

where,

$$P = \frac{\nu^2}{2}\frac{\nabla^2|\psi|}{|\psi|}. \tag{2.4}$$

from Equations (1.17) and (2.2).

Equation (2.3) is a Schrödinger-like Equation, with potential V, ν acting as $\hbar/m$ with the addition of non-linear term P. The limit $\nu \to 0$ corresponds to the

Wentzel-Kramers-Brillouin (WKB) limit for the wave equation where quantum effects are small and the system behaves alomst classically; see Spiegel [61] and Johnston et al. [62] for further details. In the cosmological context we take V to be the gravitational potential determined via the *Poisson Equation* (now in comoving coordinates)

$$\nabla^2 V = 4\pi G\rho, \tag{2.5}$$

and we get the , the Schrödinger-Poisson (SP) system of coupled Partial Differential Equations (PDEs).

Although ψ is governed by the same equation as the evolution of a single-particle wave function, that is not how it should be interpreted here. In particular, $|\psi|^2$ represents a physical density not a probability density, and its evolution is completely unitary - there is nothing like the wave-function collapse that occurs in standard quantum mechanics in this system.

It's important to note a crucial advantage of this description, namely that because $\rho = |\psi|^2$ the condition that $\rho \geq 0$ is automatically enforced if one applies, e.g., perturbation theory to ψ. This is not the case for approaches based on standard Eulerian perturbation theory applied to $\delta = (\rho - \rho_0)/\rho_0$ which predict $\rho < 0$ when $\delta < -1$ and are therefore very unsuitable for describing voids. Note also that because the wavefunction describes a delocalized particle there are no singularities analogous to the caustics that form in the ZA.

The non-linear term, P, in Equation (2.3) is known as the *quantum pressure*. It is difficult to see where this name comes from. Some combine P and V to create a new effective potential for the system. However, we find it more useful to refer to it as a pressure, because it acts like a pressure in the sense that it acts like an opposing force to the gravitational collapse in a similar way a pressure

would act like this in gas. In saying this, it is not essential that P be kept in Equation (2.3), as $P = 0$ describes a purely wave-mechanical system. One can then conclude that the SP system is extremely versitile in describing cosmological structure formation. Keeping P as its defined in Equation (2.4), is consistent with the Eulerian fluid description for CDM, and setting $P = 0$ describes a wave-mechanical dark matter particle, often called Fuzzy Dark Matter (FDM).

Furthermore, if we wish to use SP to describe FDM, ν in Equation (2.3) must be

$$\nu = \frac{\hbar}{m}, \tag{2.6}$$

where $m \sim 10^{-22}\mathrm{eV/c^2}$. Dark matter particles with this mass have a deBroglie wavelength that is cosmologically significant, hence the *fuzzy* in FDM; see for example Schwabe et al. [63], Dentler et al. [64], Hui [65] and references therein.

Similarly to the quantum pressure, ν can be as described in Equation (2.6), or it can be used a coarse-graining tool. In this thesis we keep the discussion as general as possible to account for either interpretation (FDM or Eulerian Fluid).

On the matter of using ν as a coarse grain tool, larger ν leads to waveier solutions. We wish to strike a balance between accuracy to the fluid description and smaller ν making calculations more difficult, but more on that later (Chapter 4).

2.2 One-dimensional "Free Particle" Collapse

In the previous section (Section 2.1), we concluded with a system of two coupled PDEs in Equations (2.3) and (2.5), which is not exactly solvable in its current state. Even with the use of computational methods, coupled systems of PDEs are notoriously difficult to solve. In this subsection, we will utilse the fact that the potential changes very slowly to ignore it, essentially. We use the approximation

where the gravitational potential is calculated at each time-step, but not included in the Schrödinger equation explicitly. In other words, the gravitational potential is updated as the fluid moves but the effect of this evolution of the fluid motion is ignored. This has the effect that the fluid moves as a collection of *free particles*, a shortcut that has shown to be remarkably accurate for some applications; see Short and Coles [66], Coles and Spencer [67]. Here, we demonstate here this for reference in later chapters.

We also ignore the quantum pressure term in Equation (2.3) for the free particle theory. Using similar reasoning to the gravitational potential, we notice that P (Equation (2.4)) changes very slowly when compared to the density field ρ. Therefore, we conclude that it will not affect the evolution of the system greatly, at least in early timesteps. We will say more about this later.

I want to stress that the free particle approximation is very effective due to implications of Equation (2.2). We see that the gravitational potential is encoded into the velocity potential in the initial instance, and then the free particle approximation functions similar to the ZA, where the particles get an initial "kick" due to gravity, and then evolve.

I will only show this result in $(1+1)D$, as a proof of concept, and note that it is possible to extend into $(3+1)D$.

The free particle equations are as follows,

$$i\nu\frac{d\psi}{dt} = -\frac{\nu^2}{2}\frac{d^2\psi}{dx^2}, \tag{2.7}$$

$$\frac{d^2V}{dx^2} = 4\pi G|\psi|^2. \tag{2.8}$$

It is clear in Equations (2.7) and (2.8) that the system is now decoupled, and much easier to solve.

Figure 2.1 shows the solution to Equations (2.7) and (2.8) for three different

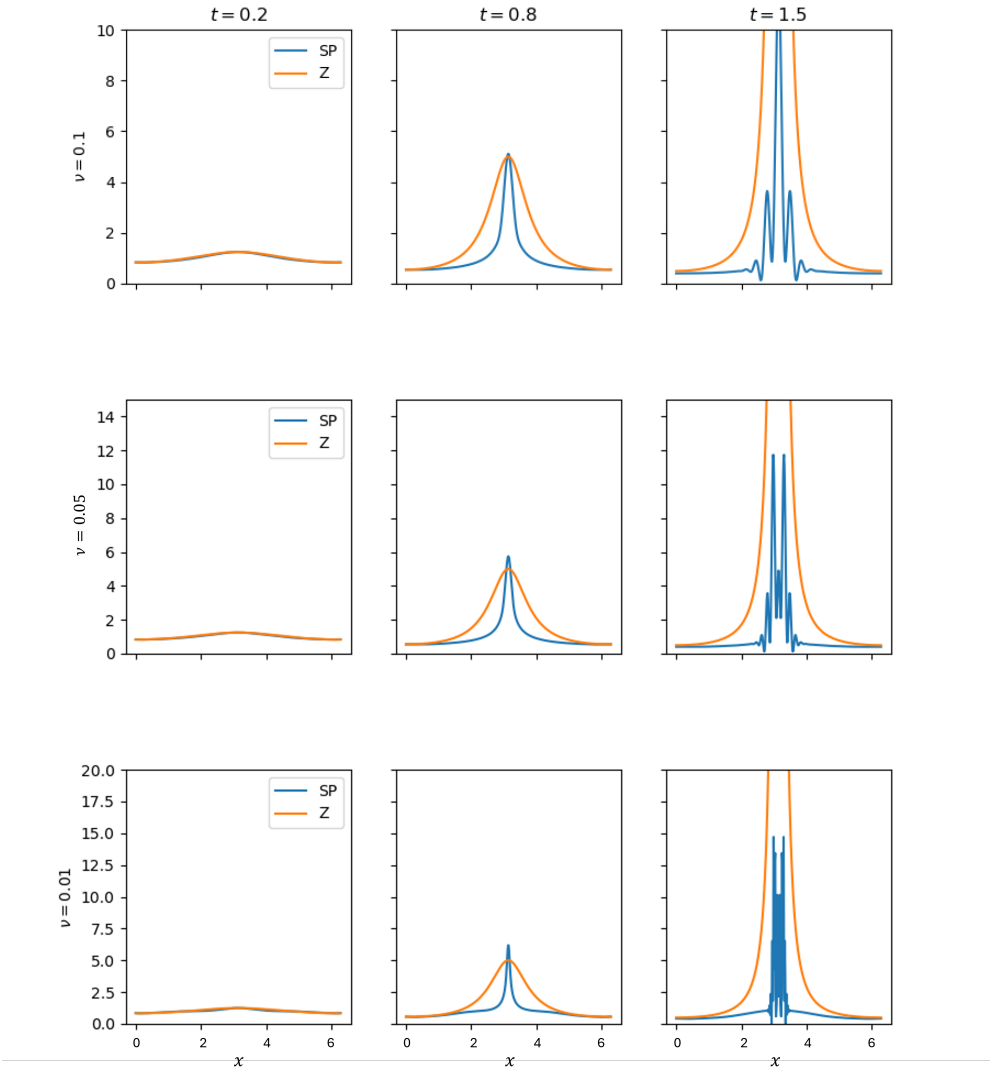

Figure 2.1: In this figure, we can see the Zel'dovich Approximation (orange) and Schrödinger-Poisson Formalism (Blue) compared for a simple one dimensional collapse of a plane wave, with period of 2π. The columns depict 3 different timesteps and the rows depict 3 different values of our scale parameter ν, which the Zel'dovich is not affected by.

values of the scale parameter ν to demonstrate its effect on the evolution of the system, along with showing the differences with between the SP system and ZA. It is clear in Figure 2.1 that at early timesteps there is little difference between the two different systems, but as we get closer to shell-crossing we can see the two diverge. The main take-away from this comparison is that at the point of shell-crossing ZA becomes undefined and blows up, whereas the wave-nature of the SP particles kicks in and the particles in different streams begin to interfere with each other and we no longer have an undefined density field post-shell crossing. This is the main motivation for using SP over ZA. It is also interesting to note, that while ZA is becoming singular at the centre of the overdensity, SP spreads out as it is interfering with itself. This becomes more relevant when we consider one of the current issues with CDM being the cusp-core porblem, an FDM field described by SP would not have this issue.

2.2.1 Spherical Collapse

As shown in Section 2.2, SP is useful for peering into the multistreaming region. As well as one-dimensional Cartesian analysis, it is a useful exercise to look at one-dimensional spherical analysis, since [50] showed that matter condensations around large perturbations were nearly spherical. As well as being able to predict that the typical mass, size and density of galaxy clusters should have a roughly similar density as their collapse. Due to this result, we can learn a lot about early density perturbations by analysing the end-point of a simple spherical collapse model.

The ideas for this section were presented in Johnston et al. [62], and should be consulted for more details of what's to follow.

To understand the collapse of a spherical overdensity, we turn our attention to the so called *top-hat* model, as shown in Figure 2.2. It is called this because it kind of looks like a top-hat, with a small sphere in the center, which is the

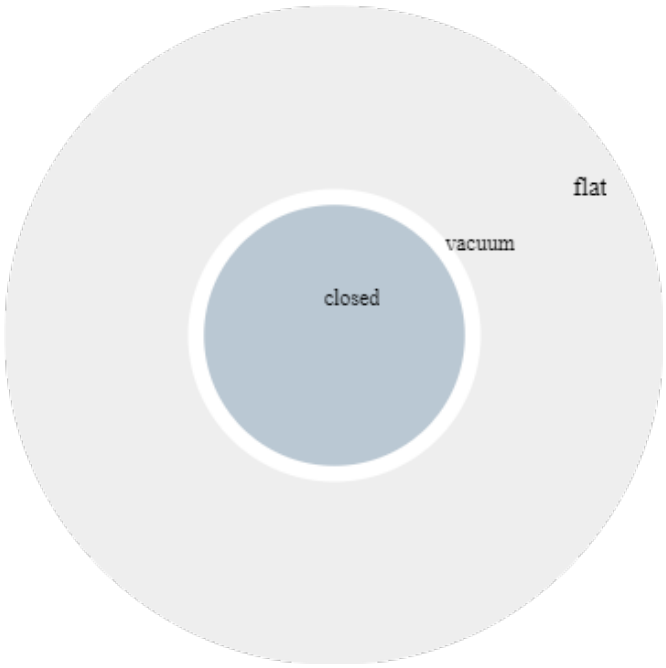

Figure 2.2: Top hat diagram for spherical collapse. The inner region is the overdense region, the shell is a thin layer of vacuum separating the overdensity from the rest of the universe, which is the outer region. We model the inner region as a closed universe and the outer region as a flat universe.

overdense region, a thin layer of vacuum to separate this region from the rest of the universe which surrounds the over dense region.

We separate the inner region from the outer region with this shell in our theoretical model because this region is where we would expect a multistreaming region to occur, and this is quite difficult to work with.

The overdense reion is modelled by a closed universe. Full details of the calculation are found in [62]. The rest of the universe is assumed to be flat and the solution to this is found with the solution to the closed universe.

The aformentioned solutions are only valid in this very specific case which is great but not the most useful. To get a more useful understanding of the problem we need to solve the system more generally.

To solve this system in three dimensions is very computationally intensive, but to make it more manageable we can make some assumptions. If we assume that the object will remain spherically symmetric as it collapses we can get a

one-dimensional solution to a three-dimensional problem. The equations to the spherically symetric problem are as follows,

$$i\nu\frac{\partial\psi}{\partial t} = -\frac{\nu^2}{2}\left(\frac{\partial^2\psi}{\partial r^2} + \frac{2}{r}\frac{\partial\psi}{\partial r}\right) + V\psi + P\psi, \tag{2.9}$$

which is obtained from Equation (2.3), and Equation (2.5) becomes

$$\frac{\partial^2 V}{\partial r^2} + \frac{2}{r}\frac{\partial V}{\partial r} = 4\pi G|\psi|^2. \tag{2.10}$$

These analytic solutions are valid because we consider a thin shell of vacuum between the two fluids so that we don't have issues with the multistreaming region. This is a great way to get an analytic solution but is not the most physical description. To get a more physical solution, without having to consider the multistreaming region, we can split the fluid in two again, but this time without the vacuum shell. Now with a two-fluid description we have a new system of equations;

$$i\nu\frac{\partial\psi_1}{\partial t} = -\frac{\nu^2}{2}\left(\frac{\partial^2\psi_1}{\partial r^2} + \frac{2}{r}\frac{\partial\psi_1}{\partial r}\right) + V\psi_1 + P\psi_1, \tag{2.11}$$

$$i\nu\frac{\partial\psi_2}{\partial t} = -\frac{\nu^2}{2}\left(\frac{\partial^2\psi_2}{\partial r^2} + \frac{2}{r}\frac{\partial\psi_2}{\partial r}\right) + V\psi_2 + P\psi_2, \tag{2.12}$$

$$\frac{\partial^2 V}{\partial r^2} + \frac{2}{r}\frac{\partial V}{\partial r} = 4\pi G\big(|\psi_1|^2 + |\psi_2|^2\big). \tag{2.13}$$

I constructed the initial conditions to align as well as possible to the top-hat model described by Figure 2.2, this can be seen in Figure 2.3. The initial gravitational field is calculated from Equation (2.13), and shown in Figure 2.4. The velocity potential for fluids one and two are given to be quadratic and quartic

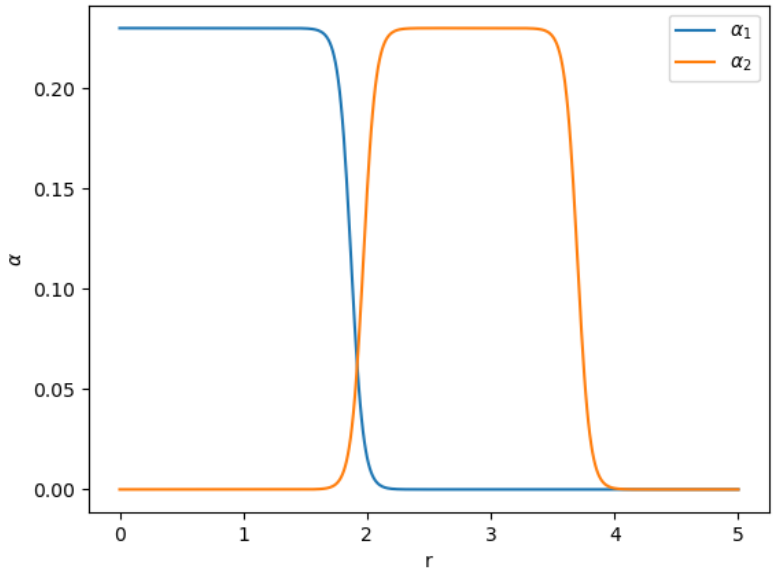

Figure 2.3: Initial conditions for density field of two fluid collapse.

respectively, as this is what we would expect for these fluids with this gravitational potential. The velocity potential is shown in Figure 2.5.

The system of Equations (2.11-2.13) were solved by a finite-difference method and appropriate boundary conditions [62] to produce the results seen in Figures 2.6-2.8.

The two-fluid approach is particularaly compelling becuase it allows for a detailed examination of the multistreaming region. The two fluid model, as presented in [62] acts like a window into the multistreaming region, and allows us to analytically go beyond shell crossing in this particular case.

Having established the foundational principles and key results that frame this work, we now turn to their implications and explore how they inform the central questions of wave-mechanical structure formation. With the results of spherical collapse in mind, we turn our attention to an analogous result of examining the evoltuion of an isolated void in a similar expression as the results presented in this section. Icke [68] found that the spherically symmetric model is more applicable to model voids than collapse due to the *Bubble Theorem*, which states that voids

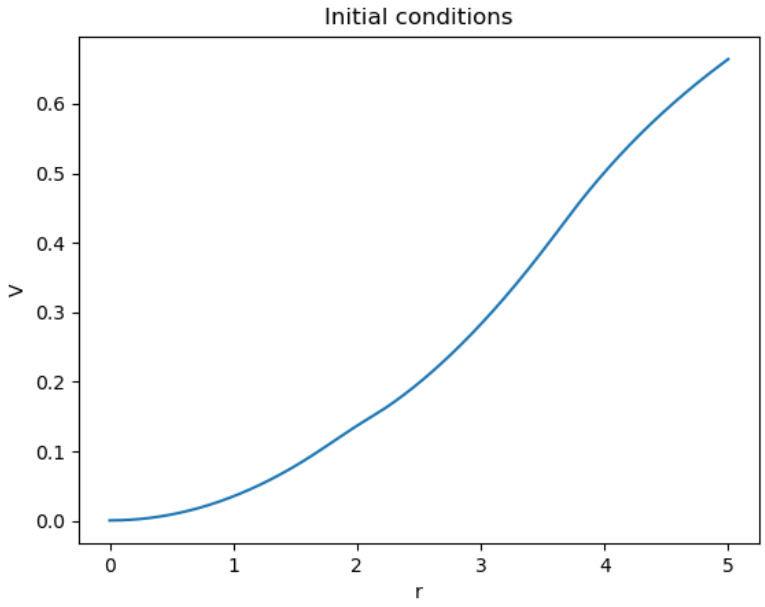

Figure 2.4: Initial gravitational potential for density field in Figure 2.3.

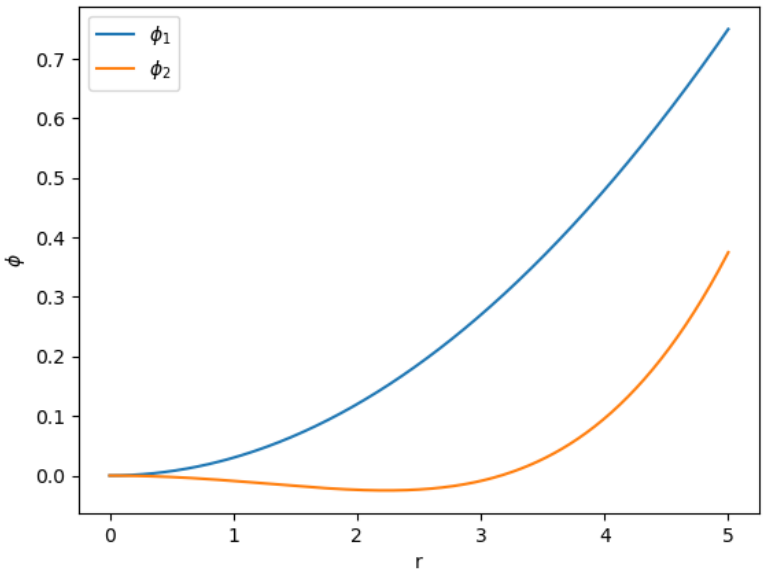

Figure 2.5: Initial velocity potential for two fluid spherical collapse.

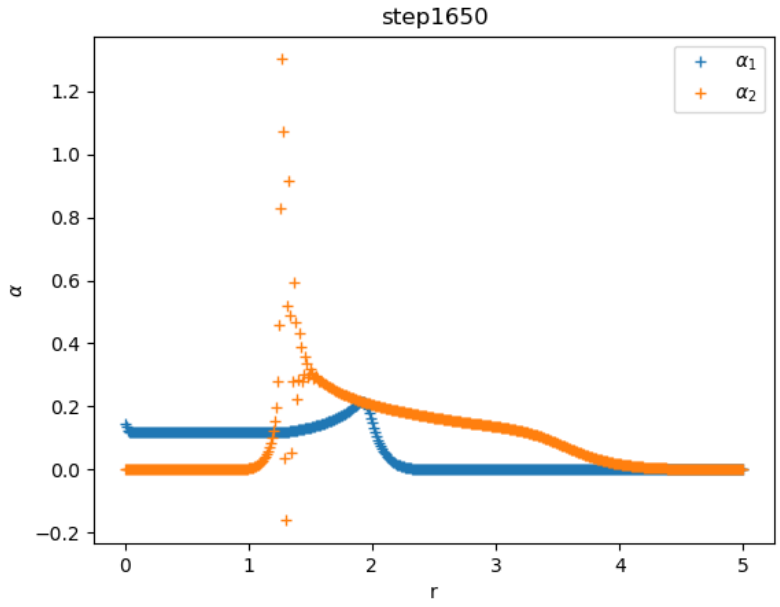

Figure 2.6: Late time-step density field for two fluid spherical collapse.

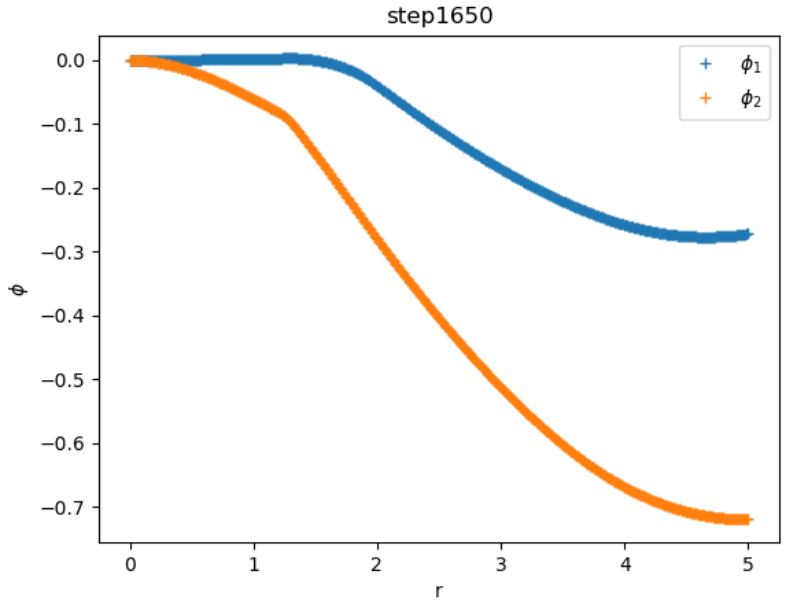

Figure 2.7: Late time-step velocity potential field for two fluid spherical collapse.

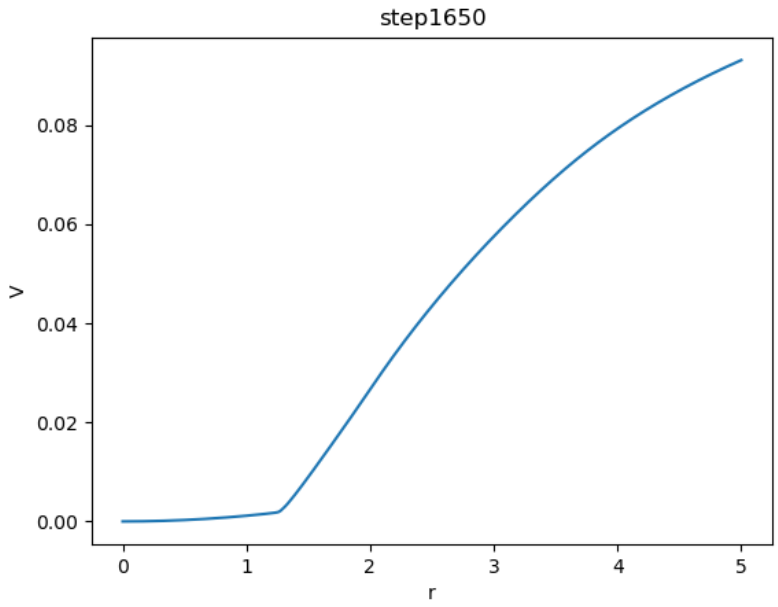

Figure 2.8: Late time-step graviational potential for the two fluid spherical collapse.

tend to become more spherically symmteric as they expand. Of course, this is more applicable in the slightly unrealistic isolated void case, which is the focus of the next chapter.

However, we don't let the limitations of simple models disuade us from undertaking a study, Doroshkevich's work helped establish a statistical and dynamical framework for understanding galaxy clustering and large-scale structure. It bridged the gap between early cosmological perturbations and the observed distribution of galaxies, making it a foundational contribution to modern cosmology. His insights into anisotropic collapse and tidal torques remain integral to theoretical and computational models of structure formation.

Thus, the another key theme of this thesis will be the study of simple semi-analtic models with the goal of gaining some insight, which could later inform more complex models, theories and techniques.

Chapter 3

Evolution of Cosmic Voids

It was first demonstrated by Lynden-Bell [69] and Lin, Mestel and Shu [70] that density inhomegeneities are likely to collapse in such a way that any slight departure from sphericity is systematically magnified in evolution. However, the case for the void is the opposite. The same argument for loss of sphericity holds for voids, except that it is reversed. So while the condensations collapse, the voids expand. Centrella and Melott [71] showed that *as the void becomes bigger, its asphericities will tend to disappear*. This result is often referred to as the "Bubble Theorem", Icke [68, 72, 73]; also see [74] for more numerical calculations.

The expansion of a spherically symmetric void is therefore more realistic than the collapse of a spherically symmetric over-density. Moreover, [71] shows that condensations are more likely to form sheets or filaments as they collapse, forming the Cosmic Web, leading to voids dominating space in terms of volume fraction.

As well as these physical aspects of void evolution, White [75] shows that voids contain information about the entire hierarchy of n-point correlation functions at all orders. For these reasons, among others, a great deal of interest has been generated in the behaviour of cosmic voids; see e.g. Sheth and Weygaert [76], Bos et al. [77], Achitouv et al. [78], Demchenko et al. [79] and Pisani et al. [80].

In this Chapter, I detail the interesting case of evolution of cosmic voids by

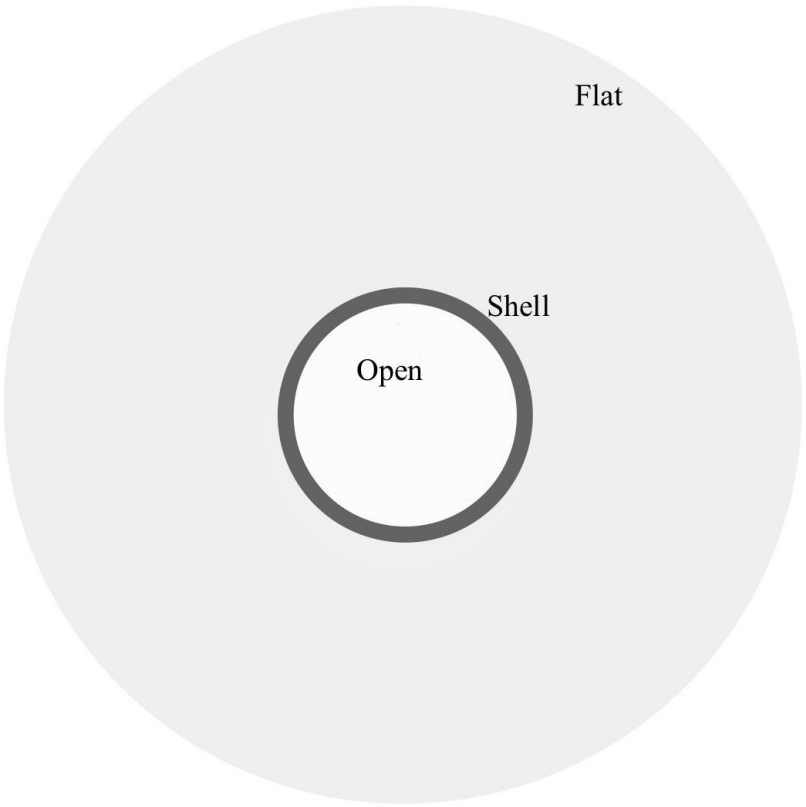

Figure 3.1: The centre (white) region is underdense, the outermost (light grey) region is flat space surrounding the underdense region. Between these two regions (dark grey) is a shell of overdensity, that forms as the void evolves.

the Schrödinger-Poisson formalism, introduced in [4]. The case presented in this Chapter compliments the previously explained spherical collapse, see Section 2.2.1 and [62].

3.1 Analytic model of an isolated void

Figure 3.1 shows a simple isolated void. Similarly to [62] the outermost region depicted in Figure 3.1 is flat space, simply the "rest of the universe" surrounding the innermost underdense region, the void. The underdense space is modelled by an open universe, expanding. When the underdensity expands, it pushes into the flat space surrounding it, resulting in a shell of overdense space encasing the void.

3.1.1 Spatially flat universe

For the following we assume a flat universe (with $\kappa = 0$). We begin here by taking the well known cosmological result for the evolution of the density field under a globally defined cosmic time, t, given by

$$\rho(t) \equiv |\psi|^2 = \frac{\Lambda c^2}{8\pi G}\text{cosech}^2\Big(\frac{3}{2}\sqrt{\frac{\Lambda c^2}{3}}t\Big). \tag{3.1}$$

Under spherical symmetry the Laplacian operator is simply

$$\nabla^2 \equiv \frac{\partial^2}{\partial r^2} + \frac{2}{r}\frac{\partial}{\partial r},$$

where r here is now the radial variable $r = |x|$. This density evolution obtained previously can be substituted into Equation (2.5) to obtain an equation for the gravitational potential V. This allows the calculation of ϕ by substitution into Equation (2.3), resulting in the wave-function ψ, as shown in [62]:

$$V = \frac{\Lambda c^2}{12}(\coth^2(\lambda t) - 3)r^2, \tag{3.2}$$

and

$$\psi = \sqrt{\frac{\Lambda c^2}{8\pi G}}\text{cosech}\,(\lambda t)\exp\Big(\frac{i}{v}\sqrt{\frac{\Lambda c^2}{12}}\coth\left[\lambda t\right]r^2\Big), \tag{3.3}$$

where $\lambda \equiv \frac{3}{2}\sqrt{\Lambda c^2/3}$. We therefore also find

$$\phi = \sqrt{\frac{\Lambda c^2}{12}}\coth(\lambda t)r^2. \tag{3.4}$$

Also following [62], a series expansion of $\rho = \alpha^2$ and ϕ/r^2 about $\Lambda = 0$ provides the well known results of $\rho \propto t^2$ and $V = r^2/9t^2$ for this particular case.

3.1.2 Open Universe

Working in a similar way to Section 3.1.1, we find solutions for a universe with negative curvature, $\kappa = -1$, an open universe, to be

$$\rho = \frac{\gamma}{A^3(\cosh(\eta) - 1)^3}, \tag{3.5}$$

$$V = \left\{ \frac{G\pi\gamma}{12A^3 \left[\sinh\left(\frac{\eta}{2}\right)\right]^3} \right\} r^2, \tag{3.6}$$

and

$$\psi = \frac{C}{\sqrt{2A}\left[\sinh\left(\frac{\eta}{2}\right)\right]^3} \exp\left[\frac{i}{v} C \coth\left(\frac{\eta}{2}\right) \operatorname{cosech}\left(\frac{\eta}{2}\right) r^2\right], \tag{3.7}$$

where $A \equiv 4\pi G\rho_0/3$, $C = \gamma^{1/2}/4A$, $\mu = 3M/4\pi$ and γ is a constant. For a simpler derivation we have converted to conformal time by using $ad\eta = dt$ where a is the scale factor of the open universe.

Having established this simple solution we can now proceed to study the dynamics of a void, taking into account the fact that the density surrounding the void will not remain homogeneous as the interior expands.

Using the solutions described in both Sections 3.1.1 and 3.1.2 above, we aim to construct an analytical model of an isolated void in one-dimension. We construct the model of the void with an inner region and an outer fluid separated by a shell. The inner fluid is modeled by the open universe solutions and the outer fluid is modeled by the flat universe solutions. Both fluids are evolved completely

independently and the overall behaviour inferred from there. Both fluids are homogeneous but the fluid in the inner region is less dense than the outer fluid so we expect it to expand quicker, pushing into the surrounding medium and evacuating the void.

Using the cosmological solutions shown above, and following the same procedure as [62], we compute an expression for the expansion of the radii of both sections of the void, in conformal time η. We have R_o for the open-universe section of the void and R_f for flat universe section of the void.

$$R_o = \mu^{1/3} \frac{2A}{\gamma^{1/3}} (\sinh^2(\eta/2)), \tag{3.8}$$

$$R_f = B \left(\sinh(\eta) - \eta\right)^{2/3}, \tag{3.9}$$

where B is a free parameter corresponding to the inital conformal time η_0 when the configuration is set up, at which point $R_o = R_f$. The evolution is illustrated by Figure 3.2 which shows the evolution of each of these radii with respect to conformal time with an arbitrary scaling on the vertical axis just to show that the inner region of the void expands much quicker than the outer region, and an overlapping region develops after some time as the inner void expands into a region that was previously in the space exterior to the void.

It is clear that this is not enough to truly model the behaviour of Schrödinger fluids around a void, since this system cannot be solved exactly in this case. Therefore, the system requires numerical methods to get a solution.

3.2 The Zel'dovich void

To best be able to understand the evolution of voids within SP, it makes sense that we would compare how voids behave in this regime with how they behave

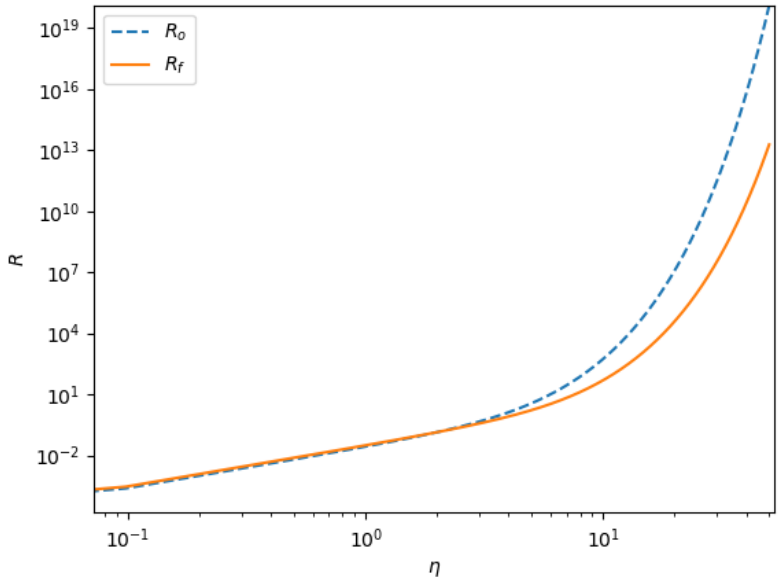

Figure 3.2: The evolution with respect to conformal time of the radius of an underdense region as modelled by an open universe (blue) and the radius of the flat space which occupies the region surrounding the underdensity (orange), plotted on a log scale.

in the popular and effective Zel'dovich approximation, for which full details were shown in Section 1.3.3.

Simplifying Equation (1.35), to one which describes a one-dimensional comoving density field,

$$\rho(q,t) = \frac{\rho_0}{1 - b(t)\frac{\partial s}{\partial q}}, \tag{3.10}$$

while continuing to use $b(t)$, as described by Equation (1.32), as our time coordinate for ZA.

Modelling void expansion with ZA is a challenge, since shell-crossing effectively occurs immediately. As the void begins to evacuate, the matter on the "edge" of the void pushes into the the rest of the matter that forms the "walls" of the void. This creates a little bump on the edge of the void. This bump at-

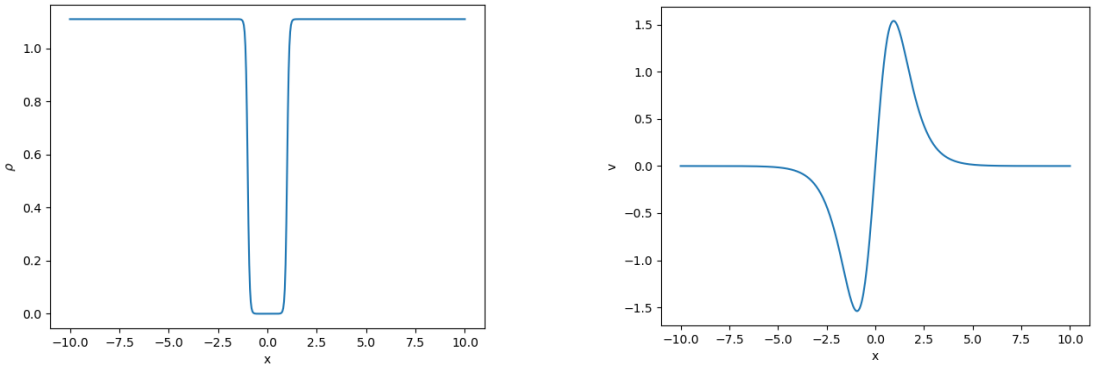

Figure 3.3: Initial compensated void (left), initial velocity potential (right).

tracts a small amount to matter to it, thus creating a multistreaming region at the edge of the void as it expands. As we know, multistreaming regions are not handled well by the Zel'dovich approximation, and this model of the void breaks down.

Figure 3.3 shows ideal initial conditions for a compensated void density field and velocity potential. A compensated void is such that the mean density is set to be 1. To get this shape we used a smoothed tanh function. See Spencer and Coles [67] for motivation on this chosen velocity potential. We are using periodic boundary conditions, with the void placed significantly far away from the boundary so that we have an effective boundary-at-infinity, to truly have an isolated void.

Figure 3.4 shows three different timesteps of evolution of these intial conditions by ZA. It is clear that ZA is only valid for very early time-steps. It models the forming of the "shell" very well, but fails to capture the expansion of the void, as once shell-crossing occurs it form these two peaks at the "edge" of the void where the multistreaming region exists.

3.3 The "free-particle" void

Using the same initial conditions as for ZA (Figure 3.3), we wish to compare its evolution as a collection of free particles as described in Section 2.2 to the

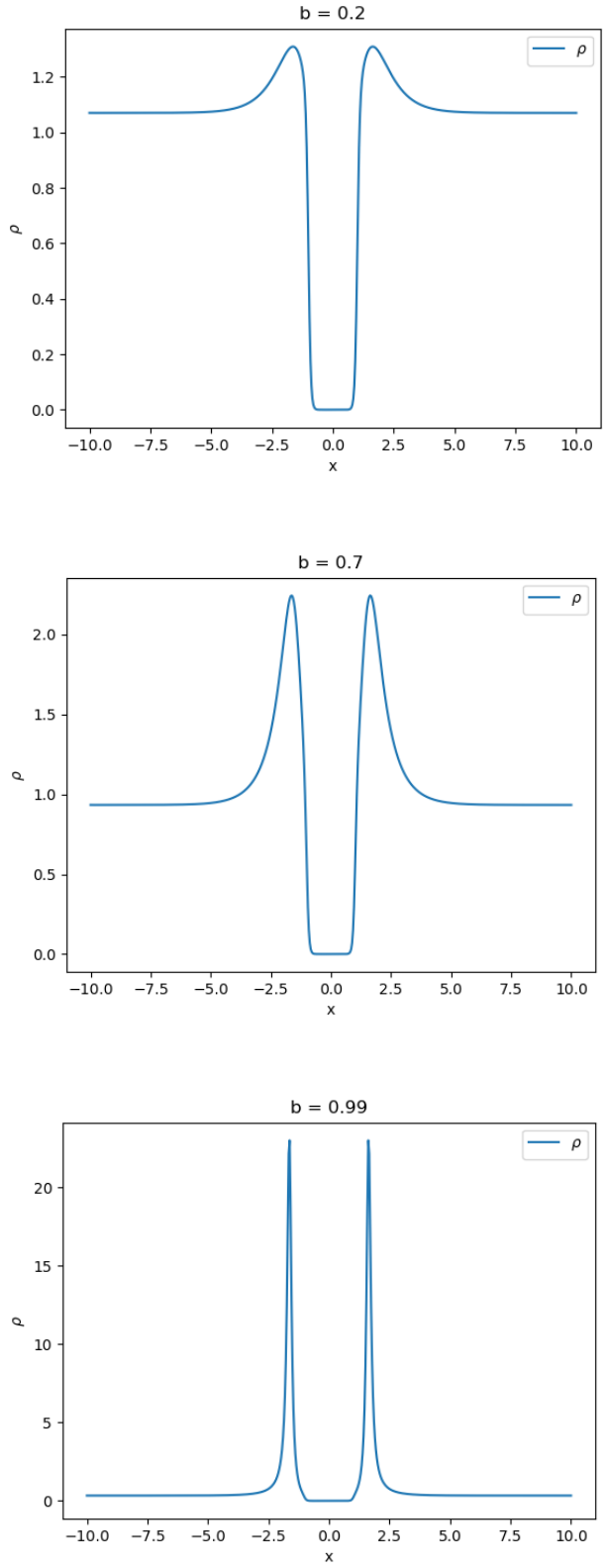

Figure 3.4: Three time-steps of the evolution of a void under the Zel'dovich approximation.

Zel'dovich void. Figure 3.5 shows three time-steps of void evolution in both regimes. The top plot shows that the free partilce void and ZA agree for early time-steps. However, the centre plot shows both regimes diverging. Both regimes form peaks at the edge of the void, creating the necessary conditions to form multistreaming region in these peaks. Figure 3.4 showed the Zel'dovich void breaking down and failing to effectively model the behaviour expected after shell-crossing. The bottom plot of Figure 3.5 shows that once the interference effects from the wave-mechanical approximation kick in, the evolution is not hindered by the existance of shell-crossing, and we can effectively model the void expansion. These interference effects are an important part of SP dynamics, and occur in the multistreaming region, see [52, 67] for further details. This is contrasting to the collapse model, in collapse we find shell crossing inside the collapsed object, however in the void case shell-crossing occurs outside of the void. This provokes the idea that the model of the void in this case could be thought of as more accurate as the inner void is unaffected by shell-crossing complications.

We also remark that a field level model is better suited to modelling voids as opposed to a particle model. Uniform resolution is a key feature of field models, they permit more accurate modeling of the empty regions, compared to particle models where the resolution is best where there are particles and we effectively have no resolution in void regions.

We can conclude that even the most basic of wave-mechanical approximations (free-particle) is more effective at modelling a one-dimensional isolated void. But why stop there? SP has more complexity and when used to its full potential, could further improve its ability to model such objects. In the next section, we compare the inclusion of the P, the quantum pressure term, and re-coupling Equations (2.7) and (2.8).

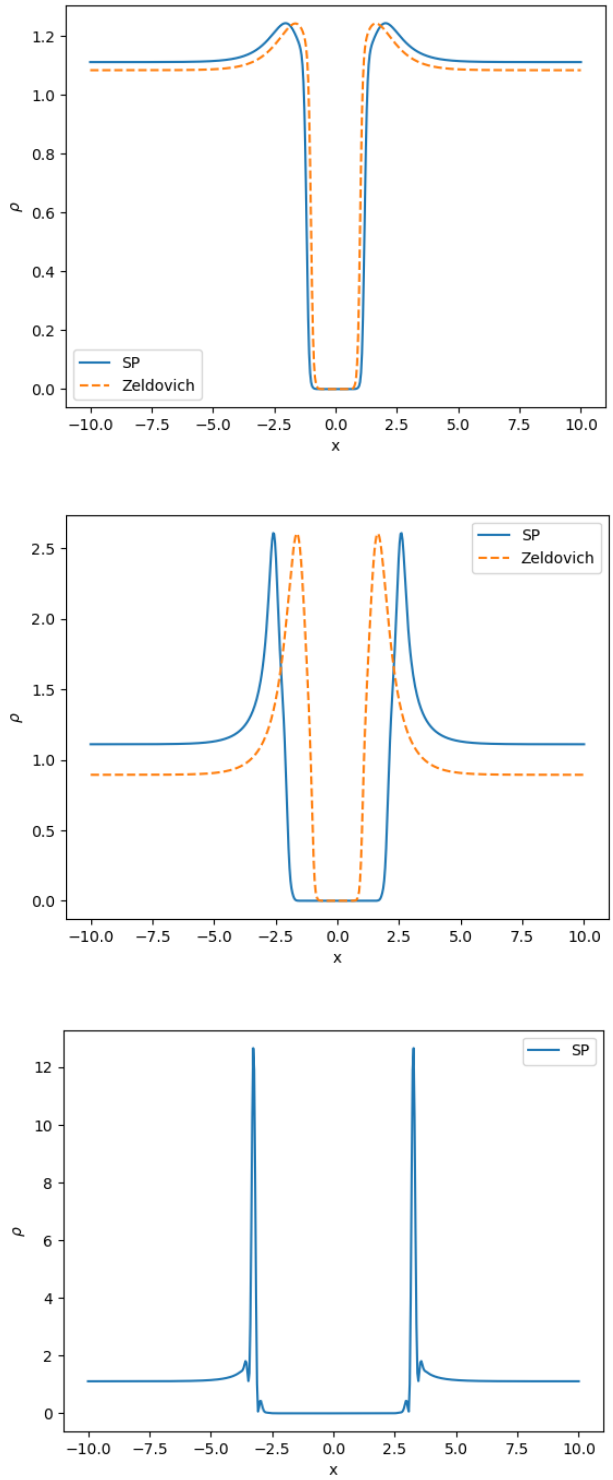

Figure 3.5: Three stages of evolution of the free particle void (blue, solid) with the Zel'dovich void layered over it (orange, dashed), where possible. The first plot is an early timestep. The second is an intermediate timestep before shell-crossing. The third plot is after shell-crossing.

3.4 Including Other terms

The free particle approximation works well, as shown in Sections 2.2 and 3.3. The free particle approximation, models the behaviour of the void and collapse quite accurately for simple models, however, it is important to note that while using this approximation we are neglecting terms that could improve our result and understanding of these systems. In this section, I will show results similar to that of the previous section, but including either the potential, the pressure or both.

3.4.1 Potential

It is important to detail the difficulties of implementing the inclusion of a potential term. Including the potential term, turns the problem from a PDE problem to a coupled PDE problem, which is exponentially more difficult.

We can circumvent the complexity of the coupled PDE problem by calculating the gravitational potential of the intial condition and including a constant gravitational potential, V_0 instead of solving the coupled PDE problem. This method has the benefits of the free particle approximation's ease and speed on a computational front, but still encapsulates some of the additional dynamics of including a potential. The second derivative nature of the potential ensures that it is changing very slowly compared to that of the density field, leading us to believe that including only V_0 will still add significantly to our model.

Figure 3.6 shows that early on in the evolution of the void (top) in this regime we deviate from the free particle approximation. In both earlier timesteps (top, center) shown here in Figure 3.6 we see that the free particle approximation, when compared to the inclusion of the potential, shows traits more like that of the ZA (see Figure 3.4), the sharp peaks at the edge of the void, and the slower void expansion. It is only in late times (bottom) that we begin to see a differentiation

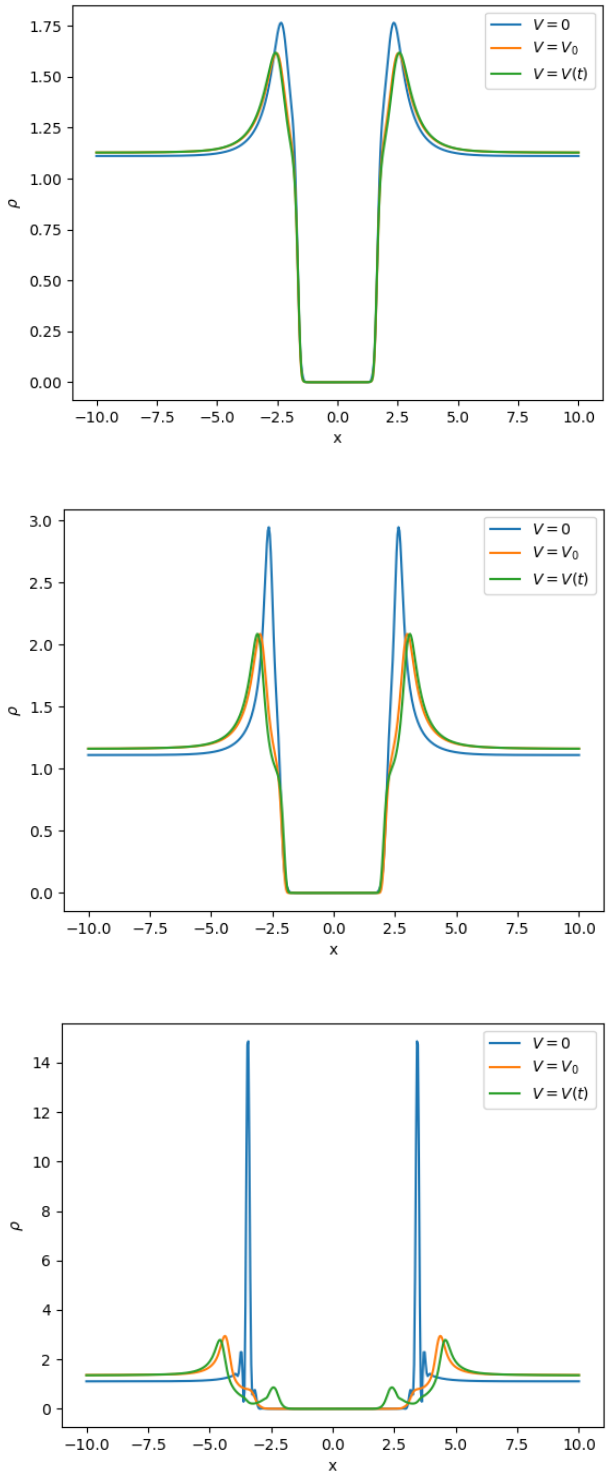

Figure 3.6: Comparison for how the gravitational potential affects the evolution of the SP void when included in 3 different ways. $V = 0$ (blue), $V = V_0$ (orange), $V = V(t)$ (green). The three plots are taken at the same timesteps as the three plots in Figure 3.5

between the method used for including the potential. Including only the intial potential V_0 (orange) empties out the void, and is showing to expand slightly slower than that of the time-dependent potential (green). The time-dependent potential is not completely evacuating the void, and is forming some (small) structure, within the empty region of the void. This is the most realistic picture of the void out of the three. The gravitational potential accelerates the expansion of the void, as expected. Even in this simple model, we see that the void is not totally evacuated with the inclusion of a time-dependent potential, more similar to what we observe in our universe today.

We also conclude that the inclusion of an intial potential is a very attractive method moving forward, as it is as computationally intensive as the free particle approximation, but shows behaviours much more similar to that of the time-dependent potential.

Not considered here, however, it could be worthwile including V (or P, or both) in a similar way to the Zel'dovich-Bernoulli method, detailed later in Chapter 5. To save time on computation, but to limit loss of accuracy, V would be calcuated and updated at a convenient interval of timesteps (e.g. every 50 timesteps).

3.4.2 Quantum Pressure

Inclduing the quantum pressure term P, dissassociates this model from FDM, and is now a wave-mechanical approximation for CDM. The second derivative nature of P as described by Equation (2.4), means that P changes very slowly compared to ρ, so we expect this to have little effect on the evolution of the void. Figure 3.7 shows the evolution of the SP void (left), with P included (orange) and $P = 0$ (blue). Figure 3.7 also shows the isolated quantum pressure (right) at these same timesteps. It is clear from Figure 3.7 that including P has little to no affect on the evolution of the void.

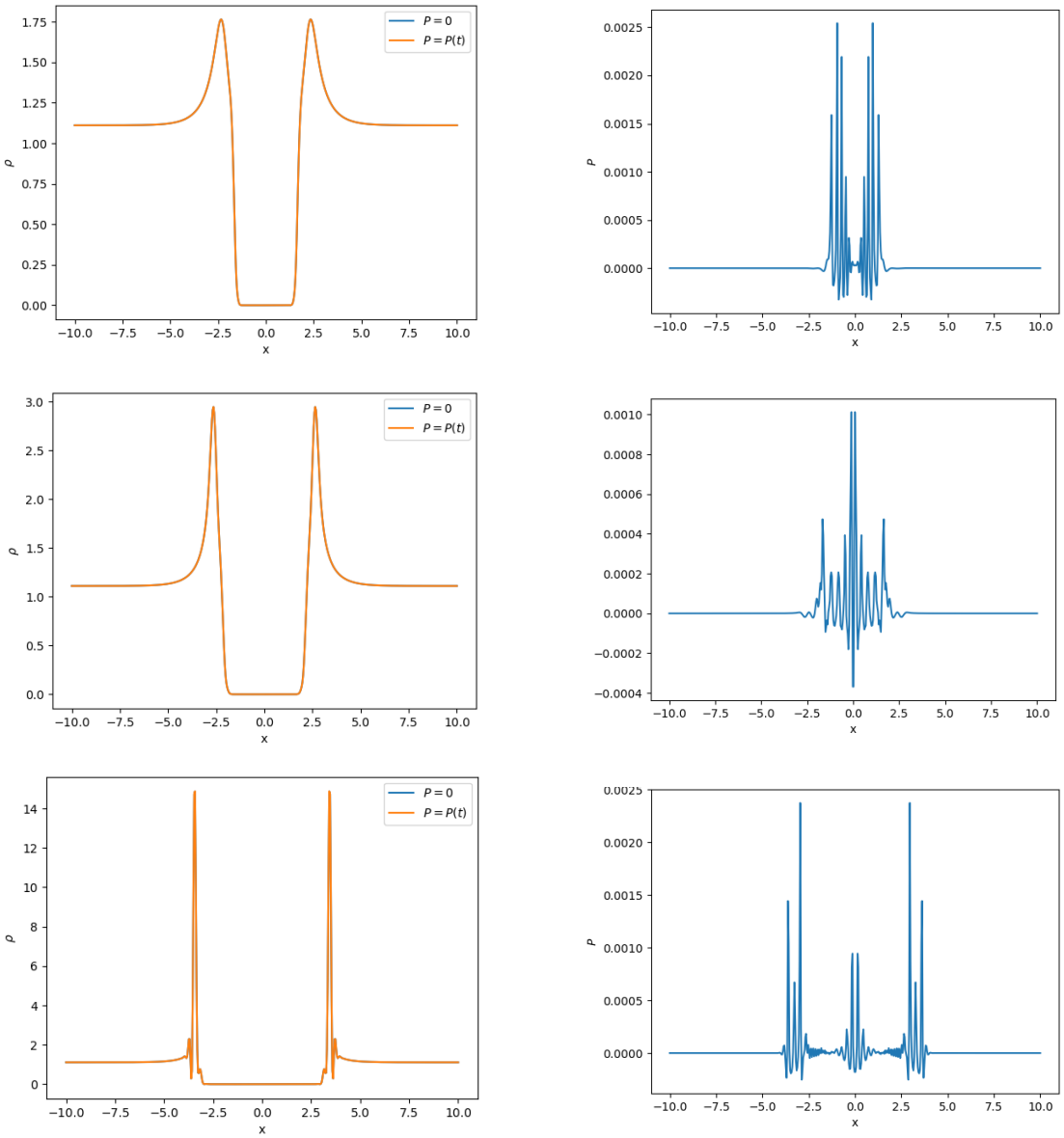

Figure 3.7: Comparison of including the quantum pressure term (left column) in the evolution of the SP void, where the timesteps shown are the same as Figure 3.5. The isolated quantum pressure term for the SP void (right column), at the same timesteps as the left.

The scale on the right column plots shows how small the contributions from P are to the evolution, as well as most of the contribution from P being on the empty regions of the void, with some action happening right at the edge of the void, but still very negligible. We can therefore conclude that one can safely neglect quantum pressure when considering the evolution of isolated voids.

The question of its impact on other aspects of this model are still undetermined. Considering P as a pressure, can further link this model with its ancestors in fluid dynamics. We can also extend the fluid dynamical analogy by considering ν in Equation (2.3) as a viscosity, considering that ν is expressed in units of kinematic viscosity. These ideas are explored more in Chapter 4.

Chapter 4

Analogies with Fluid Dynamics

We follow on from the analysis in Chapter 3 on the quantum pressure by considering it more seriously as a pressure in the fluid analogy of this model. We discuss to which extent a quantum pressure can indeed be interpreted as a pressure in the fluid analogy. Pressure in fluids is typically split into two catgeories, hydrostatic and dynamic pressure. Hydrostatic pressure refers to the pressure of a fluid that is not moving; dynamic pressure refers to pressure of a moving fluid in a closed body of fluid. Considering cosmological fluids are not in a closed container but are definitely moving, they fall under hydrostatic in this case, similarly to that of the ocean being a hydrostatic fluid, where the pressure changes due to the motion of the fluid are negligible. Pressure within fluids can be calculated in many situations by the Bernoulli Equation (2.2). However, this equation required the fluid be an ideal fluid, requiring the fluid have zero viscosity.

It has been previously remarked that the coefficient ν, from the Madeulung Transformation, has the same dimensions as kinematic viscosity; see, for example Short and Coles [66, 81] for a discussion. This is particularaly interesting in the context of the so called adhesion approximation [82], an extension of the Zel'dovich approximation achieved by introducting an effective viscosity term to make particles "stick" at shell-crossing. An extension of this model is presented

by Jones [83] and analysed from a wave-mechanical perspective in [62].

Assuming a potential flow, the velocity field $\boldsymbol{v}$ can be expressed as $\boldsymbol{\nabla}\phi$, the adhesion approximation reduces to the following equation for ϕ:

$$\frac{\partial\phi}{\partial\tau} - \frac{1}{2}|\boldsymbol{\nabla}\phi|^2 + \mu\nabla^2\phi = 0, \tag{4.1}$$

where μ is the (constant) viscosity. It is shown in [66] that the same in the wave-mechanical representation has the following form,

$$\frac{\partial\phi}{\partial\tau} - \frac{1}{2}|\boldsymbol{\nabla}\phi|^2 + P = 0, \tag{4.2}$$

where P is the quantum pressure as described in Equation (2.4). There is an important role played by ν in the dynamics of this system, just as μ does in the former case. Further connections between the adhesion model and SP approach are explored in [84].

The question thus arises, to which extent can we treat ν as a descriptor of vsicosity in a quantum system. The viscosity of a fluid is its ability to resist change in shape. It quantifies the internal friction of the fluid; see Stokes [85]. It is a common train of thought that viscosity refers to a "stickiness" of a fluid. More viscous fluids stick to themselves more than inviscid fluids.

Viscous fluids are often associated with vorticity, and our representation requires a potential flow, for which the vorticity is zero by definition. On the other hand, there is a sizable liturature [86] on the subject of potential flows in viscous fluids, so we feel it is worth taking this discussion further, though we are limited in what we can expanding the description of velocity fields beyond the current simple form. An example of an application of this general approach to a fluid with viscosity is given in [59].

4.1 Viscosity and the Navier-Stokes Equations

The full form of the Navier-Stokes equation takes the following form,

$$\frac{\partial \boldsymbol{v}}{\partial t} + (\boldsymbol{v} \cdot \boldsymbol{\nabla})\boldsymbol{v} + \frac{\boldsymbol{\nabla} P}{\rho} - \frac{\boldsymbol{\nabla} \cdot \sigma}{\rho} = \mathbf{0}, \tag{4.3}$$

where σ is the viscous stress tensor,

$$\sigma_{ij} = \eta\left(\frac{\partial v_i}{\partial x_j} + \frac{\partial v_j}{\partial x_i} - \frac{2}{3}\delta_{ij}\frac{\partial v_k}{\partial x_k}\right) + \zeta\delta_{ij}\frac{\partial v_k}{\partial x_k}, \tag{4.4}$$

in which ζ is the bulk viscosity, η is the shear viscosity and v_i are components of the velocity field $\boldsymbol{v}$, and we use Einstein's summation convention to sum over k here.

The first point to be made is that there is little point in talking about fluid analogies wihtout including a full classical description. We define the *material derivative* for velocities in a fluid to be

$$\frac{D}{Dt} = \frac{\partial}{\partial t} + \boldsymbol{v} \cdot \boldsymbol{\nabla}, \tag{4.5}$$

and we can rewrite the Navier-Stokes equation using the material derivative,

$$\rho\frac{D\boldsymbol{v}}{Dt} = -\boldsymbol{\nabla} P + \boldsymbol{\nabla} \cdot \boldsymbol{\sigma}. \tag{4.6}$$

We also need to include a description of heat transfer, including viscous dissipation, and associated as entropy production, which requires the introduction of a temperature T and entropy s, as well as thermal conductivity κ. The general

form being

$$\rho T \frac{Ds}{Dt} = \boldsymbol{\nabla} \cdot \kappa \boldsymbol{\nabla} T + \frac{\eta}{2} \left(\frac{\partial v_i}{\partial x_j} + \frac{\partial v_j}{\partial x_i} - \frac{2}{3} \delta_{ij} \boldsymbol{\nabla} \cdot \boldsymbol{v} \right)^2 + \zeta \big(bm \nabla \cdot \boldsymbol{v} \big)^2, \tag{4.7}$$

in which $\boldsymbol{\nabla} \cdot \kappa \boldsymbol{\nabla} T$ represents thermal conductivity, and the other two terms describe viscous dissipation. To construct a full fluid analogy would therefore involve complexities beyond the scope of this work. However, we can attempt to extract a better description by starting with the Schrödinger equation and working towards the fluid analogy. We are guided by Fernández de Córdoba et al. [87] to whom we refer the reader for further comments.

Consider the Schrödinger equation for a particle of mass m in a time-independent potential $V(\boldsymbol{x})$,

$$i\hbar \frac{\partial \psi}{\partial t} + \frac{\hbar^2}{2m} \nabla^2 \psi - V\psi = 0, \tag{4.8}$$

for which we can make the Madelung transformation in the following form

$$\psi = \psi_0 e^{S + i\phi} = \psi_0 N e^{i\phi}, \tag{4.9}$$

where ψ_0 is a normalisation constant. It can be included in N, but it is useful to keep separate for the description of the Boltzmann entropy, assumed to only depend on density,

$$\mathcal{S} = k_B \ln \left(\left| \frac{\psi}{\psi_0} \right|^2 \right), \tag{4.10}$$

which is related to S.

We choose to define density $\rho = m|\psi|^2$.

There is a natural length scale, $\lambda = |\psi_0|^{2/3}$, that arises due to the normalisation of ψ. This leads to

$$\rho = \frac{m}{\lambda^3} e^{2S} = \frac{m}{\lambda^3} N^2. \tag{4.11}$$

Thus, we now have two equations as a result of the Madelung transformation,

$$\frac{\partial S}{\partial t} + \frac{\hbar}{m} \boldsymbol{\nabla} \cdot \boldsymbol{\nabla} \phi + \frac{\hbar^2}{2m} \nabla^2 \phi = 0, \tag{4.12}$$

and

$$\hbar \frac{\partial \phi}{\partial t} + \frac{\hbar}{2m} (\nabla \phi)^2 + V + U = 0, \tag{4.13}$$

where,

$$U = -\frac{\hbar^2}{2m} \frac{\nabla^2 N}{N} = -\frac{\hbar^2}{2m} [(\nabla S)^2 + \nabla^2 S], \tag{4.14}$$

which we will name the quantum potential. In the general case, V, could be an external potential, or as we have used it in this thesis, the gravitational potential. Taking the gradient of Equation (4.13), and defining the velocity field $\boldsymbol{v} = \hbar/m \boldsymbol{\nabla} \phi$, we get

$$\frac{\partial \boldsymbol{v}}{\partial t} + (\boldsymbol{v} \cdot \boldsymbol{\nabla}) \boldsymbol{v} + \frac{1}{m} \boldsymbol{\nabla} (U + V) = \mathbf{0}. \tag{4.15}$$

It is argued in [87] that in order to make Equation (4.15) compatible with a

pressureless Navier-Stokes equation,

$$\frac{D\boldsymbol{v}}{Dt} = \frac{4\eta}{3\rho}\nabla^2\boldsymbol{v} = \mathbf{0}, \tag{4.16}$$

here, we also combine bulk and shear viscosity to one term, $\eta \to \zeta + 4\eta/3$, it is necessary to impose two separate conditions. First,

$$\frac{\boldsymbol{\nabla}P}{\rho} = \frac{\boldsymbol{\nabla}V}{m}, \tag{4.17}$$

which is tantamount to the assumption that we are dealing with hydrostatic pressure, and also means that if $V = 0$, we must have $P = 0$, for consistency. Second, we must identify the term in U with the viscosity, i.e.

$$\frac{1}{m}\boldsymbol{\nabla}U = -\frac{\eta}{\rho}\nabla^2\boldsymbol{v}. \tag{4.18}$$

These conditions imply that the gradient of the quantum potential must exactly balance the viscosity term in the equations of motion. Internal frictional forces arising in a system described by these equations are therefore inherently wave-like in nature. Equation (4.18) yeilds

$$\frac{\eta}{\rho}\nabla^2\boldsymbol{v} = -\frac{1}{m}\boldsymbol{\nabla}U = -\frac{1}{m}\boldsymbol{\nabla}\left(\frac{-\hbar^2}{2m}\frac{\nabla^2 N}{N}\right), \tag{4.19}$$

Thus, the viscosity term is in general spatially dependent and very complicated, but of order $\hbar$, which is the salient point. If we want to describe this system using the Navier-Stokes equations (which have constant η) we have to take the

classical limit $\hbar \to 0$ and that spatial variations of ψ are small. This, in turn, means that $\nabla^2\phi \simeq 0$, which is easy to show and requires that the fluid be almost incompressible, and the flow be almost isentropic (negligible entropy production).

One could go further by analysing the behaviour found in the one-dimensional calculations presented in Chapter 2. We can then replace the partial derivatives by ordinary derivatives, and reduce $\boldsymbol{v}$ to one spatial dimension v and write

$$\eta(x) = \rho(x)\frac{A(x)}{B(x)}, \tag{4.20}$$

where,

$$\rho(x) = \frac{m}{\lambda}N^2, \tag{4.21}$$

$$A(x) = -\frac{\hbar^2}{2m^2}\frac{d}{dx}\left(\frac{1}{N}\frac{d^2N}{dx^2}\right) = -\frac{\hbar^2}{2m^2}\frac{d}{dx}\left[\left(\frac{dS}{dx}\right)^2 + \frac{d^2S}{dx^2}\right] \tag{4.22}$$

and

$$B(x) = \frac{d^2v}{dx^2} = \frac{d^2}{dx^2}\left(\frac{\hbar}{m}\frac{d\phi}{dx}\right) = \frac{\hbar}{m}\frac{d^3\phi}{dx^3}. \tag{4.23}$$

We can immediately see that this definition of η is of order $\hbar$. Therefore, for a qualitative understanding, we need not include factors of λ, m or $\hbar$. We only need

$$|\eta(x)| \propto \frac{N^2\frac{d}{dx}\left(\frac{1}{N}\frac{d^2N}{dx^2}\right)}{\frac{d^3\phi}{dx^3}} = \frac{N\frac{d^3N}{dx^3} - \frac{d^2N}{dx^2}\frac{dN}{dx}}{\frac{d^3\phi}{dx^3}}. \tag{4.24}$$

Assuming a given form of $N(x)$ and $\phi(x)$ would straighforwardly given an effective value behaviour of $\eta(x)$ for a given configuration, if one were interested in doing

so.

Therefore we cannot find similar system of equations to the SP system defined in Chapter 2 in the full Navier-Stokes viscous regime. The system found in this section is only consistent in the $\hbar \to 0$ limit, in which case $\eta \to \infty$. This case is not irrelevant, it is, for example, the limit taken in analytic treatments of the adhesion model.

4.2 Wave Propagation in Viscous Fluids

When considering the validity of a viscosity in these wave mechanical cosmic fluids, it makes sense to consider propagation of waves within such fluid. The internal friction as a consequence of having a viscosity, causes dissipation of energy and dampens waves as they travel through the fluid. This results in attenuation of amplitude over distance, often known as the attenuation of sound.

To determine an attenuation of sound for cosmic fluids we begin with conservation of both mass and momentum. Conservation of mass is given by the *Continuity Equation*,

$$\frac{\partial \rho}{\partial t} + \nabla \cdot (\rho \boldsymbol{v}) = 0, \tag{4.25}$$

and conservation of momentum is given by,

$$\rho \frac{D\boldsymbol{v}}{Dt} + \nabla P = \frac{4\mu}{3} \nabla^2 \boldsymbol{v}. \tag{4.26}$$

The *dynamic viscosity* is included in Equation (4.26) as μ. Dynamic viscosity relates to kinematic viscosity by $\mu = \nu\rho$. We use ν here instead of η (as in Equations (4.3) and (4.4)) to consider ν as it appears in the SP system as the

kinematic viscosity for this analysis.

For fluids, the equation of state relates pressure, density and entropy, by expressing pressure as a function of density and entropy. For cosmic fluids we have the pressure as a function of density in the form of the quantum pressure,

$$P = \frac{\nu^2}{2}\frac{\nabla^2(\sqrt{\rho})}{\sqrt{\rho}}. \tag{4.27}$$

To move forward with this as our equation of state, we will use the more convenient form

$$P = \nu^2\left(\frac{\nabla^2\rho}{2\rho} - \left(\frac{\nabla\rho}{2\rho}\right)^2\right) \tag{4.28}$$

4.2.1 Small-signal approximation for attenuation of sound

For convenience and brevity we will use notation where the subscript denotes derivative, for example,

$$\rho_t = \frac{\partial\rho}{\partial t}.$$

Sound waves typically disturb the fluid only around a small region, therefore, the quantities associated with sound, excess pressure, excess density and particle velocity can be assumed to be small and of first order. Assuming

$$|\delta\rho| \ll \rho_0, \tag{4.29}$$

where ρ_0 is the background density and does not depend on x and t. Now in one

dimension for simplicity, the continuity Equation (4.25) can be expanded to the following,

$$\delta\rho_t + v\delta\rho_x + v_x\rho_0 + v_x\delta\rho = 0. \tag{4.30}$$

It can be seen that this reduces to

$$\delta\rho_t + v_x\rho_0 = 0, \tag{4.31}$$

by keeping only first-order terms. Following the same procedure, we can see that equation Equation (4.26) becomes

$$\rho_0 v_t + P_x = \frac{4\nu}{3}\rho_0 v_{xx}, \tag{4.32}$$

and Equation (4.28) becomes

$$P = \frac{\nu^2}{4}\frac{\delta\rho_{xx}}{\rho_0 + \delta\rho}. \tag{4.33}$$

The small signal approximation is summarised by Equations (4.31-4.33). Combining these equations to find a final form of the viscous wave equation, from

Equation (4.32) we get,

$$\begin{aligned} \rho_0 v_x &= -\delta\rho_t, \\ \rho_0 v_{xx} &= -\delta\rho_{tx}, \\ \rho_0 v_{tx} &= -\delta\rho_{tt}, \\ \rho_0 v_{xxx} &= -\delta\rho_{txx}, \end{aligned} \tag{4.34}$$

Differentiating Equation (4.32) with respect to x and use identities found in Equation (4.34) to get,

$$-\delta\rho_{tt} + P_{xx} = -\frac{4\nu}{3}\delta\rho_{txx} \tag{4.35}$$

Differentiating Equation (4.33) with respect to t and discarding any higher order terms we get,

$$P_t = \frac{\nu^2}{4}\frac{\delta\rho_{txx}}{\rho_0 + 2\delta\rho}. \tag{4.36}$$

Rearranging gives,

$$\delta\rho_{txx} = \frac{4}{\nu^2}\rho_0 P_t. \tag{4.37}$$

Substituting into Equation (4.35) gives,

$$-\delta\rho_{tt} + P_{xx} = -\frac{16}{3\nu}\rho_0 P_t. \tag{4.38}$$

Then, differentiating with respect to x twice gives,

$$-\delta\rho_{ttxx} + P_{xxxx} = -\frac{16}{3\nu}\rho_0 P_{txx} \tag{4.39}$$

Differentiating Equation (4.37) with respect to t,

$$\delta\rho_{ttxx} = \frac{4}{\nu^2}\rho_0 P_{tt}. \tag{4.40}$$

Combining Equations (4.39) and (4.40) to get the final form of the viscous wave equation

$$\frac{\nu^2}{4}P_{xxxx} - \rho_0 P_{tt} - \frac{4\nu}{3}\rho_0 P_{txx}. \tag{4.41}$$

To solve Equation (4.41) it is fair to assume a general wave solution and look for a particular solution. Assume,

$$P = P_0 e^{i(\omega t - kx)}. \tag{4.42}$$

We seek a dispersion relation ($k = k(\omega)$) of the form,

$$k = \beta - i\alpha, \tag{4.43}$$

where α will be the attenuation coefficient, and β will define the phase velocity $c = \omega/\beta$.

Solving Equation (4.41) with Equation (4.42) for $k(\omega)$ gives

$$k = \pm\frac{2\sqrt{\rho_0}\omega\sqrt{\frac{\nu^2}{4} + i\frac{4\nu}{3}\rho_0\omega}}{\sqrt{\frac{\nu^4}{16} + \frac{16\nu^2}{9}\rho_0^2\omega^2}}. \tag{4.44}$$

Clearly, this is a complicated expression from which α is not easily extracted. We

found that α takes the following form,

$$\alpha = \mp \frac{2\sqrt{\rho_0 \omega}}{\left(\frac{\nu^4}{16} + \frac{16\nu^2}{9}\rho_0^2\omega^2\right)^{1/4}} \sin\left(\arctan\left(\frac{4\rho_0\omega}{3\nu}\right)\right). \tag{4.45}$$

However complicated α may be, the key here is that it exists and can be found by specifying initial conditions. The existance of attenuation of sound waves in an FDM fluid could impact the way density perturbations evolve in the early universe. The damping of sound waves might suppress the formation of small-scales structures, contrary to the predictions of CDM.

4.3 Reynolds number

Now having an analogy to viscosity for SP fluids, we can also define a Reynolds number analogy for them, we first introduced this for SP fluids in my first paper [4]. We define the Reynolds number,

$$R = \frac{ul}{\nu}, \tag{4.46}$$

as introduced by Stokes [88], popularised by Reynolds [89], but named by Sommerfeld [90], where u is a velocity, l a length scale, and ν the viscosity. All three components are chosen to be reasonably associated with the motion. Although ν is now well defined, it is not clear how one would define the other two quantities. There are many velocity quantities present in this model and it is not exactly clear which one we should choose. There is a momentum associated with the wave-function, but this is not uniform in space and it is not clear how one could convert this to a single number.

There is also the issue of a length-scale associated with the motion. It may be obvious that we choose to use the size of the object we are studying, however, in dealing with both collapse and void expansion this length is constantly changing

(Also, this length is only unique in one-dimension, but we will stick to one-dimension for this work.)

For our work on this scaling in [4] we chose the initial size of the void to be the length. For the velocity, we measured an expansion speed for the void.

Expansion Speed

It can be seen in Figures 3.5 and 3.6 that the edges of the void move outwards as we increase the timestep. The peak created at the edge of the void serves as a positional marker for the edge of the void, so we measure the change in position of this peak over change in timestep. These peaks are sharply defined, at least until the strong interference pattern develops after shell-crossing.

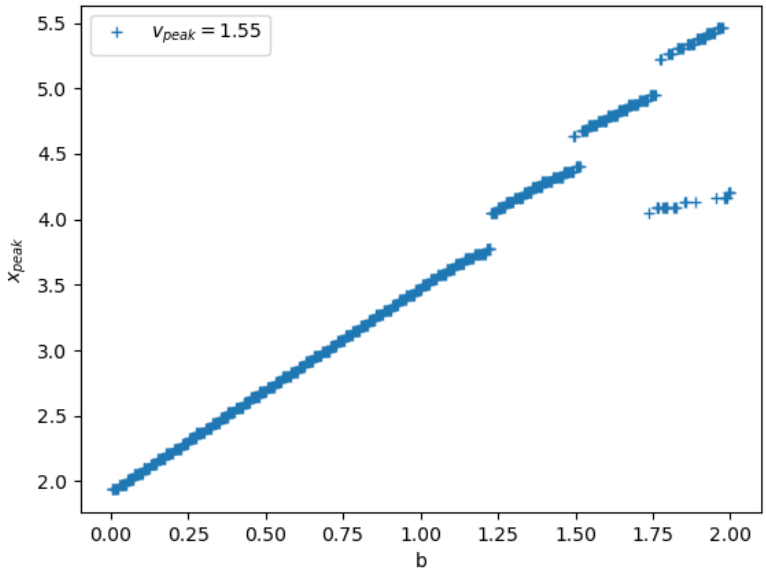

Figure 4.1: The position of the maximum value of the density field plotted against timestep. Maximum value of the density field taken to be the "edge" of the void.

Figure 4.1 shows the position of these peaks as a function of timestep. It is interesting to note, that Figure 4.1 shows an almost linear relationship between time and position with some jumps once the interference pattern starts to develop. This indicates a free expansion of the void region discussed by e.g. [74, 91]. At

very late times one expects a void embedded in a baryonic fluid to enter an adiabatic phase described by the Sedov solution for blast waves [92], but the physical behaviour of the quantum fluid described here would probably be quite different and in any case we only look at the initial phase of the expansion here.

With all of the parameters defined, not perfectly, but in a systematically consistent way for void expansion, we now must test the reliability of a pseudo-Reynolds number. Does this system behave in a way that a Reynolds number would even make sense?

To test the reliability of this pseudo-Reynolds number, we looked at the relationships between the quantities used to define it. Since u is the calculated value v_{peak}, we started by fixing l, and comparing various ν values with the v_{peak} produced by this. As seen in Figure 4.2 it is clear that ν and v_{peak} are proportional to one another.

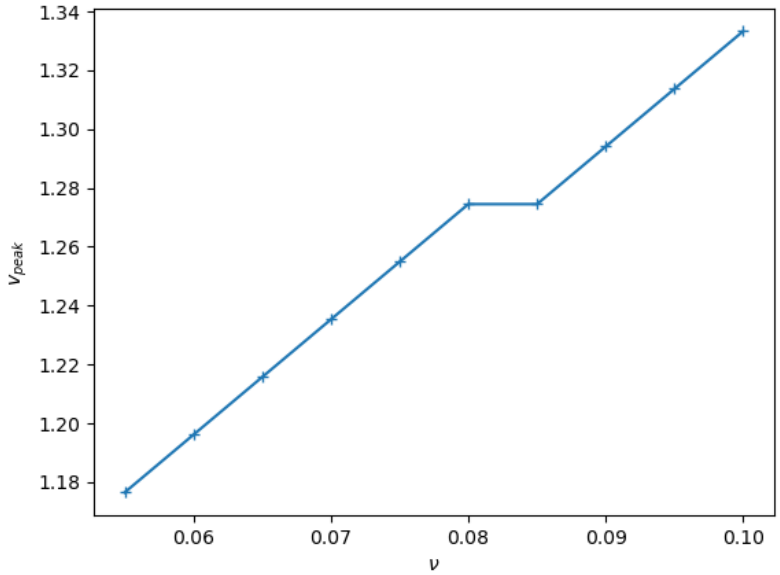

Figure 4.2: Peak velocity of a one dimensional SP void as measured in Figure 4.1, plotted against viscosity parameter ν

Then we fixed ν and calculated v_{peak} for various l values and as seen in Figure 4.3, it is clear that l and v_{peak} have an inversely proportional relationship.

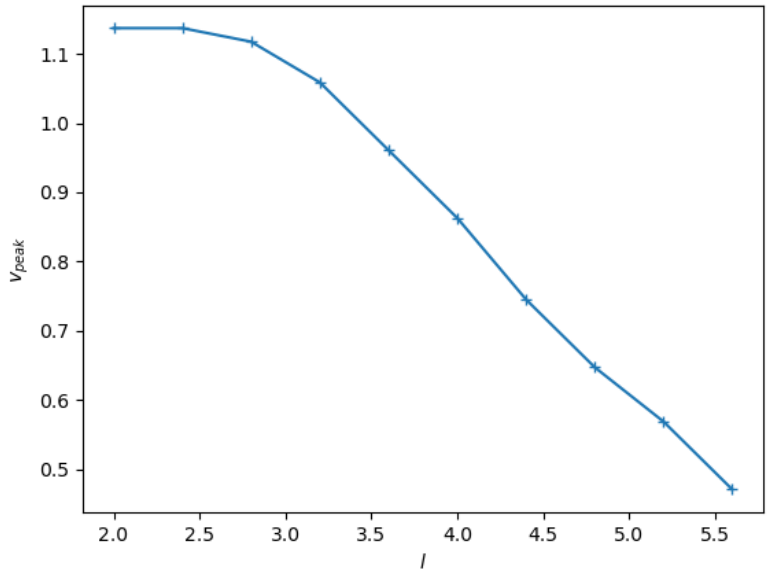

Figure 4.3: Peak velocity of a one dimensional SP void plotted against its length scale.

Due to the nature of how v_{peak} is calculated it is not possible to fix u and look at the relationship between ν and l, but this suffices for a quick illustration.

However, this definition of the Reynolds number is only valid for voids. We wish to define a Reynolds number which can be assigned to many different types of motion of cosmic fluids. Continuing to use the length scale to be the size of the object as our length-scale. This becomes more difficult in higher dimensions, but we will stick to one dimension.

The question of velocity for other types of motion in this regime is not so clear. In one-dimensional collapse, for example, we don't have an expansion speed, and it would be difficult to define a similar collapse speed. To overcome this we've opted to choose the peak positive velocity at the moment of shell-crossing. We find this by extracting the velocity field from the velocity potential at the moment of shell-crossing, at the location of the most positive peak. We believe this is a velocity which encapsulates the dynamics of the fluid at an important moment in the evolution.

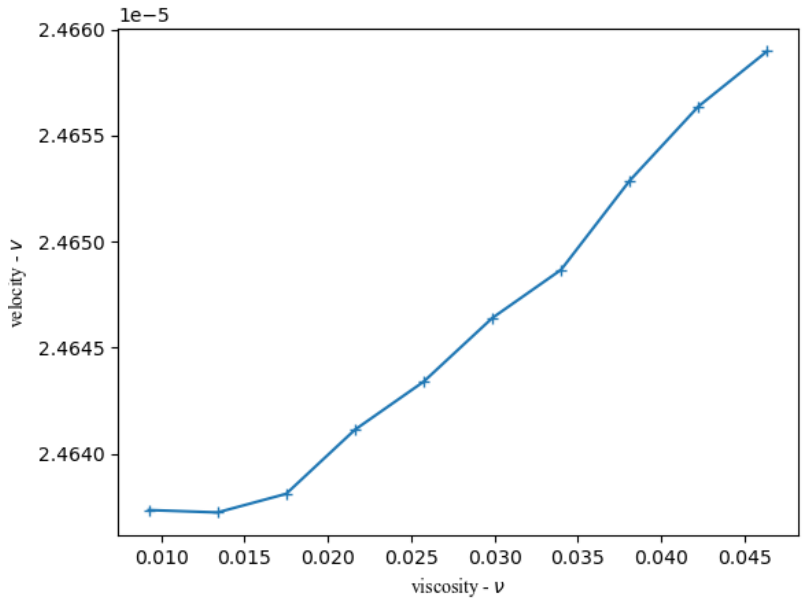

Figure 4.4: Positive peak velocity at shell-crossing measured for different values of viscosity for one-dimensional SP collapse.

Continuing with the importance of the moment at which shell-crossing occurs, we also choose our length to be the distance between peaks of the object at this time. Similarly, as for the void, we wish to see if it is reasonable to define a Reynolds number with these parameters for one-dimensional collapse.

Figure 4.4 shows the relationship between viscosity and velocity for one-dimensional collapse of a Schrödinger fluid. However small, we still see a positive linear relationship. Similarly, Figure 4.5 shows a positive linear relationship between viscosity and length. Each parameter has the appropriate relationship to deduce a Reynolds number can be calculated for these quantities, and a scaling solution exists.

With a Reynolds number defined for one-dimensional collapse and one-dimensional void expansion, this is a sufficient proof of concept for a reynolds number of cosmic fluids. For example, in our code units, we calculated the Reynolds number for the void evolution shown in Figure 3.5. This cosmic fluid has a viscosity $\nu = 0.05$, initial void size $l = 2.0$ and expansion speed $u = 1.55$. This results in a Reynolds

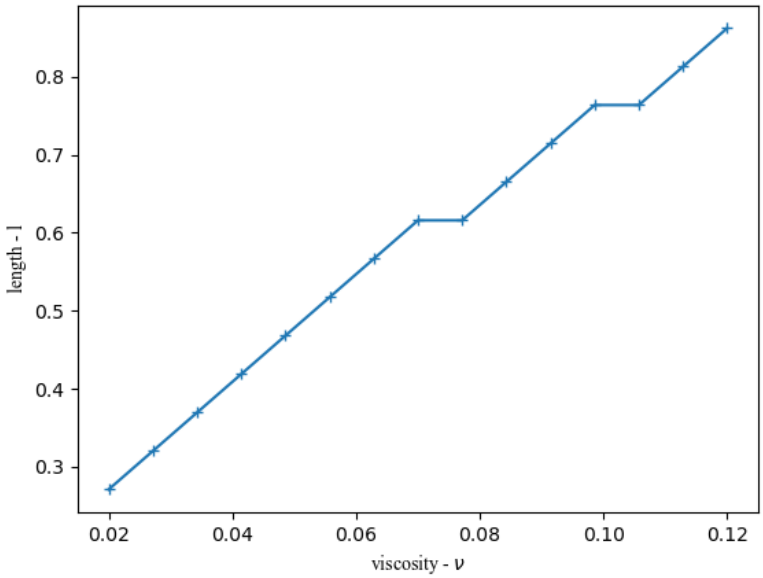

Figure 4.5: length at shell-crossing measured for different values of viscosity for one-dimensional collapse of an SP fluid.

number $R = 62.0$. This is equivalent to a void spanning 30Mpc, expanding with a speed of $27\text{km}s^{-1}$ and a viscosity of $\nu = 4 \times 10^{10}\text{km}^2s^{-1}$. Both the size and speed of this void are possible in the observable universe; for the viscosity of such more realistic cosmic fluids we turn to Gibson [93].

This thesis wishes to push the limitations of the SP formalism beyond its current state. Chapter 4, discusses the limitations of the fluid analogy by attempting a Navier-Stokes focussed version of the Madelung Transformation that initially gave us the SP system, analysing the implications of considering the quantum pressure as a pressure, and discussing the possibility of a scaling solution via the viscosity parameter and a psuedo-Reynolds number. In the next chapter, we wish to push this model in another way. Chapter 5 attempts a proof-of-concept reconstruction of initial condition density field maps of the early universe. We use the hard test of map reconstruction to test the validity of the SP approximation as a model for large-scale structure formation.

Chapter 5

Reconstruction

Recovering the initial density and velocity fields of the universe from present observations is one of the most important tasks in cosmology. These fields contain information about the physical processes which operated in the early universe. It is easy to follow the initial density and velocity fluctuations in the linear regime. However, the non-linear gravitational evolution at recent epochs makes this recovery more challenging, and we can no longer reproduce the initial conditions by analytical means exactly. A popular method for recovering the growing mode of the initial fluctuations of a cosmological gravitating system from the present large-scale density field is based on the Bernoulli Equation (2.2) for evolution of the velocity potential in the Zel'dovich approximation (Section 1.3.3), first proposed by Nusser & Dekel [94]. For a further discussion and good description of the Zel'dovich Bernoulli (ZB) method, see [95]. It is useful to have a full map reconstruction of both the density field and the velocity field. This is often referred to as field reconstruction or map reconstruction, of initial conditions. Galaxy surveys provide three-dimensional redshift-space maps of the large-scale structure of the universe that contain anisotropies along the line of sight due to redshift space distortions (RSD) [96] (stemming from gravitationally-induced peculiar velocities). Therefore, our observations are not independent of how we

observe them and it is incredibly important to reconstruct the map of the galaxy survey in real space.

The Alcock-Paczynski effect (AP) [97] (differential geometrical stretching along and transverse to the line of sight of the cosmological model used to translate redshifts to distances), makes it difficult to know if we are reconstructing the real space map correctly. The Baryon Acoustic Oscillation (BAO) peak provides a feature in the galaxy clustering power spectrum that is unaffected by RSD and therefore allows us check the accuracy of the cosmological model used to translate between real and redshift space. The power spectrum is best understood as the Fourier transform of the autocorrelation function of the density contrast. It describes how density fluctuations vary with scale, providing a statistical measure of structure formation.

There are various methods used to reconstruct in all meanings of the word in the field of cosmology. The most popular being the Zel'dovich Bernoulli (ZB) which is used to analyse large data sets for big collaborations; see [98–100]. Many people have turned the problem into an optimization problem, see; [101, 102]. And many have tasked this same optimisation problem to neural networks, for example [103].

In this chapter, I will discuss the implications of using the Schrödinger-Poisson model, as described in Section 2.1, as a possible method of recovering the initial conditions of the universe, namely the map reconstruction of the density and the velocity fields. In this section we will compare the robustness of SP reconstruction to that of ZB reconstruction and linear fluid approach (LFA).

Linearised Fluid Approach

The use of linear approximations to reconstruct the initial conditions of the universe stems from the early theoretical framework for understanding large-scale structure formation. This approach builds on the assumption that the universe

began with small initial density fluctuations, which grew over time due to gravitational instability. As seen in Section 1.3 linear perturbation theory is our first line of defence.

We saw in Section 1.3.2 that in the linear regime, we get evolution by means of a linear growth factor, as described by Equation (1.30). In this case, to reconstruct past maps we reverse the order of our time coordinate $D_{\text{rev}} = D(-t)$ and we evolve a "final state" backward by the same law,

$$\delta = D_{\text{rev}}\delta_f. \tag{5.1}$$

LFA is quite a simple approach and can only be used when density fluctuations are low, $|\delta| << 1$. They are also still quite effective in low density regions and on very large scales, where fluctuations remain low. Their computational simplicity often means they are the only means by which we can do reasonable analysis when resources are low. They also provide the basis for which more complicated models are built up from. The Zel'dovich-Bernoulli (ZB) method builds upon the LFA by incorperating the non-linear dynamics of the Zel'dovich approximation and a Bernoulli-like condition, enabling more accurate reconstruction in moderately non-linear regimes.

Zel'dovich-Bernoulli

As the name suggests, the Zel'dovich-Bernoulli (ZB) method uses a technique that combines the Zel'dovich Approximation (Section 1.3.3) for tracing the evolution of cosmic structure with a Bernoulli-like constraint (Equation (2.2)) to account for non-linear gravitational dynamics. It employs an iterative approach, re-calculating the velocity potential at regular intervals to recover the initial density field. This reasonably captures the non-linear gravitational effects while

remaining computationally efficient. For an insight into the capabilities of this model see White [104].

Time-reversal symmetry implies that reversing the direction of time also reverses the motion of the particles within the system. Since velocity is defined as $\frac{\partial \boldsymbol{x}}{\partial t}$, reversing time changes the sign of the time variable, thus inducing a change in sign of the velocity as well, $\boldsymbol{v} \to -\boldsymbol{v}$. In the ZA, the velocity field is responsible for generating the displacement vector (Section 1.3.3), therefore, to invoke the change of sign needed in the velocity field we reverse the sign of the eigenvalues of the deformation tensor, which yields a ZB reconstructed density field given by,

$$\rho_{rec}(\boldsymbol{q}, t) = \frac{\overline{\rho}}{[1 + b(t)\alpha(\boldsymbol{q})][1 + b(t)\beta(\boldsymbol{q})][1 + b(t)\gamma(\boldsymbol{q})]}. \tag{5.2}$$

The ZB method, while quite effective, has its limitations. Since ZB builds on ZA, it inherits its weaknesses such as its inability to handle multi-stream flows and difficulty with virialised structures. However, it is more accurate than the ZA because of the Bernoulli-like condition that updates and provides a situationally more accurate displacement field at appropriate intervals.

The Zel'dovich approximation, as described by Equation (1.31), can be written in the Eulerian formalism by using the convective derivative, that relates the Lagrangian regime to the Eulerian,

$$\frac{d}{dt} \equiv \frac{\partial}{\partial t}\Big|_{\boldsymbol{q}} = \frac{\partial}{\partial t}\Big|_{\boldsymbol{x}} + (\boldsymbol{v} \cdot \nabla_{\boldsymbol{x}}), \tag{5.3}$$

in comoving coordinates. This implies that Equation (1.31) is equivalent to

$$\frac{\partial \boldsymbol{v}}{\partial t} + (\boldsymbol{v} \cdot \nabla_{\boldsymbol{x}})\boldsymbol{v} = \boldsymbol{0}, \tag{5.4}$$

which guarantees a velocity potential, $\boldsymbol{v} = \nabla_{\boldsymbol{x}}\phi$.

Using the *linear growth law* (Equation (1.30)) to invert the continuity equation (1.17), we can deduce that ϕ satisfies

$$\delta = D\nabla^2\phi. \tag{5.5}$$

This same Bernoulli condition can also be applied to SP reconstruction. However, it is only necessary in SP reconstruction to use this to find the initial condition, since SP updates the velocity potential as it evolves the state.

5.1 Reconstructing with Schrödinger-Poisson

There are many advantages to using the SP approach for reconstruction. Its ability to naturally model the full phase-space distribution of dark matter without the need for artificial assumptions about particle crossing or smoothing. This is hugely advantageous in the highly non-linear regime, where the previous more traditional methods struggle. The reversibility of the Schrödinger equation allows for a more detailed phase-space reconstruction than either LFA or ZB. The likelihood of FDM as a dark matter candidate does not need to feature in this section as SP continues to be a useful tool inspite of these possibilities. Of course, the reality of the nature of dark matter will greatly inform which is the best reconstruction model in the future as our ability to model structure formation is the backbone of reconstuction.

The SP method does not disappoint in terms of computational simplicity. It is more complicated and time consuming than the traditional LFA or ZB, but not by anything significant enough to dissuade users from using it.

5.1.1 Time-reversal of the Schrödinger Equation

In quantum mechanics it is widely accepted that time-reversal is possible. It is more possible here than anywhere else in physics, since we don't have to deal with entropy. This is part of the reason why reversing time in this model is so much more attractive. Time reversal in quantum mechanics is done by applying the time-reversal operator.

We wish to consider taking $\psi(x, -t)$ as a solution to the Schrödinger Equation 2.3. This is not possible since the Schrödinger equation is first order in time, so the left hand side would change sign under $t \to -t$ but the right hand side does not. However, if we take the complex conjugate of Equation (2.3), we can see that $\psi^*(x, -t)$ is a solution to the Schrödinger equation, since the complex conjugation changes the sign of i on the left hand side, which compensates for the change in sign $t \to -t$. Therefore, we define time-reversed motion of this model by the rule

$$\psi_{\mathrm{r}}(x, t) = \psi^*(x, -t) = \sqrt{\rho} e^{-i\phi/\nu}, \tag{5.6}$$

where, subscript r stands for reversed.

This is interesting because taking the complex conjugate ψ^*, in the context of this thesis, refers to changing the direction of the velocity potential. So, in order to move the particles backwards in time, we reverse the direction of time, and also reverse the direction of the velocities. It is also interesting to note that since the velocity potential is linked to the gravitational potential, we are also reversing that as well. A more in-depth discussion on time reversal in quantum mechanics and the Time-Reversal Operator is discussed in many texts on quantum mechanics such as [105].

With all of this in mind, our Schrödinger equation becomes,

$$i\nu\frac{\partial\psi_{\rm r}}{\partial t} = \frac{\nu^2}{2}\nabla^2\psi_{\rm r} + V\psi_{\rm r}. \tag{5.7}$$

Inspiration for this work

The work in this chapter has been inspired by work done by Short in his thesis, [106]. His thesis explores the free-particle approximation as an alternative to methods popular at the time. It includes a chapter with a more rigorous mathematical analysis and a reconstruction comparison of different methods on *GADGET* N-body simulations. Short ran *GADGET* locally and thus his analysis was conducted on a more simple power law power spectrum. The work in this thesis expands upon Short's work by conducting a similar reconstruction analysis on *IllustrisTNG* [107], which employs ΛCDM .

Similarly to Figures 5.4 and 5.6 Short compares the ability of the different approximations at different smoothing radii and different redshifts. Figure 5.1 shows point-by-point comparisons of the reconstructed density contrast δ with a Gaussian filter smoothing radius of $g = 8\mathrm{h}^{-1}\mathrm{Mpc}$, at 3 different redshifts. Similarly, Figure 5.2 shows point-by-point comparisons of the same but with a smoothing radius of $g = 4\mathrm{h}^{-1}\mathrm{Mpc}$.

It is clear from both Figure 5.1 and Figure 5.2 that the free particle approximation greatly out-performs both the Zel'dovich-Bernoulli approximation and the Linearised Fluid Approach at both smoothing radii and all three reconstructed redshifts for a power-law power spectrum. Given these results it is clear that further analysis was needed to test the validity of the free-particle approximation and further again the Schrödinger-Poisson approach.

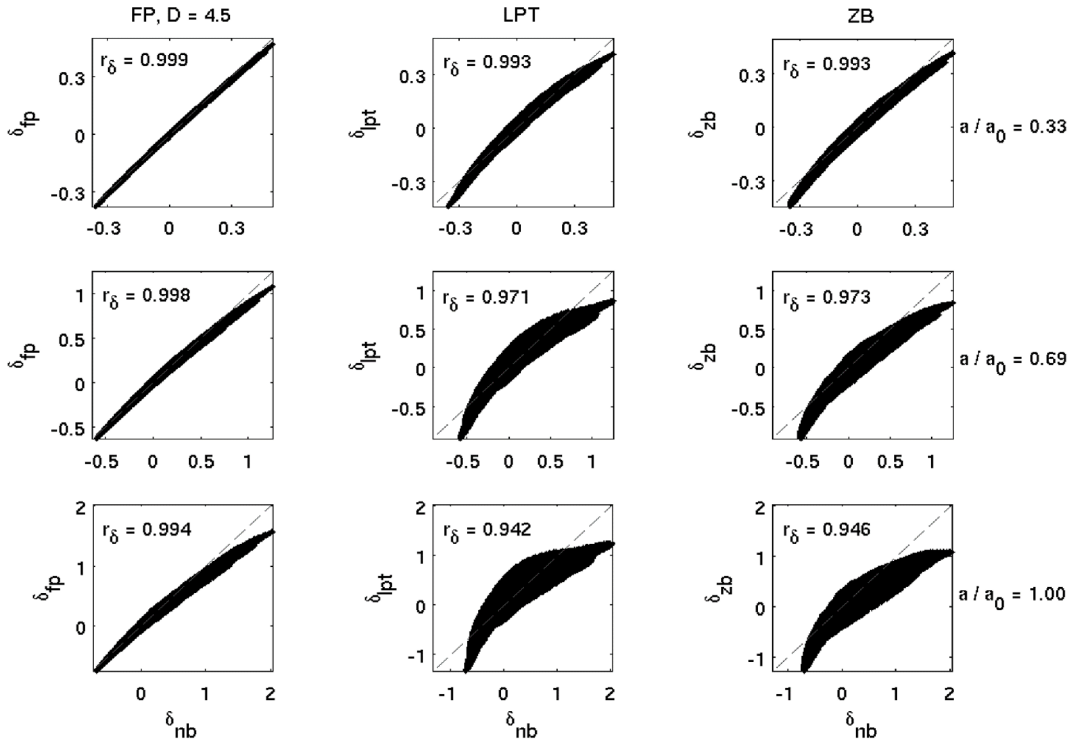

Figure 5.1: Point-by-point comparison of reconstructed density contrast δ and the intial condition with $8h^{-1}$Mpc smoothing. Image credit to [106]

5.2 The Real Test: N-body simulations

We used the results of the *illustrisTNG* suite of cosmological galaxy formulation simulations [107]. Each simulation in *illustrisTNG* evolves a large swatch of a mock Universe from high redshift until the present day while taking into account a wide range of physical processes that drive galaxy formation. The project consists of three volumes and 18 simulations in total. Three physical simulation box sizes with cubic volumes of roughly 50, 100 and 300Mpc side length, which are referred to as TNG50, TNG100 and TNG300, respectively, in the catalog. All of the simulations have "dark matter only" counterparts to their "baryonic physics" counterparts, which are the runs which account for many different types of physical processes. The dark matter only simulations give predictions for how the large-scale structure, the clustering of galaxies, shapes of haloes and so forth would evolve in a universe constructed of only dark matter.

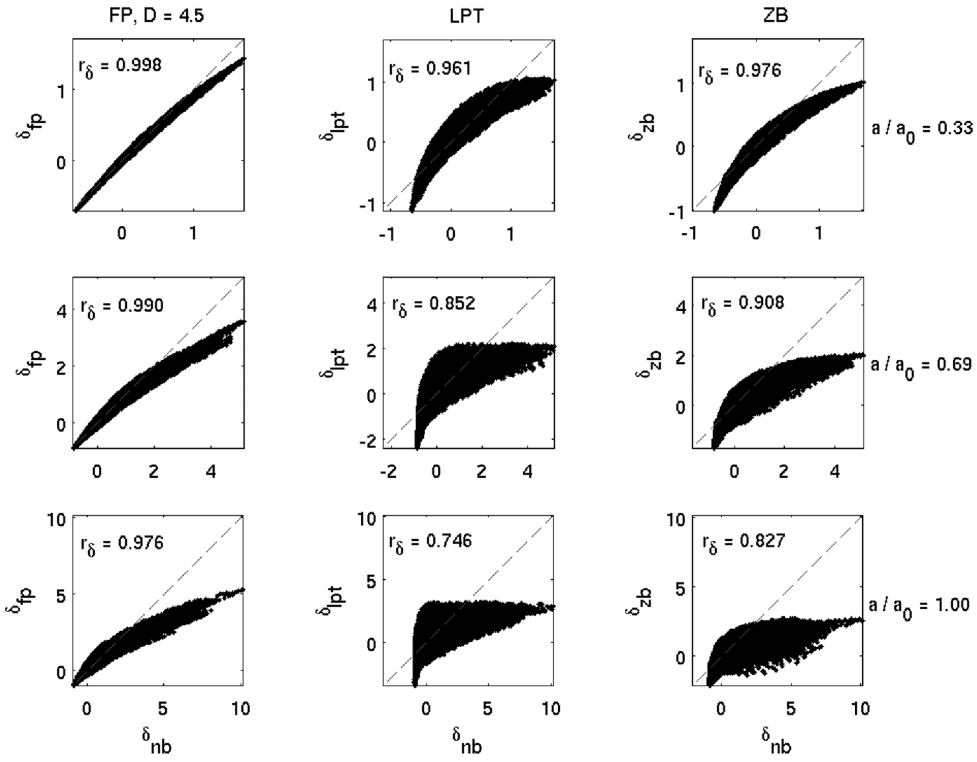

Figure 5.2: Point-by-point comparison of reconstructed density contrast δ and initial condition with $4h^{-1}$Mpc smoothing. Image credit to [106]

Volume	[Mpc^3]	51.7^3
$\mathrm{L_{box}}$	[Mpc/h]	35
N	-	2160^3
m	[$\mathrm{M}_\odot$]	4.5×10^5

Table 5.1: Specifications of TNG50 simulations.

While including all of the baryonic physics in the simulation is very important for a lot of physics, for us it is not particularly useful as this work wishes to reconstruct the large-scale struture of the universe, which is modelled very well by only considering dark matter. Therefore, for this work we have chosen to use only "dark matter only" counterparts to the TNG50 simulations.

The specifics of the TNG50-dark simulations are seen in Table 5.1. TNG50 contains roughly 100 Milky Way mass-analogs, one massive galaxy cluster ($\sim 10^{14}\mathrm{M}_\odot$), a Virgo-like analog and dozens of group sized haloes at $10^{13}\mathrm{M}_\odot$. The key science drivers of TNG50 focus on present day ($z = 0$), but also at earlier epochs, from cosmic noon ($z \sim 2$) through reionisation ($z \sim 6$).

For the purpose of proof of concept, we have decided to model SP for reconstruction in $2 + 1$ dimensions. The bulk of the analysis has been done on a two-dimensional slice of TNG50-2-dark. To demonstrate that this is a somewhat random choice, various slices from TNG50-2,3,4-dark are shown in Figure 5.7 at the end of this chapter. Two-dimensional slices were taken by taking $\mathrm{L_{box}}/10$ thick sections and flattening them to form a two-dimensional density field ρ.

With the 'final' density field compiled from the particle data, we used the Bernoulli-like condition (Equation (5.5)) to construct the initial velocity potential field from the 'final' particle density field. With both the velocity and density information of the "final state" we can begin reconstructing.

Before starting this analysis of the models effectivness at reconstructing initial conditions from N-body simulations, we ran some preliminary tests on toy models in real and redshift space just to test that the code actually worked and could recover a simple initial condition set by us. Once, we were satisfied with these

early tests, we began our analysis on results from *illustrisTNG*.

Smoothing

There is a level of smoothing necessary for all of the methods described above as we must smooth over highly non-linear regions where the linear and semi-linear approximations are unreliable and cannot be expected to produce a meaningful result. Figure 5.3 shows the same slice from the N-body simulation smoothed using a Gaussian filter of three different radii, g.

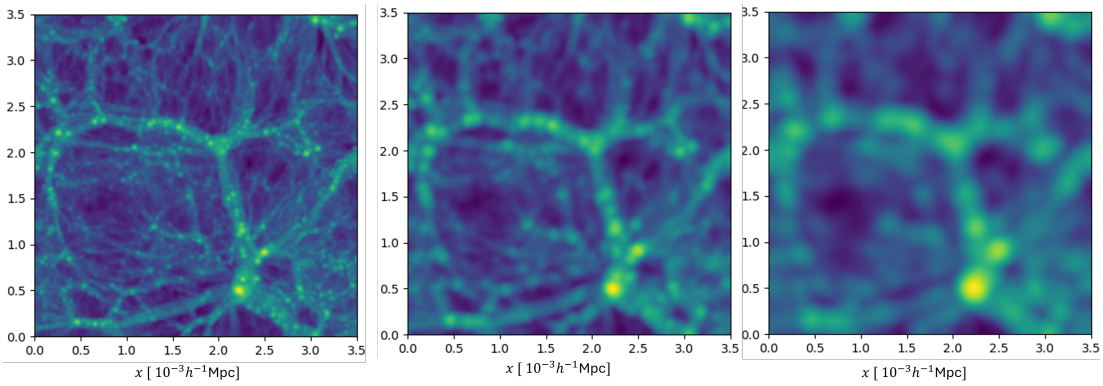

Figure 5.3: Initial condition from N-body simulation with 3 different smoothing radii. Gaussian filters of $g = 870\text{h}^{-1}\text{kpc}$ (left), $g = 2\text{h}^{-1}\text{Mpc}$ (center), $g = 4\text{h}^{-1}\text{Mpc}$ (right). Plotted on a log scale so it is easier to see the structure and the difference in the smoothing factors.

Each of these were evolved backwards in time by three different regimes, SP, ZB and LFA, as described above in their respective sections. To compare these schemes, Figure 5.4 shows a point-by-point comparison of the density field of each scheme to the N-body simulation of the appropriate snapshot for the evolution. Density fields are plotted and compared on a log scale so their differences are more clear bye eye. We also wish to assign a singular number which encompasses how well these schemes could recover their N-body initial state. For this we refer to the *Pearson product-moment correlation coefficient* [108],

$$r = \frac{\Sigma(x_i - \overline{x})(y_i - \overline{y})}{\sqrt{\Sigma(x_i - \overline{x})^2 \Sigma(y_i - \overline{y})^2}}, \tag{5.8}$$

where x_i, y_i are the individual data points and $\overline{x}, \overline{y}$ are the mean average of the data points.

The r-value for each density field is below in Table 5.2, where all r-values are compared and contrasted with the constraints of each reconstruction.

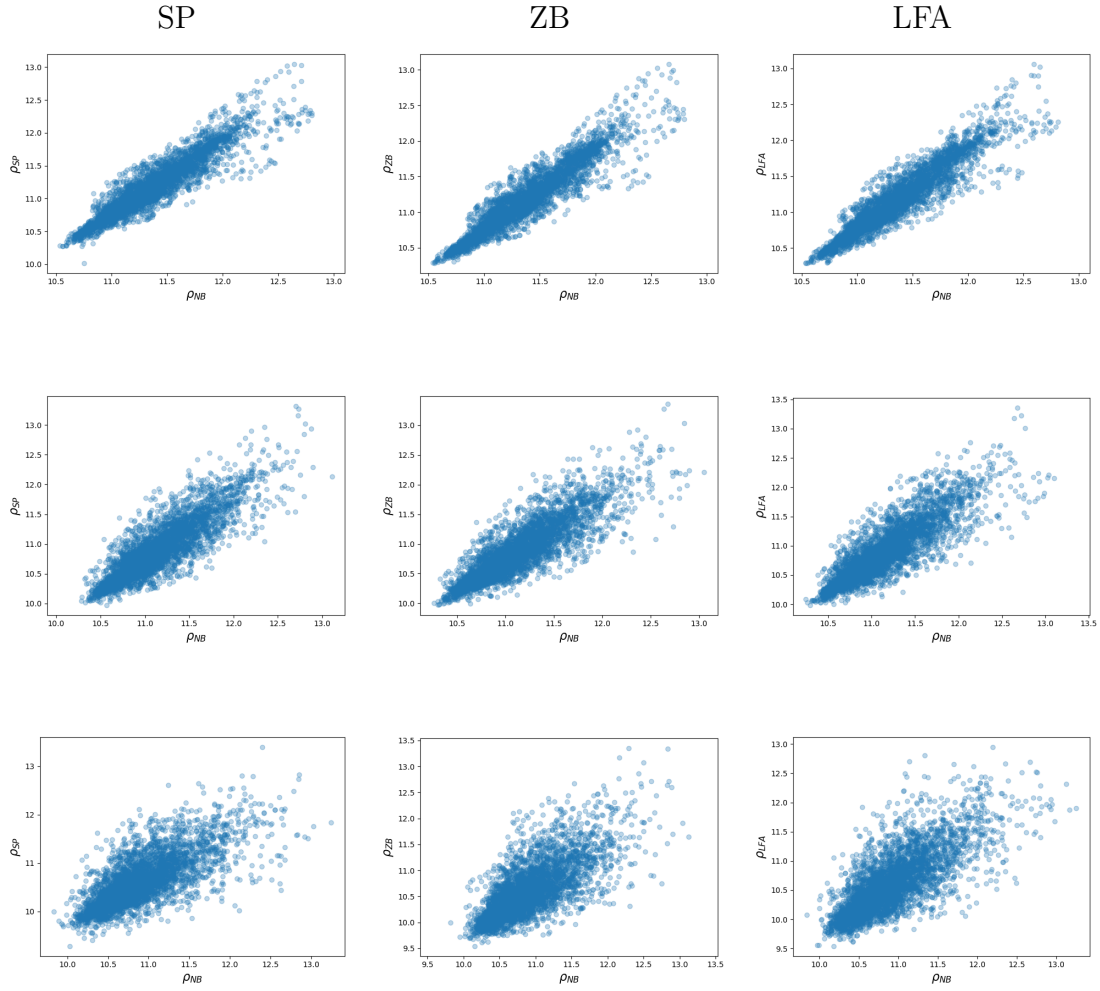

Figure 5.4: Point-by-point comparison of base 10 log density fields reconstructed by the three approximation schemes, each column shows a different methods of reconstruction; SP (first column), ZB (second column), and LFA (third column). Each row depicts a different level of smoothing applied to the initial condition (Figure 5.3); $g = 4\text{h}^{-1}\text{Mpc}$ (first row), $g = 2\text{h}^{-1}\text{Mpc}$ (second row), and $g = 870\text{h}^{-1}\text{kpc}$ (third row). These plots show a sample of the data randomly selected with uniformly distributed $p = 1/64^2$, to be comparable to Figures 5.1 and 5.2.

It is clear that in row 1 of Figure 5.4 that all approximations can reasonably well recover the intial state with smoothing radius $g = 4\mathrm{h}^{-1}\mathrm{Mpc}$. In row 2 of Figure 5.4 we cannot distinguish between SP and ZB reconstruction and we can see in Table 5.2 that 4 significant figures are needed to distinguish between the two regimes. It is at the lowest smoothing radius, $g = 870\mathrm{h}^{-1}\mathrm{kpc}$, that we begin to see large differences between the capabilities of the different approximations. We conclude, by eye, that at the lowest smoothing SP better reconstructs the initial state that the other two approximate schemes. LFA is unable to predict the initial state at this smoothing radius as the structures are highly non-linear. As we move to more non-linear initial density fields the SP and ZB models better predict the initial state, which is to be expected.

In the SP method there exits another level of smoothing built into the model. The viscosity parameter, ν, can in some ways act like a smoothing. Larger ν means our waves have a larger wavelength, and smaller ν gives a smaller wavelength. Figure 5.5 shows a point-by-point comparison of SP reconstruction with three different values of ν.

We chose to use $g = 2\mathrm{h}^{-1}\mathrm{Mpc}$ as our smoothing radius, to best be able to see the difference between ν values. Using different values of ν does not have a huge affect on the reconstruction, since we need 3 significant figures in r-value to distinguish between them. With this in mind, for the rest of the analysis we have chosen to continue using the ν value which gives us the best correlation, $\nu = 0.01$. We understand that in order to truly know the best value of ν we would need to carry out a full optimisation, but for our proof of concept this will be sufficient.

Redshift

The above scatter plots all refer to a reconstruction of redshift $z = 0.5$ from $z = 0$, we also wish to compare the abilities of the approximate schemes to reconstruct higher redshifts. Figure 5.6 shows similar point-by-point comparison plots as seen

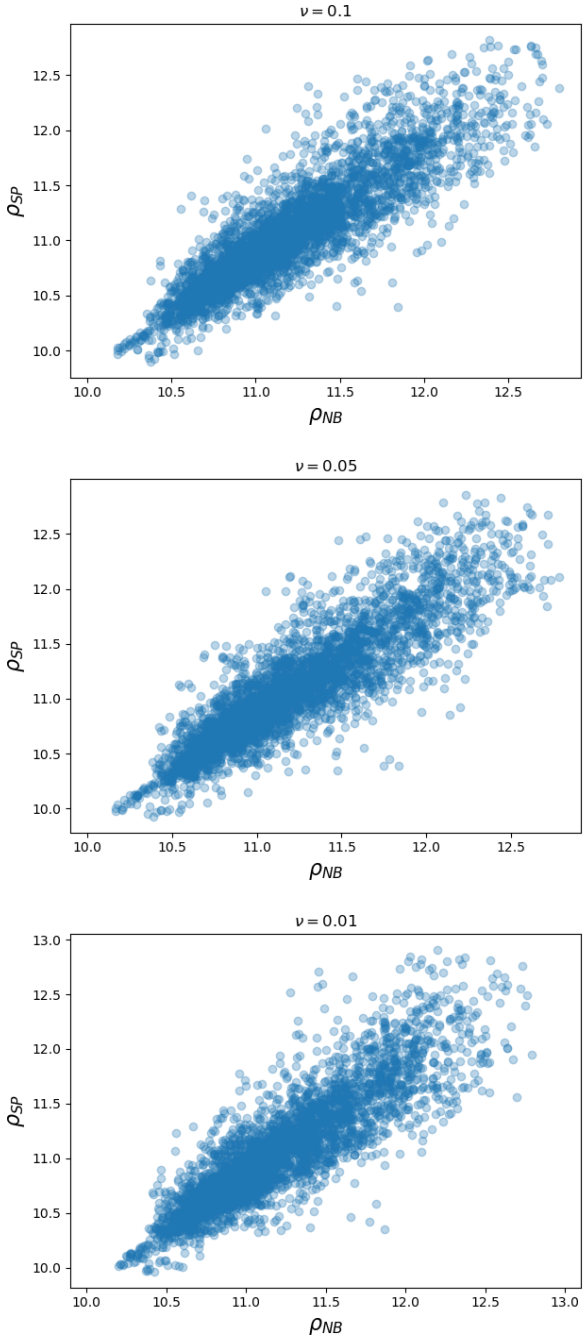

Figure 5.5: Point-by-point comparison of SP reconstruction with different values of ν; $\nu = 0.1$ (top), $\nu = 0.05$ (center), $\nu = 0.01$ (bottom).

in the subsection above.

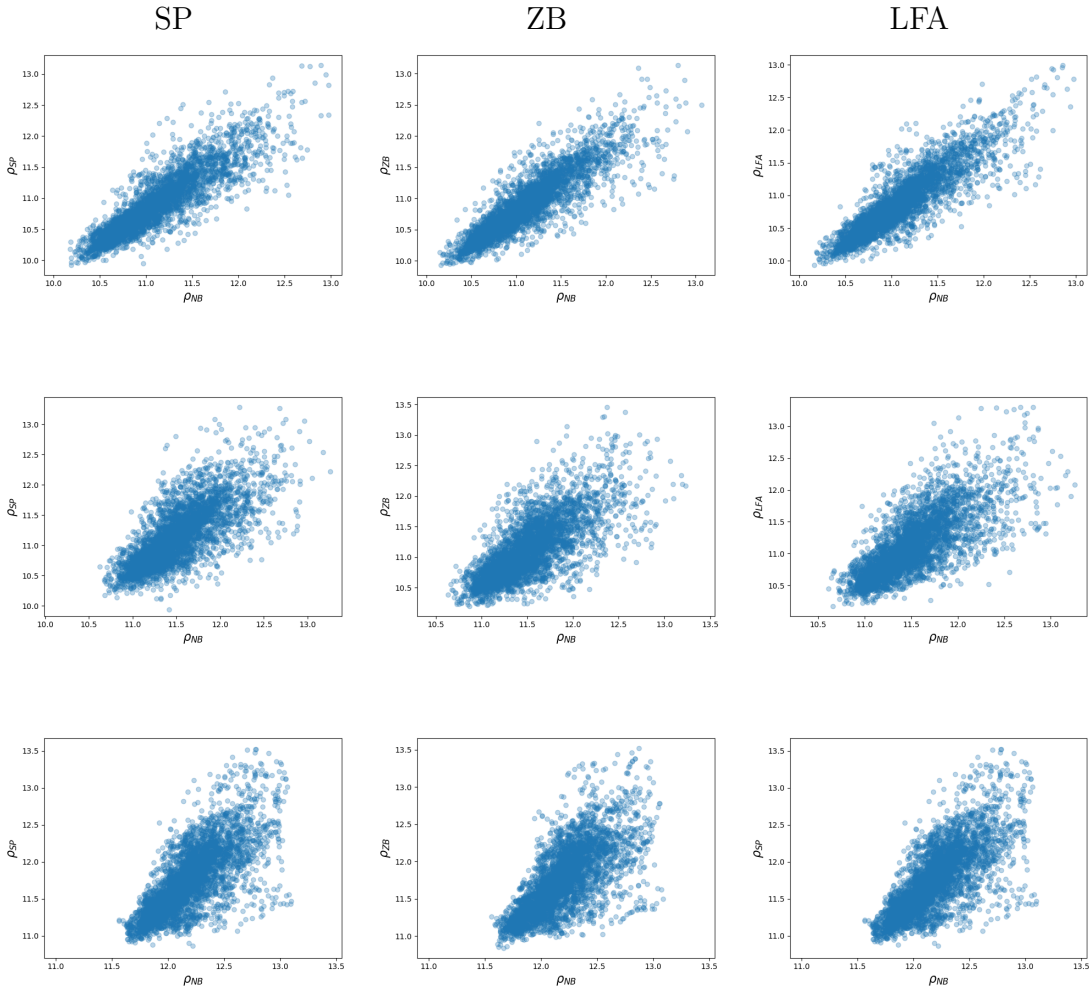

Figure 5.6: Point-by-point comparison of three approximation scheme density field reconstructions with N-body simulation appropriate snapshot density field. Each column shows a different methods of reconstruction; SP (first column), ZB (second column), and LFA (third column). Each row depicts a reconstruction of a different redshift of the same 2D slice of TNG50-2-Dark. First row $z = 0.5$, second row $z = 1.0$, third row $z = 2.0$. These plots show a sample of the data randomly selected with uniformly distributed $p = 1/64^2$, to be comparable to Figures 5.1, 5.2 and 5.4.

For this analysis, we chose a smoothing radius of $g = 4\text{h}^{-1}\text{Mpc}$, as we believe this best shows the difference between approximations, without putting too much strain on the system by using the lowest smoothing radius. It is clear by eye that all three approximations perform worse as they attempt to reconstruct higher redshifts. It can be seen in Table 5.2 that SP better reconstructs the initial density field at higher redshifts. This is what we expect, as we reconstruct further back

Correlation values r			
Method	Smoothing [h^{-1}Mpc] σ	Redshift z	r-value
LFA	0.87	0.5	0.7665
LFA	2	0.5	0.8876
LFA	4	0.5	0.9444
SP ($\nu = 0.01$)	2	0.5	0.8787
SP ($\nu = 0.1$)	2	0.5	0.8817
SP ($\nu = 0.05$)	2	0.5	0.8816
SP ($\nu = 0.1$)	0.87	0.5	0.7780
SP ($\nu = 0.1$)	10	0.5	0.9441
ZB	0.87	0.5	0.7684
ZB	2	0.5	0.8882
ZB	4	0.5	0.9948
LFA	2	1.0	0.7392
LFA	2	2.0	0.5587
SP ($\nu = 0.1$)	4	2.0	0.7126
SP ($\nu = 0.1$)	2	1.0	0.7504
SP ($\nu = 0.1$)	2	2.0	0.5772
ZB	2	1.0	0.7411
ZB	4	2.0	0.7093

Table 5.2: Tabel of r values for different methods, smoothings and redshifts.

in time, the linear/semi-linear regimes are not capable of predicting the evolution of fluctuations. Whereas, SP is more capable of going into the non-linear and better predicting the fluctuations at these times.

It seems that the SP approximation is minimally better than the current schemes for reconstructing smoothed density fields to redshifts up to $z = 2.0$. We acknowledge that this is not a full analysis or optimisation and with such this scheme could be an improvement upon the current regime.

We conclude this section by acknowledging that SP does not necessarily out perform the next best thing (ZB) for ΛCDM reconstruction, but it remains competitive, being able to reconstruct at each smoothing radius and tested redshift at least as good as ZB. It is important to note that field reconstruction is a challenging exercise in reconstruction, and that testing it with a point-by-point comparison is a very hard test as the field needs to match the initial condition in

both position and magnitude, and small deviations for this have a significant impact on the correlation number. It is difficult to know whether SP reconstruction would shine brighter in redshift space or power spectrum reconstruction. Therefore, with the other advantages of using SP over ZB we believe that we cannot yet rule out SP as a viable next candidate for reconstruction.

We also wish to highlight that in a truly ΛFDM universe, SP might be a better candidate. To make any sort of conclusion on this statement one would need to conduct a similar analysis to what is presented above on an FDM simulation, such as [109].

The point-by-point comparison plots shown in Figures 5.4-5.6 are sampled from a larger data-set, for easier comphrension by eye, and for easier comparison with Figure 5.1. Point-by-point comparison plots including the full data-set are included in the Appendix (Chapter A).

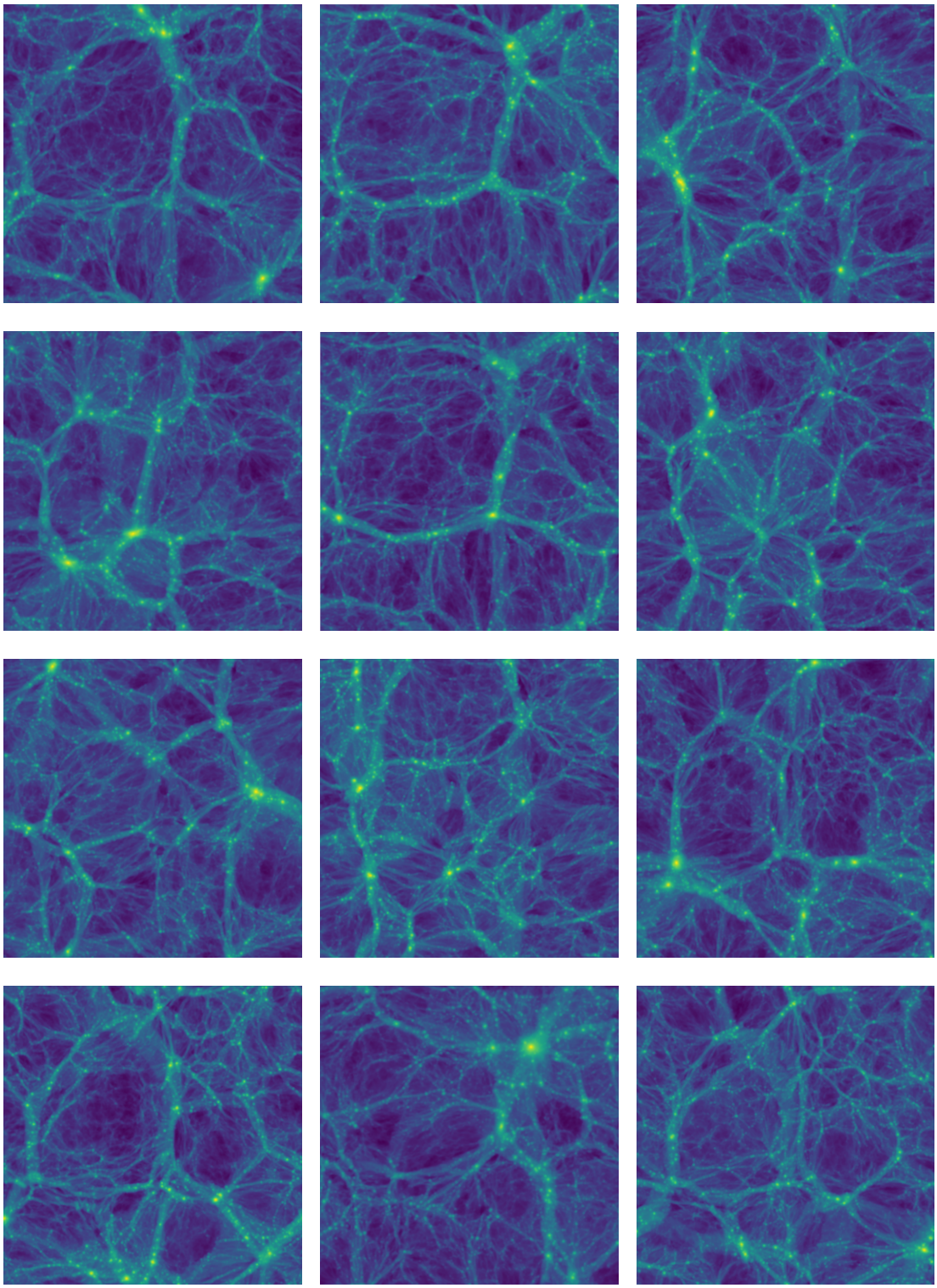

Figure 5.7: Gallery of simulation snapshots

Chapter 6

Conclusion

6.1 Summary

This thesis explored cosmological structure formation through the lens of wave mechanics, following the pioneering work of Widrow and Kaiser [3]. At its core, the main achievement of this work has been to advance the understanding of simple, foundational models using the SP framework. Developing the insights provided by such models is a crucial step in constructing a comprehensive understanding of the universe as a whole. Without these fundamental insights, it becomes challenging to bridge the gap between theoretical abstractions and the complexities of observed phenomena. Doroshkevich's seminal work [50], for instance, illustrated the power of such models by establishing a statistical and dynamical framework for understanding galaxy clustering and large-scale structure. His work bridged the divide between early cosmological perturbations and the observed distribution of galaxies, forming a cornerstone of modern cosmology. Similarly, this thesis contributes to advancing theoretical understanding while addressing practical challenges in modeling and simulation.

By framing the evolution of large-scale structures within the SP system, this research highlights the unique strengths of the wave-mechanical approach. In

particular, this formalism naturally integrates the multistreaming behavior of underdense regions with the wave-like nature and interference effects inherent to the SP framework. This ability sets it apart from traditional methods, such as the ZA, which often fail to accurately model post-shell-crossing phenomena. Furthermore, the SP approach avoids the resolution issues faced by particle-based simulations when modeling cosmic voids, offering a continuous description of the density field that remains well-defined even in underdense regions.

The introduction in Chapter 1 provided the necessary context for this work by reviewing the theoretical foundations of structure formation and identifying limitations in the standard ΛCDM model. Chapter 2 outlined the mathematical background of the SP system and established key results that underpinned subsequent chapters.

Chapter 3 presented a detailed exploration of cosmic voids within the SP framework. By focusing on the evolution of an isolated void, this study demonstrated the method's ability to model void expansion beyond shell-crossing while maintaining physical consistency. Unlike traditional approaches, the SP system circumvents the singularities inherent to ZA and captures the multistreaming region with wave-like interference patterns. This highlights the unique strength of the SP formalism in studying void dynamics, an area of growing importance given the dominant volume fraction of voids in the cosmic web.

In Chapter 4, we extended the SP framework by incorporating viscosity and exploring its limitations in relation to full Navier-Stokes dynamics. The introduction of viscosity provided a means to model internal energy dissipation, leading to a description of wave propagation in these systems. A key result was the identification of a novel scaling solution, analogous to the Reynolds number in classical fluid dynamics. The broader analysis of viscosity within the SP framework revealed fundamental insights into the interplay between small-scale wave effects and large-scale structure evolution. Collectively, these results deepen our

understanding of how perturbations grow and interact, offering a more comprehensive picture of structure formation in the nonlinear regime where traditional methods face significant challenges.

Chapter 5 explored the SP framework as a tool for reconstructing initial conditions in cosmological simulations. While this investigation was primarily a proof of concept, the results were promising. In a universe governed by power-law power spectra, SP significantly outperformed the standard ZB approach. In modern ΛCDM contexts, the SP method matched the performance of ZB while maintaining competitive accuracy in non-linear regimes. These findings suggest the potential of SP as a robust alternative for initial condition reconstruction, though further work is needed to explore its full capabilities, particularly in redshift-space reconstructions.

The collective findings of this thesis underscore the profound impact of adopting a wave-mechanical perspective in cosmology. By bridging the gap between classical fluid models and quantum-inspired approaches, this work lays a solid foundation for a deeper understanding of the universe's formation and evolution. Moreover, the SP framework provides a versatile tool for addressing longstanding challenges in computational cosmology, offering a physically grounded and mathematically elegant description of structure formation.

The future of FDM research is particularly exciting, as it offers a compelling alternative to CDM while addressing key challenges in small-scale structure formation. Recent advancements, such as the first full hydrodynamical simulations of FDM by Nori et al. [109], mark a turning point in the field. Observationally, the next generation of cosmological surveys promises to play a pivotal role in testing FDM predictions. The Euclid mission, for instance, aims to map the geometry of the dark universe through high-precision measurements of galaxy clustering and weak gravitational lensing. Such data will be invaluable for probing FDM's unique imprint on the cosmic web and void dynamics. Complementary efforts

from the Dark Energy Spectroscopic Instrument (DESI) and the Vera C. Rubin Observatory's Legacy Survey of Space and Time (LSST) will further constrain cosmological parameters, offering a clearer picture of FDM's viability as a dark matter candidate.

The convergence of advanced simulations, refined theoretical models, and cutting-edge observational capabilities promises to shed new light on the nature of dark matter. By integrating these efforts, the field is poised to redefine our understanding of cosmic structure formation and the fundamental forces shaping the universe.

6.2 Future Work

- Applications to Filament Dynamics

  While the Schrödinger-Poisson (SP) framework has proven effective in modeling isolated voids and spherical collapse, an exciting avenue of exploration would be its application to the dynamics of cosmic filaments. For instance, SP could replace ZA in analyses similar to those conducted by Feldbrugge et al. [110] and Gough et al. [55]. Additionally, replacing CDM with FDM in cosmological simulations could yield new insights into filament formation and evolution [109].

- Incorporating Self-Interacting Terms in the Schrödinger Equation

  A deeper exploration of the Schrödinger Equation (SE) could involve the inclusion of self-interacting potentials. By "turning on" various interaction terms, we could investigate how different types of FDM particles behave under such modifications. This approach would enable a broader examination of the parameter space for FDM and its implications for structure formation.

- Power Spectrum and Redshift-Space Reconstruction

  There is significant potential to test the SP framework's performance in reconstructing the power spectrum and redshift-space maps. A proof-of-concept study could compare SP-based reconstructions to existing methods, building on the analysis conducted in Chapter 5. Such an investigation could determine whether SP offers improved accuracy or new advantages for these types of reconstructions.

- Full Optimisation for Reconstruction

  While this thesis demonstrated the SP framework in two dimensions as a proof of concept, a fully optimised, three-dimensional reconstruction technique would be necessary for real-world applications. This development would require addressing computational challenges and ensuring the method's scalability and robustness for observational datasets.

- Integration with Observational Data

  Should the SP framework prove superior for reconstruction, the next step would be to develop a pipeline for integrating it into observational analyses. This would involve testing the method's efficacy in reconstructing initial conditions from real-world data and evaluating its potential as a model for dark matter. For instance, an SP-based ΛFDM framework could serve as a promising candidate for explaining cosmic structure formation and evolution.

Appendix A

Full Data Plots

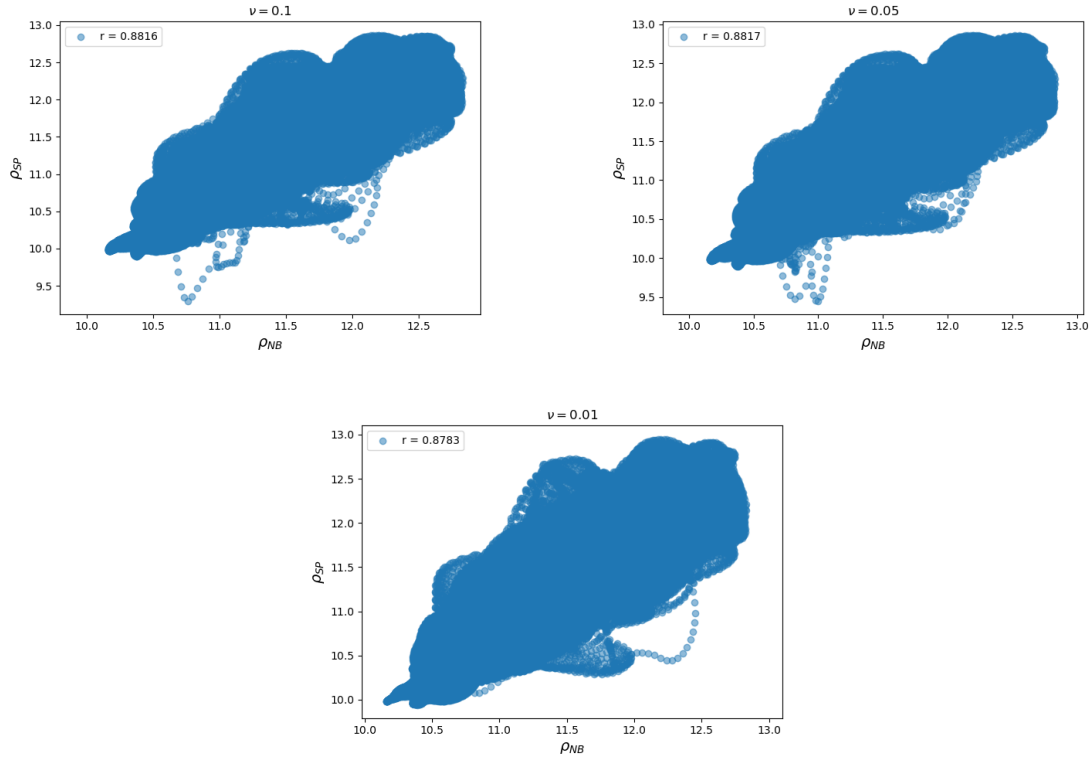

Figure A.1: Full resolution point-by-point comparison of SP reconstruction with different values of ν; $\nu = 0.1$ (top), $\nu = 0.05$ (center), and $\nu = 0.01$ (bottom)

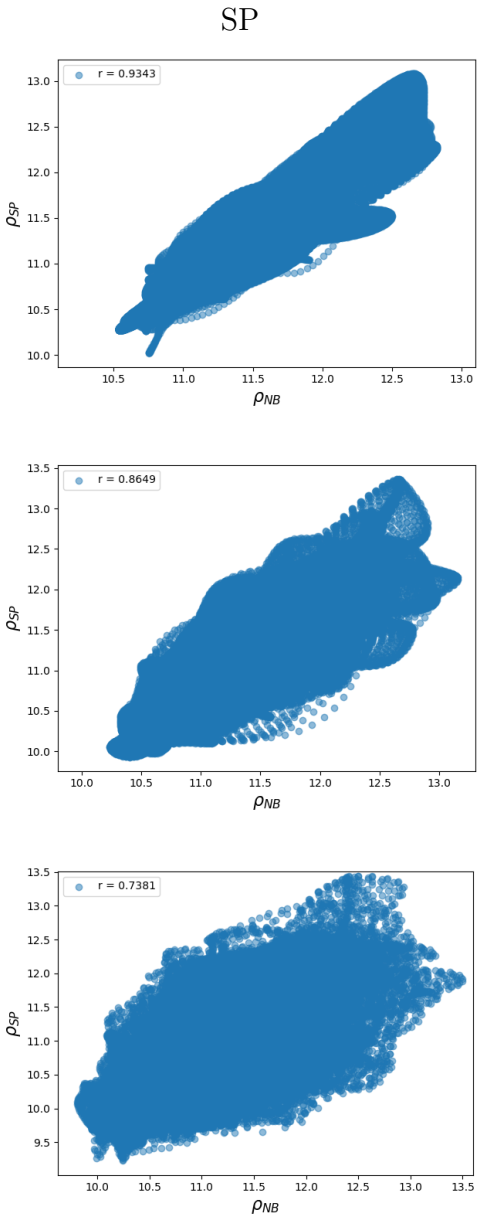

Figure A.2: Full resolution point-by-point comparison of SP reconstruction with different values of g; $g = 4\mathrm{h}^{-1}\mathrm{Mpc}$ (top), $g = 2\mathrm{h}^{-1}\mathrm{Mpc}$ (center), and $g = 870\mathrm{h}^{-1}\mathrm{kpc}$ (bottom)

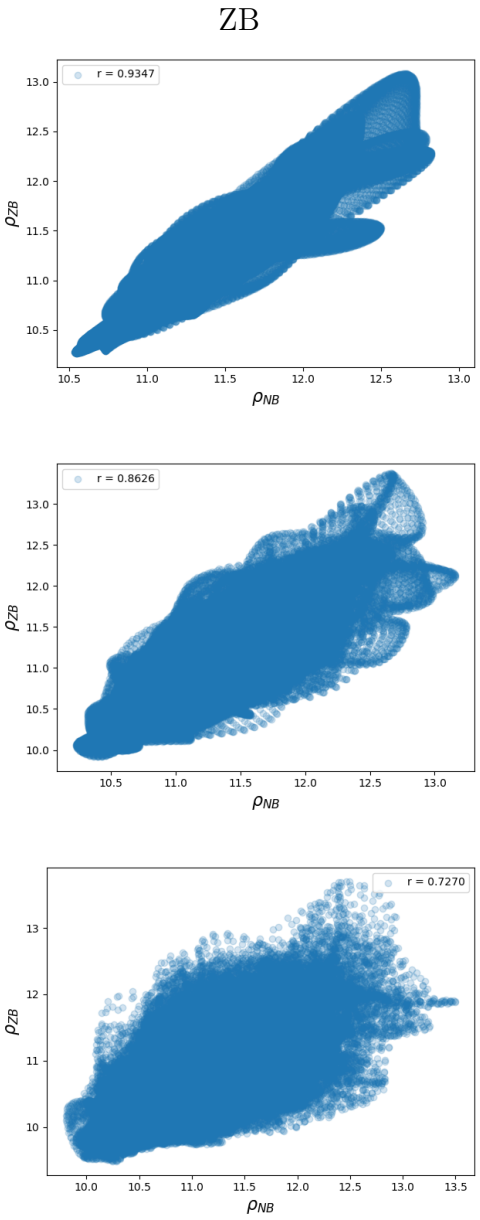

Figure A.3: Full resolution point-by-point comparison of ZB reconstruction with different values of g; $g = 4\mathrm{h}^{-1}\mathrm{Mpc}$ (top), $g = 2\mathrm{h}^{-1}\mathrm{Mpc}$ (center), and $g = 870\mathrm{h}^{-1}\mathrm{kpc}$ (bottom)

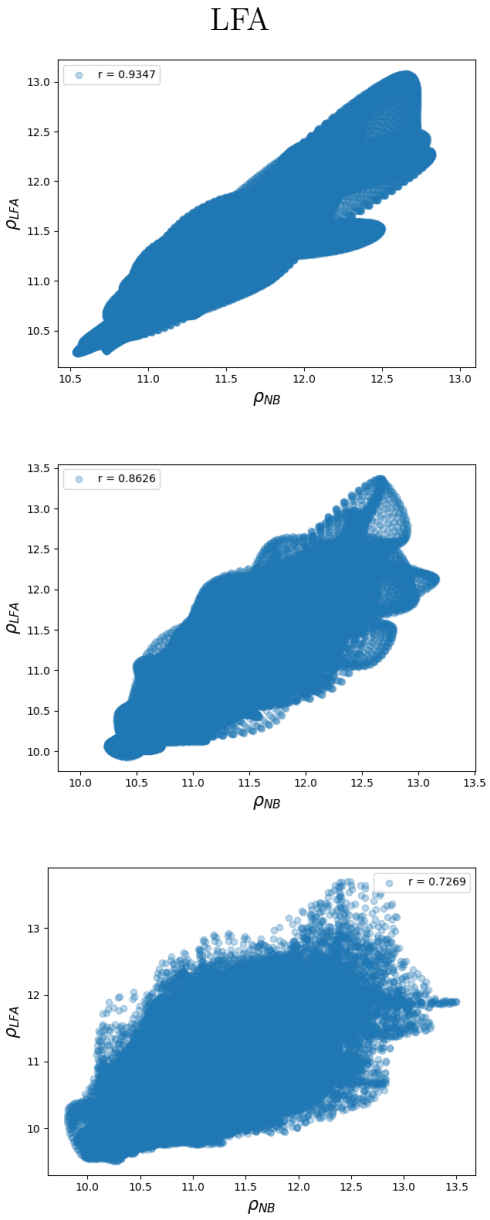

Figure A.4: Full resolution point-by-point comparison of LFA reconstruction with different values of g; $g = 4h^{-1}$Mpc (top), $g = 2h^{-1}$Mpc (center), and $g = 870h^{-1}$kpc (bottom)

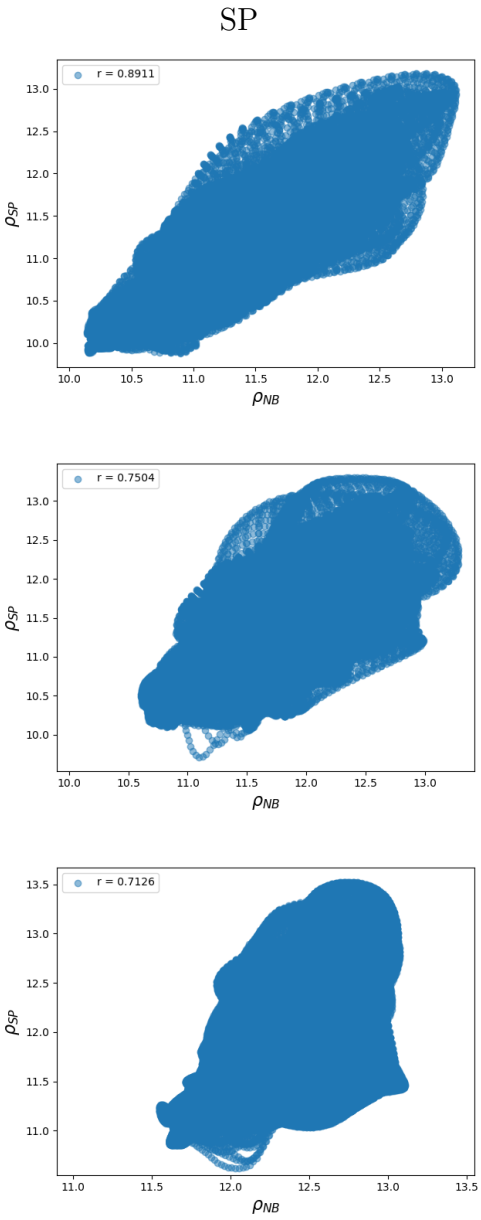

Figure A.5: Full resolution point-by-point comparison of SP reconstruction of different redshift initial conditions z; $z = 0.5$ (top), $z = 1.0$ (center), $z = 2.0$ (bottom).

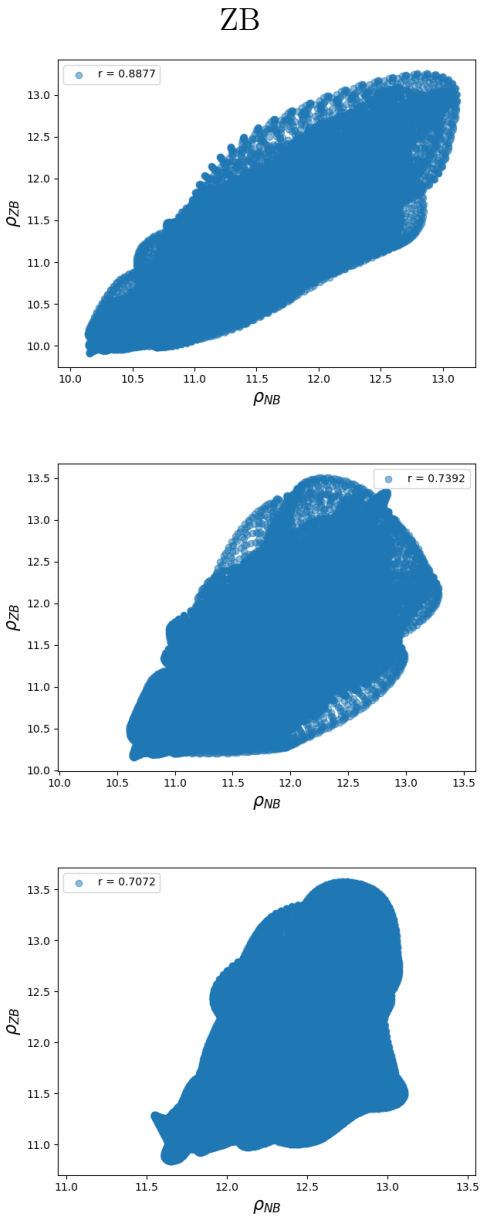

Figure A.6: Full resolution point-by-point comparison of ZB reconstruction of different redshift initial conditions z; $z = 0.5$ (top), $z = 1.0$ (center), $z = 2.0$ (bottom).

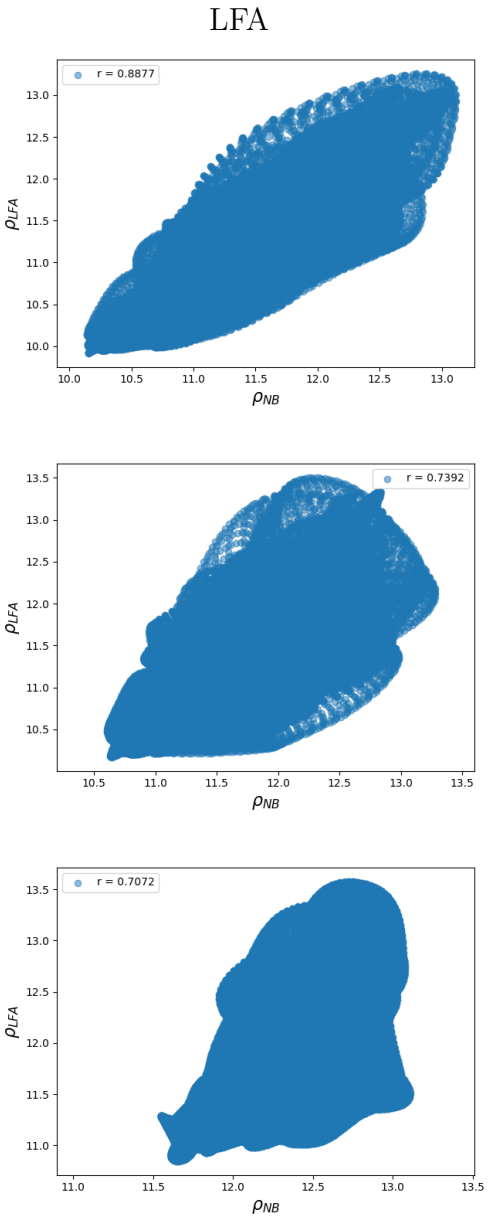

Figure A.7: Full resolution point-by-point comparison of LFA reconstruction of different redshift initial conditions z; $z = 0.5$ (top), $z = 1.0$ (center), $z = 2.0$ (bottom).

Bibliography

[1] *The SAO Astrophysics Data System*. URL: https://ui.adsabs.harvard.edu/.

[2] *arXiv ¿ astro-ph*. URL: https://arxiv.org/list/astro-ph/new.

[3] Lawrence M. Widrow and Nick Kaiser. "Using the Schrödinger Equation to Simulate Collisionless Matter". In: *Astrophysical Journal Letters* (1993). DOI: https://doi.org/10.1086/187073.

[4] Aoibhinn Gallagher and Peter Coles. "Evolution of Cosmic Voids in the Schrödinger-Poisson Formalism". In: *The Open Journal of Astrophysics* (2022). DOI: 10.21105/astro.2208.13851.

[5] Peter Coles and Aoibhinn Gallagher. "Classical Fluid Analogies for Schrödinger-Newton Systems". In: *preprint* (2025). arXiv: 2507.08583 [astro-ph.CO]. URL: https://arxiv.org/abs/2507.08583.

[6] A. Einstein. "*Die Grundlage der allgemeinen Relativitätstheorie* [The Foundation of the General Theory of Relativity]". In: *Annalen Der Physik in German* 354 (1916). DOI: 10.1002/andp.19163540702.

[7] Isaac Newton, Andrew Motte, and N.W. Chittenden. *Newton's Principia. The mathematical principles of natural philosophy*. New-York, D Adee, 1848, http://hdl.loc.gov/loc.gdc/scd0001.00035669784.

[8] Edwin Hubble. "A Relation between Distance and Radial Velocity among Extra-Galactic Nebulae". In: *Proceedings of the National Academy of Science* 15.3 (Mar. 1929), pp. 168–173. DOI: 10.1073/pnas.15.3.168.

[9] S. Perlmutter et al. "Measurements of Ω and Λ from 42 High-Redshift Supernovae". In: *The Astrophysical Journal* 517.2 (June 1999), p. 565. DOI: 10.1086/307221. URL: https://dx.doi.org/10.1086/307221.

[10] Gerson Goldhaber. "The Acceleration of the Expansion of the Universe: A Brief Early History of the Supernova Cosmology Project (SCP)". In: *Sources and Detection of Dark Matter and Dark Energy in the Universe*. Ed. by David B. Cline. Vol. 1166. American Institute of Physics Conference Series. AIP, Sept. 2009, pp. 53–72. DOI: 10.1063/1.3232196.

[11] Planck Collaboration. "Planck 2015 results: XI. CMB power spectra, likelihoods, and robustenss of parameters". In: *Astronomy and Astrophysics* 594.A11 (Sept. 2016). DOI: 10.1051/0004-6361/20156926.

[12] William C. Keel. *The Road to galaxy formation*. Springer Praxis Books, 2007. ISBN: 9783540725350.

[13] G. F. Smoot et al. "Structure in the COBE Differential Microwave Radiometer First-Year Maps". In: *The Astrophysical Journal Letters* 396 (1992).

[14] C. L. Bennett et al. "Four-Year COBE* DMR Cosmic Microwave Background Observations: Maps and Basic Results". In: *The Astrophysical Journal* 464.1 (June 1996), p. L1. DOI: 10.1086/310075. URL: https://dx.doi.org/10.1086/310075.

[15] G. Hinshaw et al. "Nine-year Wilkinson Microwave Anisotropy Probe (WMAP) Observations: Cosmological Parameter Results". In: *The Astrophysical Journal Supplement Series* 208.2, 19 (Oct. 2013), p. 19. DOI: 10.1088/0067-0049/208/2/19. arXiv: 1212.5226 [astro-ph.CO].

[16] Planck Collaboration. "Planck 2018 results - V. CMB power spectra and likelihoods". In: *Astronomy and Astrophysics* 641 (2020), A5. DOI: 10.1051/0004-6361/201936386. URL: https://doi.org/10.1051/0004-6361/201936386.

[17] The Planck Collaboration. *The Angular Power Spectrum*. 2013. URL: https://www.esa.int/ESA_Multimedia/Images/2013/03/Planck_Power_Spectrum.

[18] Adam G. Riess et al. "Large Magellanic Cloud Cephid Standards Provide a 1% Foundation for the Determination of the Hubble Constant and stronger Evidence for Physics beyond ΛCDM ". In: *The Astrophysical Journal* 876.1 (May 2019). DOI: 10.3847/1538-4357ab1422.

[19] M. Milgrom. "A modification of the Newtonian dynamics as an alternative to the hidden mass hypothesis". In: *The Astrophysical Journal* 270 (1983), pp. 365–370. DOI: 10.1086/161130.

[20] M. Milgrom. "A modification of the Newtonain dynamics - Implications for galaxies". In: *The Astrophysical Journal* 270 (1983), pp. 371–383. DOI: 10.1086/161131.

[21] Joan Solà. "Cosmologies with a time dependent vacuum". In: *Journal of Physics: Conference Series* 283 (Feb. 2011), p. 012033. ISSN: 1742-6596. DOI: 10.1088/1742-6596/283/1/012033. URL: http://dx.doi.org/10.1088/1742-6596/283/1/012033.

[22] J. Richard Gott III et al. "A Map of the Universe". In: *The Astrophysical Journal* 624.2 (2005), pp. 463–484. ISSN: 1538-4357. DOI: 10.1086/428890.

[23] A. Drlica-Wagner et al. "Milky Way Satellite Census. I. The Observational Selection Function for Milky Way Satellites in DES Y3 and Pan-STARRS DR1". In: *The Astrophysical Journal* 893 (2020), p. 47. DOI: 10.3847/1538-4357/ab7eb9.

[24] M.L. Mateo. "Dwarf Galaxies of the local group". In: *Annuall Review of Astronomy and Astrophysics* 36.1 (1998), pp. 435–506. DOI: 10.1146/annurev.astro.36.1.435.

[25] Ben Moore et al. "Dark Matter Substructure within Galactic Halos". In: *Astrophysical Journal Letters* 524.1 (1999), pp. L19–L22. DOI: 10.1086312287.

[26] Anatoly Klypin et al. "Where are the missing galactic satellites?" In: *Astrophysical Journal* 522.1 (1999), pp. 89–92. DOI: 10.1086/307643.

[27] Michael Boylan-Kolchin, James S. Bullock, and Manoj Kaplinghat. "Too big to fail? The puzzling darkness of massive Milky Way subhaloes". In: *Monthly Notices of the Royal Astronomical Society: Letters* 415.1 (July 2011), pp. L40–L44. ISSN: 1745-3925. DOI: 10.1111/j.1745-3933.2011.01074.x. URL: http://dx.doi.org/10.1111/j.1745-3933.2011.01074.x.

[28] Ben Moore. "Evidence against dissipation-less dark matter from observations of galaxy haloes". In: *Nature* 370 (1994), pp. 629–631. DOI: 10.1038/370629a0.

[29] Sophie Koudmani et al. "Diverse dark matter profiles in FIRE dwarfs: black holes, cosmic rays and the cusp-core enigma". In: *arXiv e-prints*, arXiv:2409.02172 (Sept. 2024). DOI: 10.48550/arXiv.2409.02172.

[30] H. P. Robertson. "Kinematics and World-Structure". In: *The Astrophysical Journal* 82 (Nov. 1935), p. 284. DOI: 10.1086/143681.

[31] A. Friedman. "*Über die Krümmung des Raumes* [On the Curvature of Space]". In: *Z. Phys (In German)* 10.1 (1922), pp. 377–386.

[32] A. Friedman. "*Über die Möglichkeit einer Welt mit konstanter negativer Krümmung des Raumes* [On the Possibility of a world with Constant Neg-

ative Curvature of Space]". In: *Z. Phys (In German)* 21.1 (1924), pp. 326–332. DOI: 10.1007/BF01328280.

[33] P.J.E Peebles. *The Large-scale Sturcture of the Universe*. Princeton University Press, 1980. ISBN: 9780691082400.

[34] J. N. Islam. *An introduction to mathematical cosmology*. Cambridge University Press, 1992. ISBN: 0 521 37760 9.

[35] Chung-Pei Ma and Edmund Bertschinger. "Cosmological Perturbation Theory in the Synchronous and Conformal Newtonian Gauges". In: *The Astrophysical Journal* 455 (1995), p. 7. DOI: 10.1086/176550.

[36] S. W. Hawking. "Perturbations of an Expanding Universe". In: *The Astrophysical Journal* 145 (Aug. 1966), p. 544. DOI: 10.1086/148793.

[37] Hideo Kodama and Misao Sasaki. "Cosmological Perturbation Theory". In: *Progress of Theoretical Physics Supplement* 78 (Jan. 1984), pp. 1–166. ISSN: 0375-9687. DOI: 10.1143/PTPS.78.1. eprint: https://academic.oup.com/ptps/article-pdf/doi/10.1143/PTPS.78.1/5321391/78-1.pdf. URL: https://doi.org/10.1143/PTPS.78.1.

[38] F. Bernardeau et al. "Large-scale structure of the Universe and cosmological perturbation theory". In: *Physics Reports* 367.1-3 (Sept. 2002), pp. 1–248. DOI: 10.1016/S0370-1573(02)00135-7.

[39] A. A. Vlasov. "On Vibration Properties of Electron Gas". In: *J. Exp. Theor. Phys (In Russian)* 8.3 (1938), p. 291.

[40] Siméon Denis Poisson. "*Mémoire sur la théorie du magnétisme en mouvement* [Memoir on the theory of magnetism in motion]". In: *Mémoires de l'Académie Royale des Sciences de l'Institut de France in French* 6 (1823), pp. 441–570.

[41] Leonard Euler. "*Principes généraux du mouvement des fluides* [The General Principles of the Movement of Fluids]". In: *Mémoires de l'académie des sciences de Berlin (in French)* 11 (1757), pp. 274–315.

[42] T. Buchert. "A class of solutions in Newtonian cosmology and the pancake theory". In: *Astronomy and Astrophysics* 223.1-2 (1989), pp. 9–24.

[43] D.J. Heath. "The Growth of Density Perturbations in Zero Pressure Friedmann-Lemaître Universes". In: *Monthly Notices of the Royal Astronomical Society* 179 (1977), pp. 351–358. DOI: 10.1093/mnras/179..351H.

[44] R. B. Paris et al. *"Incomplete beta functions" in NIST Handbook of Mathematical Functions*. Cambridge University Press, 2010. ISBN: 978-0-521-19225-5.

[45] Jiro Soda and Yasushi Suto. "Nonlinear Gravitational Evolution of Phases and Amplitudes in One-Dimensional Cosmological Density Fields". In: *The Astrophysical Journal* (1992). DOI: 10.1086/171726.

[46] R. J. Scherrer, A. L Melott, and S. F. Shandarin. "A Quantitative Measure of Phase Correlations in Density Fields". In: *The Astrophysical Journal* 377.29 (1991).

[47] Ya. B. Zel'Dovich. "Gravitational instability: an approximate theory for large density perturbations." In: *Astronomy & Astrophysics* 500 (1970), pp. 13–18.

[48] Martin White. "The Zel'dovich Approximation". In: *Monthly Notices of the Royal Astronomical Society* 439 (Feb. 2014). DOI: 10.1093/mnras/stu209.

[49] Benjamin Grinstein and Mark B. Wise. "On the Validity of the Zel'dovich Approximation". In: *The Asrrophysical Journal* 320 (Sept. 1987), p. 448. DOI: 10.1086/165561.

[50] A. G. Doroshkevich. "Spatial structure of perturbations and origin of galactic rotation in fluctuation theory". In: *Astrophysics* 6.320 (1970). DOI: 10.1007/BF01001625.

[51] Thomas Buchert. "Lagrangian theory of gravitational instability of Friedman-Lemaître cosmologies and the 'Zel'dovich Aprroximation'". In: *Monthly Notices of the Royal Astronomical Society* 254.4 (1992), pp. 729–737. ISSN: 0035-8711. DOI: 10.1093/mnras/254.4729.

[52] Cora Uhlemann et al. "Semiclassical path to cosmic large-scale structure". In: 99.8 (2019). DOI: 10.1103/physrevd.99.083524. URL: https://doi.org/10.1103%2Fphysrevd.99.083524.

[53] Mateja Gosença et al. "Multifield ultralight dark matter". In: *Physical Review D* 107.8, 083014 (Apr. 2023), p. 083014. DOI: 10.1103/PhysRevD.107.083014.

[54] Alex Gough and Cora Uhlemann. "When to interfere with dark matter? The impact of wave dynamics on statistics". In: *The Open Journal of Astrophysics* 7, 60 (July 2024). DOI: 10.33232/001c.121413.

[55] Alex Gough and Cora Uhlemann. "Making (dark matter) waves: Untangling wave interference for multi-streaming dark matter". In: *The Open Journal of Astrophysics* 5.14 (1 2022). DOI: 10.48550/arxiv.2206.11918.

[56] Lawrence M. Widrow. "Modeling collisionless matter in general relativity: A new numerical technique". In: *Physical Review D* 55.10 (1997), pp. 5997–6001. ISSN: 1089-4918. DOI: 10.1103/physrevd.55.5997.

[57] Peter Coles. *The Wave Mechanics of Large-scale Structure*. 2002. eprint: astro-ph/0209576.

[58] Peter Coles. "The origin of spatial intermittency in galaxy distribution". In: *Monthly Notices of the Royal Astronomical Society* 330 (2002). DOI: 10.1046/j.1365-8711.2002.05096.x.

[59] Mark Brook and Peter Coles. "Gravitational stability of Vortices in Bose-Einstein Condensate Dark Matter". In: *The Open Journal of Astrophysics* 5 (Sept. 2022). DOI: 10.21105/astro.0902.0605.

[60] E. Madelung. "Quantentheorie in hydrodynamischer form". In: *Zeitschrift für Physik* 40 (1927), pp. 0044–3328. DOI: 10.1007/BF01400372.

[61] E.A. Spiegel. "Fluid dynamical form of the linear and nonlinear Schrödinger equations". In: *Physica D: Nonlinear Phenomena* 1.2 (1980), pp. 236–240. ISSN: 0167-2789. DOI: https://doi.org/10.1016/0167-2789(80)90015-9. URL: https://www.sciencedirect.com/science/article/pii/0167278980900159.

[62] Rebecca Johnston, A. N. Lasenby, and M. P. Hobson. "Cosmological fluid dynamics in the Schrödinger formalism". In: *Monthly Notices of the Royal Astronomical Society* (2009).

[63] Bodo Schwabe et al. "Simulating mixed fuzzy and cold dark matter". In: *Physical Review D* 102.8 (Oct. 2020). ISSN: 2470-0029. DOI: 10.1103/physrevd.102.083518. URL: http://dx.doi.org/10.1103/PhysRevD.102.083518.

[64] Mona Dentler et al. "Fuzzy dark matter and the Dark Energy Survey Year 1 data". In: *Monthly Notices of the Royal Astronomical Society* 515.4 (July 2022), pp. 5646–5664. ISSN: 1365-2966. DOI: 10.1093/mnras/stac1946. URL: http://dx.doi.org/10.1093/mnras/stac1946.

[65] Lam Hui. "Wave Dark Matter". In: *Annual Review of Astronomy and Astrophysics* 59 (Sept. 2021), pp. 247–289. DOI: 10.1146/annurev-astro-120920-010024. arXiv: 2101.11735 [astro-ph.CO].

[66] C. J. Short and P. Coles. "Gravitational instability via the Schrödinger equation". In: *Journal of Cosmology and Astroparticle Physics* (Dec. 2006). DOI: 10.1088/1475-7516/2006/12/012.

[67] P. Coles and K. Spencer. "A wave-mechanical approach to cosmic structure formation". In: *Monthly Notices of the Royal Astronomical Society* 342 (June 2003), pp. 176–184. DOI: 10.1046/j.1365-8711.2003.06529.x.

[68] V. Icke. "Voids and filaments". In: *Monthly Notices of the Royal Astronomical Society* 206 (1984), 1P–3P. DOI: 10.1093/mnras/206.1.1P.

[69] D Lynden-Bell. "On Large-Scale Instabilities during Gravitational Collapse and the Evolution of Shrinking Maclaurin Spheroids." In: *Astrophysical Journal, vol. 139, p. 1195* 139 (1964), p. 1195.

[70] C. C. Lin, L. Mestel, and F. H. Shu. "The Gravitational Collapse of a Uniform Spheroid." In: *The Astrophysical Journal* 142 (Nov. 1965), p. 1431. DOI: 10.1086/148428.

[71] J. Centrella and A. Melott. "Three dimensional simulation of large-scale structure in the Universe". In: *Nature* 305 (1983), pp. 196–198. DOI: 10.1038/305196a0.

[72] V. Icke. In: *Astronomy and Astrophysics* 27.1 (1973).

[73] V. Icke. PhD thesis. Leiden, 1972.

[74] E. Bertschinger. "The self-similar evolution of holes in an Einstein -de Sitter universe". In: *The Astrophysical Journal Supplement Series* 58 (1985), pp. 1–37. DOI: 10.1086/191027.

[75] S. D. M. white. "The hierarchy of correlation functions and its relation to other measures of galaxy clustering". In: *Monthly Notices of the Royal Astronomical Society* 186 (1979), pp. 145–154. DOI: 10.1093/mnras/186.2.145.

[76] Ravi K. Sheth and Rien van de Weygaert. "A hierarchy of voids: much ado about nothing". In: *Monthly Notices of the Royal Astronomical Society* 350.2 (2004), pp. 517–538. DOI: 10.1111/j.1365-2966.2004.07661.x.

[77] E. G. Patrick Bos et al. "The darkness that shaped the void: dark energy and cosmic voids". In: *Monthly Notices of the Royal Astronomical Society* 426.1 (2012), pp. 440–461. DOI: 10.1111/j.1365-2966.2012.21478.x.

[78] Ixandra Achitouv, Mark Neyrinck, and Aseem Paranjape. "Testing spherical evolution for modelling void abundances". In: *Monthly Notices of the Royal Astronomical Society* 451.4 (2015), pp. 3964–3974. DOI: 10.1093/mnras/stv1228.

[79] Vasiliy Demchenko et al. "Testing the spherical evolution of cosmic voids". In: *Monthly Notices of the Royal Astronomical Society* 463.1 (2016), pp. 512–519. DOI: 10.1093/mnras/stw2030.

[80] Alice Pisani et al. "Cosmic Voids: a novel probe to shed light on our universe". In: *Astro2020: Decadal Survey on Astronomy and Astrophysics, science white papers, no. 40; Bulletin of the American Astronomical Society, Vol. 51, Issue 3, id. 40 (2019)* (2020).

[81] C. J. Short and P. Coles. "Wave mechanics of the adhesion approximation". In: *Journal of Cosmology and Astroparticle Physics* (Dec. 2006). DOI: 10.1088/1475-7516/2006/12/016.

[82] S. N. Gurbatov, A. I. Saichev, and S. F Shandarin. "The large-scale structure of the universe in the frame of the model equation of non-linear diffusion". In: *Monthly Notices of the Royal Astronomical Society* 236 (1989), pp. 385–402. DOI: 10.1093/mnras/236.2.385.

[83] Bernard J. T. Jones. "The origin of scaling in the galaxy distribution". In: *Monthly Notices of the Royal Astronomical Society* 307.2 (Aug. 1999), pp. 376–386. DOI: 10.1046/j.1365-8711.1999.02592.x.

[84] A. L. Ribeiro and J. G. Peixoto de Faria. "Weakly nonlocal hydrodynamics and the origin of viscosity in the adhesion model". In: *Physical Review D* 71.6 (Mar. 2005), p. 067302. DOI: 10.1103/PhysRevD.71.067302.

[85] G Stokes. "On the Theories of the Internal friction of Fluids in Motion, and of the Equilibrium and Motion of Elastic Solids". In: *Transactions of the Cambridge Phiosophical Society* 8 (1849), pp. 287–342.

[86] Daniel D. Joseph. "Potential flow of viscous fluids: Historical notes". In: *International Journal of Multiphase Flow* 32.3 (2006), pp. 285–310. ISSN: 0301-9322. DOI: https://doi.org/10.1016/j.ijmultiphaseflow.2005.09.004.

[87] P. Fernández de Córdoba, J. M. Isidro, and J. Vázquez Molina. "Schroedinger vs. Navier-Stokes". In: *Entropy* 18.1 (2016). ISSN: 1099-4300. DOI: 10.3390/e18010034.

[88] G. G Stokes. "On the Effect of the Internal Friction of Fluids on the Motion of Pendulums". In: *Transactions of the Cambridge Philosphical Society* 9 (1851), p. 8.

[89] Osborne Reynolds. "An Experimental Investigation of the Circumstances Which Determine Whether the Motion of Water Shall Be Direct of Sinuous, and of the Law of Resistance in Parallel Channels". In: *Philosophical Transactions of the Royal Society of London Series I* 174 (Jan. 1883), pp. 935–982.

[90] Arnold Sommerfeld. *Ein Beitrag zur hydrodynamischen Erkläerung der turbulenten Flüssigkeitsbewegüngen (A Contribution to Hydrodynamics Explanation of Turbulent Fluid Motions)*. 1908. URL: https://web.archive.org/web/20161115133937/http://www.mathunion.org/ICM/ICM1908.3/Main/icm1908.3.0116.0124.ocr.pdf.

[91] Peter Coles and John D. Barrow. "Microwave background constraints on the Voronoi model of large-scale structure". In: *Monthly Notices of the Royal Astronomical Society* 244 (June 1990), pp. 557–562.

[92] Leonid Ivanovich Sedov. "Propagation of strong shock wave". In: *Journal of Applied Mathematics and Mechanics* 10 (1946), pp. 241–250.

[93] Carl H. Gibson. "Cold dark matter cosmology conflicts with fluid mechanics and observations". In: *Journal of Applied Fluid Mechanics* (2006). DOI: 10.48550/arXiv.astro-ph/0606073. URL: https://arxiv.org/abs/astro-ph/0606073.

[94] Adi Nusser and Avishai Dekel. "Tracing Large-Scale Fluctuations Back in Time". In: *The Astrophysical Journal* 391 (June 1992), p. 443. DOI: 10.1086/171360.

[95] Mirt Gramann. "An Improved Reconstruction Method for Cosmological Density Fields". In: *The Astrophysical Journal* 405 (Mar. 1993), p. 449. DOI: 10.1086/172377.

[96] Nick Kaiser. "Clustering in real space and in redshift space". In: *Monthly Notices of the Royal Astronomical Society* 227.1 (July 1987), pp. 1–21. ISSN: 0035-8711. DOI: 10.1093/mnras/227.1.1.

[97] Charles Alcock and Bohdan Paczyński. "An evolution free test for non-zero cosmological constant". In: *Nature* 281 (1979). ISSN: 5730. DOI: 10.1038/281358a0.

[98] S. -F. Chen et al. "Baryon acoustic oscillation theory and modelling systematics for the DESI 2024 results". In: *Monthly Notices of the Royal Astronomical Society* (Oct. 2024).

[99] Naonori Sugiyama. "Discreteness Effects in the Post-Reconstruction Galaxy Power Spectrum". In: *arXiv e-prints*, arXiv:2406.01001 (June 2024). DOI: 10.48550/arXiv.2406.01001.

[100] A. Burden et al. "Efficient reconstruction of linear baryon acoustic oscillations in galaxy surveys". In: *Monthly Notices of the Royal Astronomical Society* 445.3 (Dec. 2014), pp. 3152–3168. DOI: 10.1093/mnras/stu1965.

[101] Y. Brenier et al. "Reconstruction of the early Universe as a convex optimisation problem". In: *Monthly Notices of the Royal Astronomical Society* 346.2 (2003), pp. 501–524. DOI: 10.1046/j.1365-2966.2003.07106.x.

[102] Farnik Nikakhtar et al. "Displacement field analysis via optimal transport: Multitracer approach to cosmological reconstruction". In: *Physical Review D* 109.12, 123512 (June 2024), p. 123512. DOI: 10.11.03/PhysRevD.109.123512.

[103] Robert Lilow, Punyakoti Ganeshaiah Veena, and Adi Nusser. "Neural network reconstruction of density and velocity fields from the 2MASS Redshift Survey". In: *Astronomy and Astrophysics* 689, A226 (Sept. 2024), A226. DOI: 10.1051/00004-6361/202450219.

[104] Martin White. "Reconstruction within the Zeldovich approximation". In: *Monthly Notices of the Royal Astronomical Society* 450.4 (May 2015). ISSN: 0035-8711. DOI: 10.1093/mnras/stv842.

[105] J. Sakurai. *Modern Quantum Mechanics (Revised Ediation)*. 1st ed. Addison Wesley, 1993. ISBN: 0201539292. URL: https://search.worldcat.org/search?q=bn:0201539292.

[106] Chris Short. "Large-Scale Structure Formation: A Wave-Mechanical Perspective". PhD thesis. University of Nottingham, 2007.

[107] Volker Springel et al. *illustrisTNG*. 2023. URL: https://www.tng-project.org/.

[108] Statistics How To. *Correlation Coefficient: Simple Definition, Formula, Easy Steps*. https://www.statisticshowto.com/probability-and-statistics/correlation-coefficient-formula/. 2024.

[109] Matteo Nori, Shubhan Bhatia, and Andrea V. Macciò. "Fuzzy Gasoline: Cosmological hydrodynamical simulations of dwarf galaxy formation with

Fuzzy Dark Matter". In: (2024). arXiv: 2411.09733 [astro-ph.GA]. URL: https://arxiv.org/abs/2411.09733.

[110] Job Feldbrugge et al. "Caustic Skeleton and Cosmic Web". In: *Journal of Cosmology and Astroparticle Physics* 2018.027 (2018). DOI: 10.1088/1475-7516/2018/05/027.